nature biotechnology

Supplementary information

https://doi.org/10.1038/s41587-025-02905-4

# All-optical visualization of specific molecules in the ultrastructural context of brain tissue

In the format provided by the authors and unedited

## Table of Contents

## Supplementary Figures

Supplementary Figure 1: Gallery of NHS ester pan-stained synapses in dissociated mouse and rat hippocampal neurons.
Supplementary Figure 2: Gallery of Bassoon-immunolabeled and NHS ester pan-stained synapses in dissociated mouse hippocampal neurons.
Supplementary Figure 3: Gallery of Homer1-immunolabeled and NHS ester pan-stained synapses in dissociated mouse neurons.
Supplementary Figure 4: Gallery of PSD-95 immunolabeled and NHS ester pan-stained synapses in dissociated mouse hippocampal neurons.
Supplementary Figure 5: Gallery of Homer1- and Bassoon-immunolabeled and NHS ester pan-stained synapses in dissociated mouse hippocampal neurons.
Supplementary Figure 6: Ultrastructural features in neurons are not visible in non-expanded and ~5 fold expanded samples.
Supplementary Figure 7: Effect of antibody dilution factor on background noise in expanded mouse neurons.
Supplementary Figure 8: Palmitate and NHS ester differential pan-staining in dissociated mouse neurons.
Supplementary Figure 9: Gallery of subcellular features in dissociated mouse hippocampal neurons.
Supplementary Figure 10: Gallery of mitochondria in dissociated mouse and rat neurons.
Supplementary Figure 11: Effect of fixation and post-fixation on cell ultrastructure in expanded mouse brain tissue sections.
Supplementary Figure 12: Effect of fixation and post-fixation on neuropil ultrastructure in expanded mouse brain tissue sections.
Supplementary Figure 13: Effect of fixation and post-fixation on extracellular space (ECS) preservation in expanded mouse brain tissue sections.
Supplementary Figure 14: Effect of denaturation time on expansion factor and protein retention in expanded mouse brain tissue sections.
Supplementary Figure 15: pan-ExM-t reveals mouse brain tissue ultrastructure (overview 1).
Supplementary Figure 16: pan-ExM-t reveals mouse brain tissue ultrastructure (overview 2).
Supplementary Figure 17: pan-ExM-t reveals mouse brain tissue ultrastructure (overview 3).
Supplementary Figure 18: Multiciliated ependymal epithelia lining the lateral ventricles of the mouse brain.
Supplementary Figure 19: Gallery of mouse brain capillaries.
Supplementary Figure 20: Effect of sodium acrylate (SA) monomer concentration on expanded mouse brain tissue integrity.
Supplementary Figure 21: Astrocytes and neurons exhibit distinct NHS ester pan-staining patterns.
Supplementary Figure 22: BODIPY-TR-Methyl Ester (BDP) pan-staining reveals lipophilic components in 4-fold expanded mouse brain tissue sections.
Supplementary Figure 23: BODIPY-TR-Methyl Ester (BDP) and hydrophilic NHS ester differential pan-staining in a 4-fold expanded mouse brain tissue section.
Supplementary Figure 24: Effect of fixation on BODIPY-TR-Methyl Ester (BDP) pan-staining in 4-fold expanded mouse brain tissue sections.
Supplementary Figure 25: BODIPY-TR-Methyl Ester (BDP) and hydrophilic NHS ester differential pan-staining in pan-ExM-t expanded mouse brain tissue sections.
Supplementary Figure 26: Effect of osmification on pan-ExM-t expanded brain tissue integrity.
Supplementary Figure 27: BODIPY-TR-Methyl Ester (BDP) signal is higher in G-HCl-denatured than in SDS- and non-denatured ~4-fold expanded mouse brain tissue sections.
Supplementary Figure 28: BODIPY-TR-Methyl Ester (BDP) does not label neurite boundaries specifically.
Supplementary Figure 29: mCling only labels the surface of 4-fold expanded mouse brain tissue sections fixed with 3% FA + 0.1% GA.
Supplementary Figure 30: Chemical structures of pGk5b, mCling, and pacSph.
Supplementary Figure 31: Effect of UV irradiation on pacSph pan-staining in pan-ExM-t expanded mouse brain tissue sections.

Supplementary Figure 32: Examples of pacSph and NHS ester differential pan-staining in 4-fold expanded mouse brain tissue sections.
Supplementary Figure 33: | pan-ExM-t data from non-brain tissue.
Supplementary Figure 34: Quantification of tracing accuracy from pan-ExM-t data.

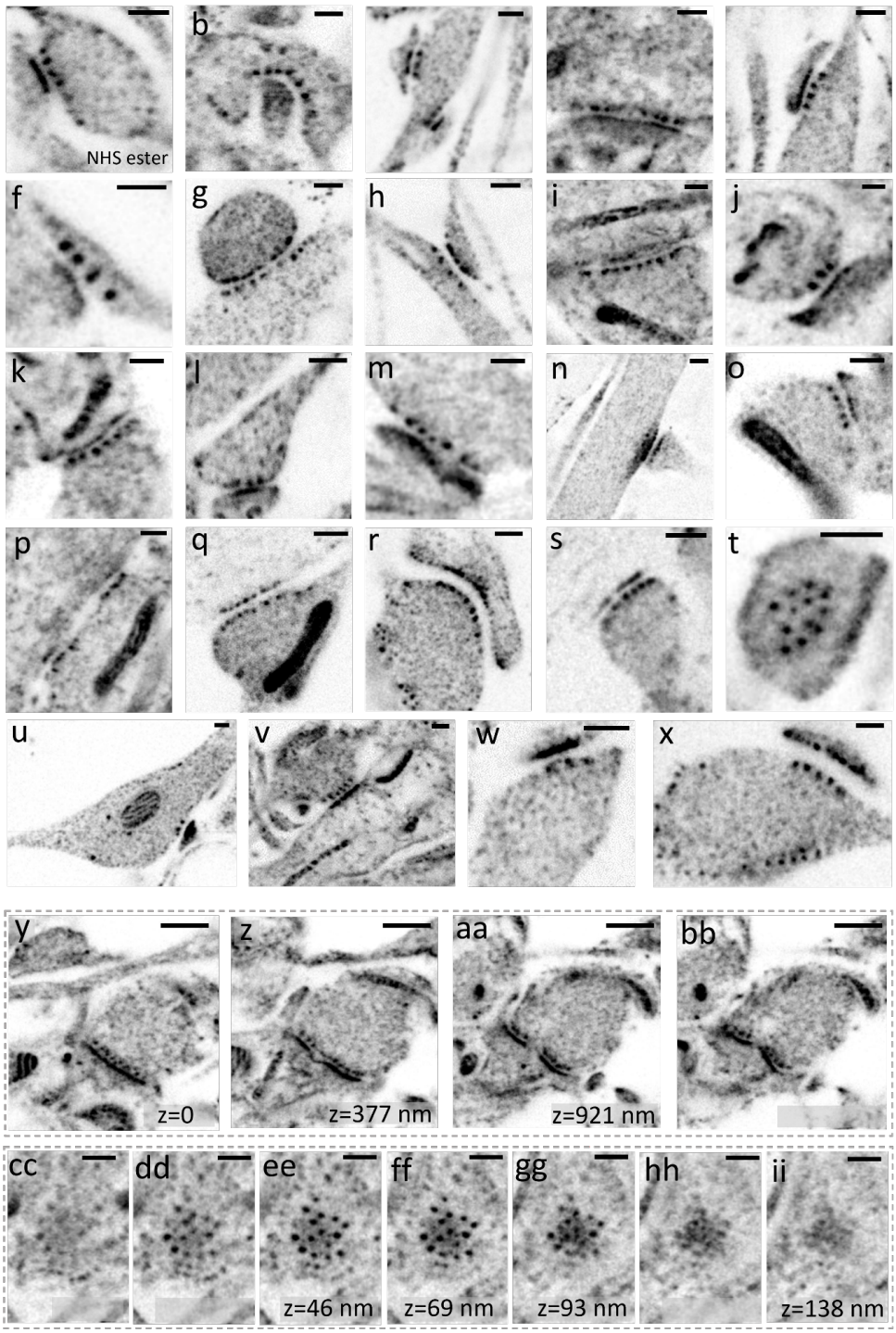
## Supplementary Tables

Supplementary Table 1: Polymerization, buffer, and fixative reagents used
Supplementary Table 2: Materials used
Supplementary Table 3: Primary antibodies used to immunolabel neuron and brain tissue samples
Supplementary Table 4: Secondary antibodies used to immunolabel neuron and brain tissue samples
Supplementary Table 5: Fluorescent pan-stains and lipid probes used
Supplementary Table 6: Overview of Labeling Conditions.

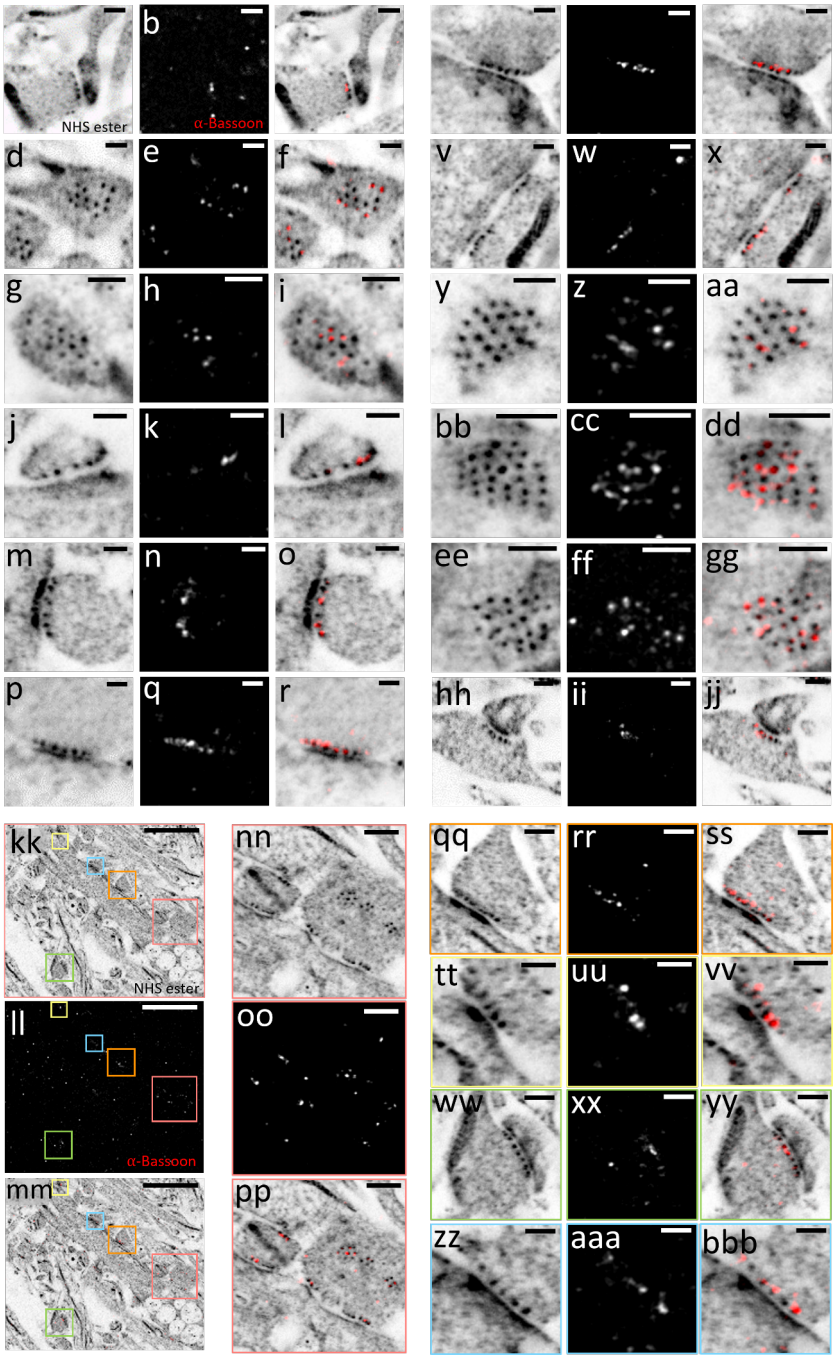
## Supplementary Methods

## Supplementary References

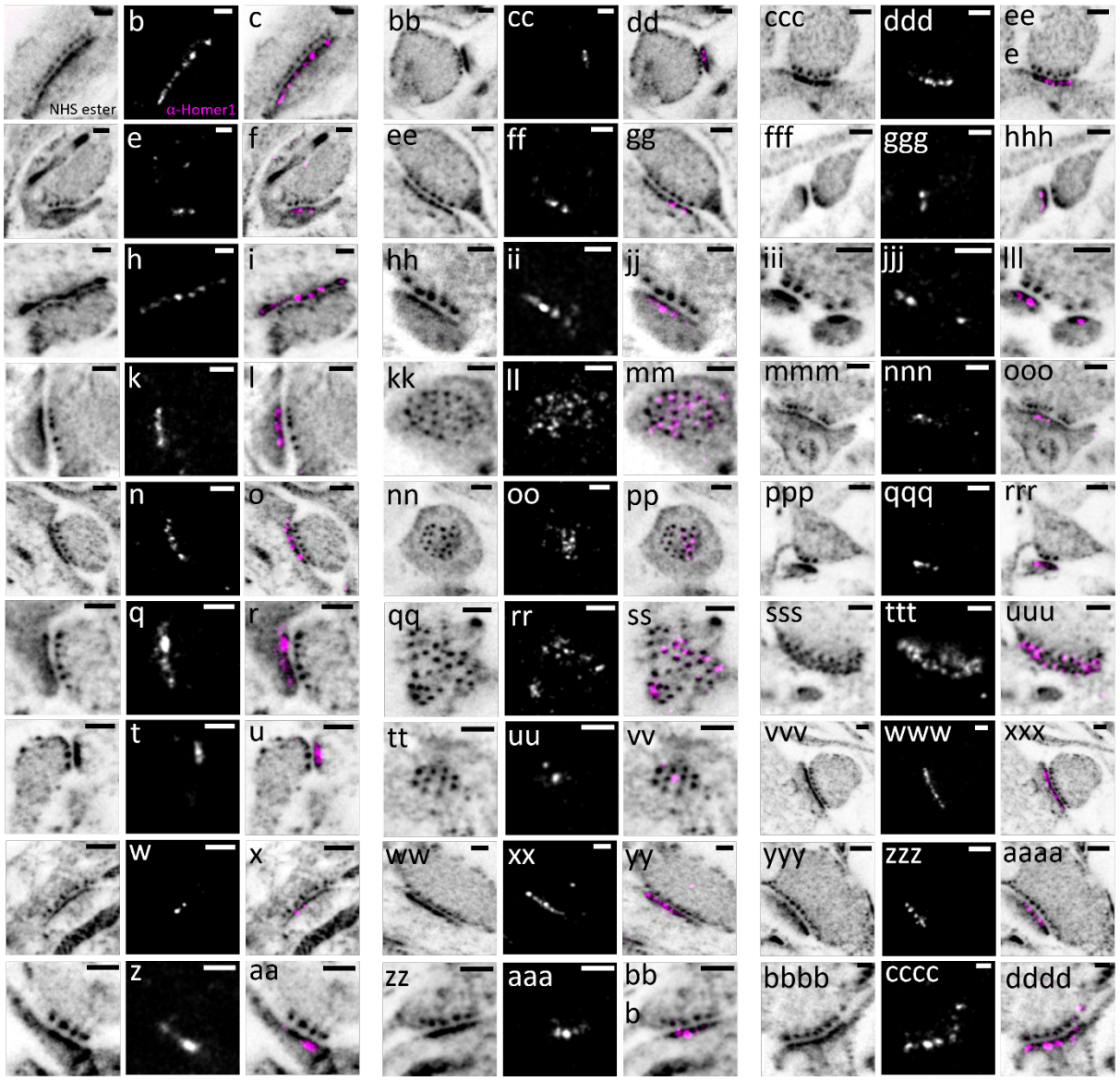
# Supplementary Figures



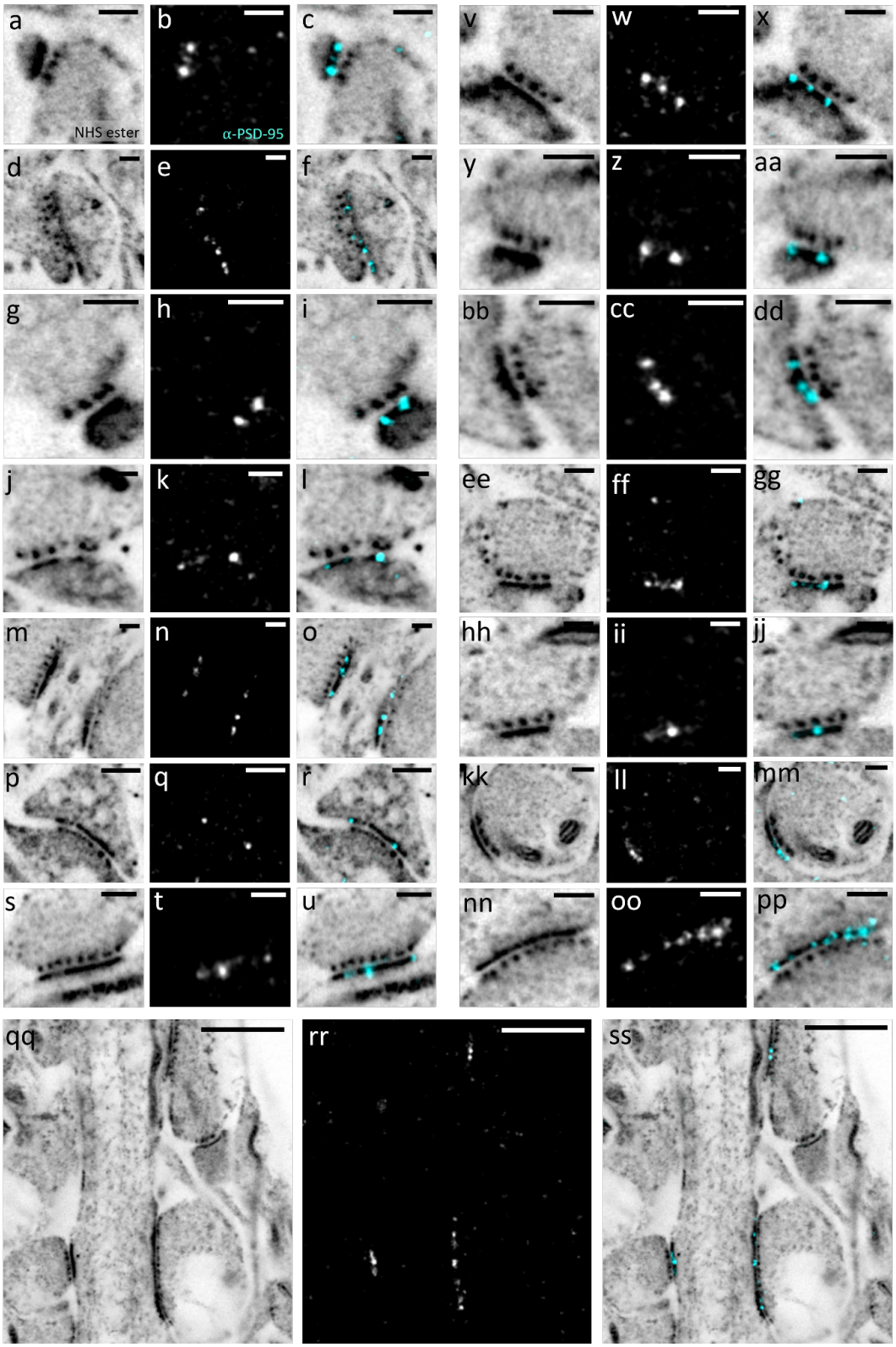

**Supplementary Figure 1: Gallery of NHS ester pan-stained synapses in dissociated mouse and rat hippocampal neurons. a-z,** axial or top views of synapses showing presynaptic dense projections (DPs) and postsynaptic densities (PSDs). **y-bb,** z-stack of a synapse (side view) spanning 990 nanometers. **cc-ii**, z-stack of a synapse (top view) spanning 138 nanometers. Image **d** was processed with a gamma value ɣ=0.5; image **l** with ɣ=0.6; images **b**, **g, i,** and **u** with ɣ=0.7; images **h**, **j**, **k**, **m**, **n**, **o**, **q**, **s**, **t**, **v**, **w**, **x**, **cc-ii** with ɣ=0.8; and image **r** with ɣ=0.9. Scale bars are corrected for the expansion factor, (**a-ii**) 200 nm.



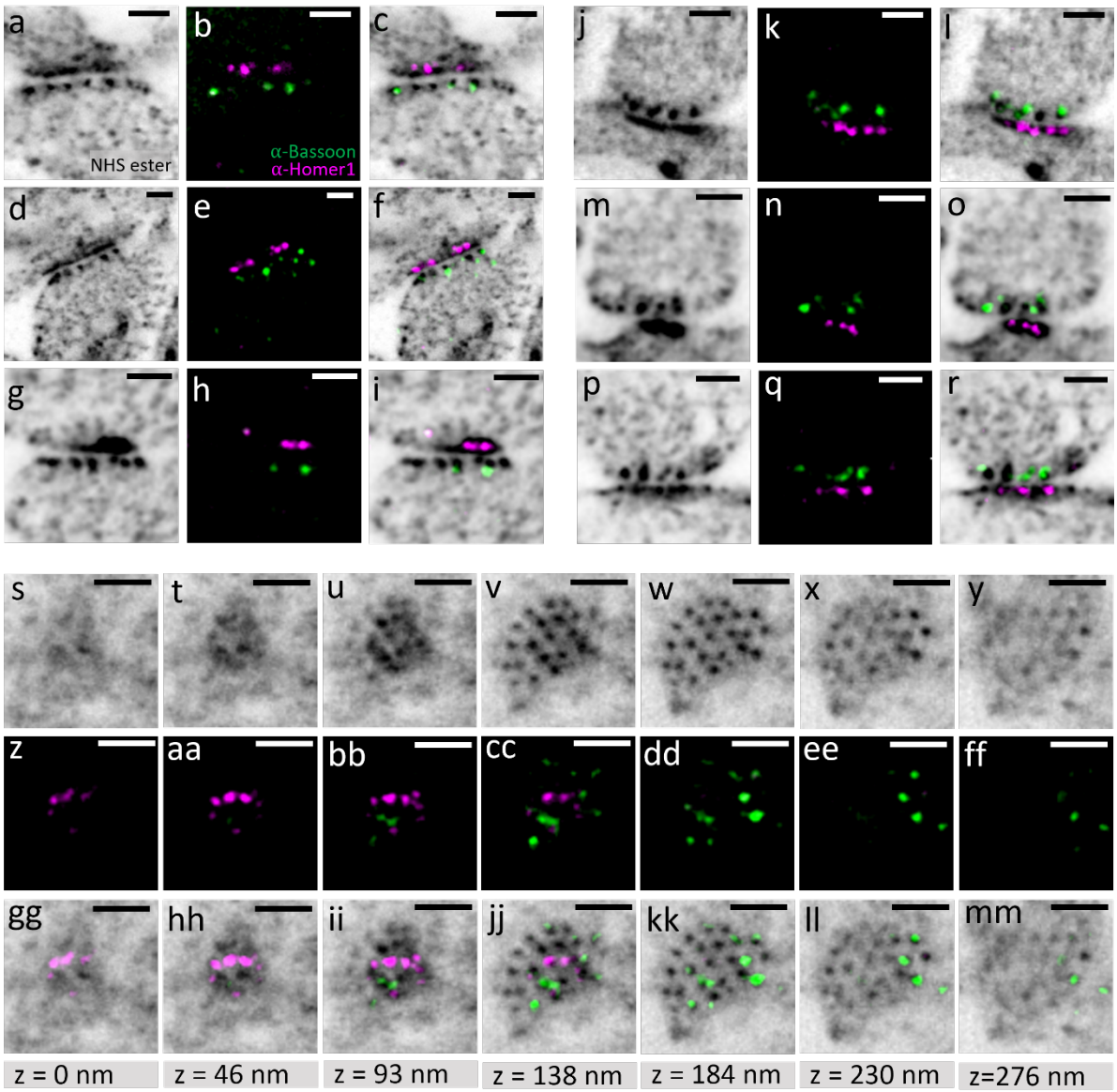

**Supplementary Figure 2: Gallery of Bassoon-immunolabeled and NHS ester pan-stained synapses in dissociated mouse hippocampal neurons. a**, **d**, **g**, **j**, **m**, **p**, **s**, **v**, **y**, **bb**, **ee**, **hh**, axial or top views of synapses pan-stained with NHS ester. **b**, **e**, **h**, **k**, **n**, **q**, **t**, **w**, **z**, **cc**, **ff**, **ii**, Bassoon immunolabeling distributed near dense projections. **c**, **f**, **i**, **l**, **o**, **r**, **u**, **x**, **aa**, **dd**, **gg**, **jj**, overlay. **kk**, ~35 µm FOV image of NHS ester pan-stained neurites. **ll**, Bassoon immunolabeling of the same area. **mm**, overlay of **kk** and **ll**. **nn**, **oo**, **pp**, magnified views of the areas outlined in the salmon boxes in **kk**, **ll**, and **mm**, respectively. **qq**, **rr**, **ss**, magnified views of the areas outlined by the orange boxes in **kk, ll,** and **mm,** respectively. **tt**, **uu**, **vv**, magnified views of the areas outlined by the yellow boxes in **kk**, **ll**, and **mm**, respectively. **ww**, **xx**, **yy**, magnified views of the areas outlined by the lime boxes in **kk**, **ll**, and **mm**, respectively. **zz**, **aaa**, **bbb**, magnified views of the areas outlined by the light blue boxes in **kk**, **ll**, and **mm**, respectively. Images **d**, **v**, **hh**, **kk**, **nn**, **qq**, **tt**, **ww**, and **zz**, were processed with a gamma value ɣ=0.7 and image **a** with ɣ=0.8. Scale bars are corrected for the expansion factor, (**a-jj**, **nn-pp**) 200 nm. (**kk-mm**) 5 µm.



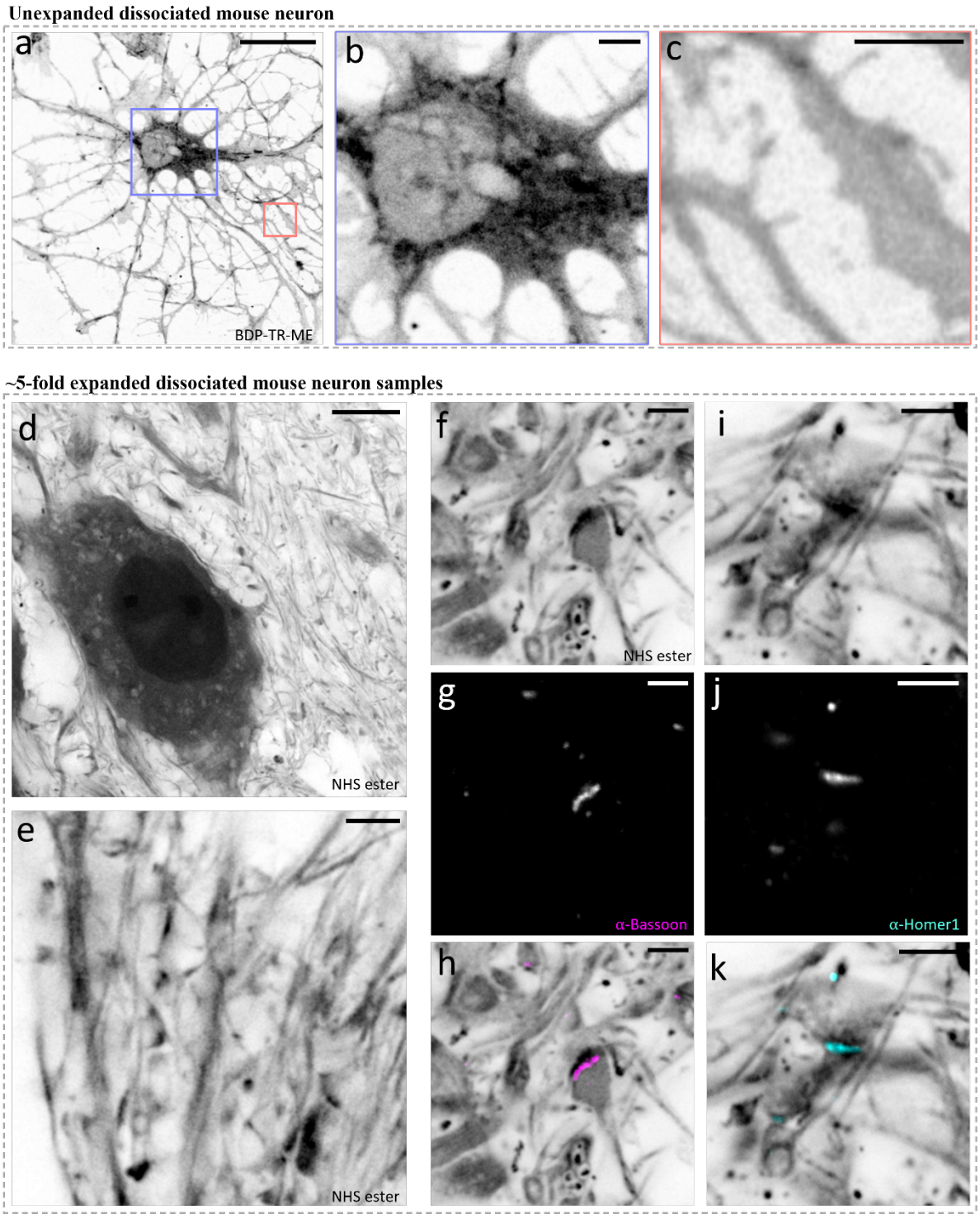

**Supplementary Figure 3: Gallery of Homer1-immunolabeled and NHS ester pan-stained synapses in dissociated mouse neurons. a**, **d**, **g**, **j**, **m**, **p**, **s**, **v**, **y**, **bb**, **ee**, **hh**, **kk**, **nn**, **qq**, **tt**, **ww**, **zz**, **ccc**, **fff**, **iii**, **mmm**, **ppp**, **sss**, **vvv**, **yyy**, **bbbb**, axial or top views of synapses pan-stained with NHS ester. **b**, **e**, **h**, **k**, **n**, **q**, t, **w**, **z**, **cc**, **ff**, **ii**, **ll**, **oo**, **rr**, **uu**, **xx**, **aaa**, **ddd**, **ggg**, **jjj**, **nnn**, **qqq**, **ttt**, **www**, **zzz**, **cccc**, Homer1 immunolabeling localized in the postsynaptic density. **c**, **f**, **i**, **l**, **o**, **r**, **u**, **x**, **aa**, **dd**, **gg**, **jj**, **mm**, **pp**, **ss**, **vv**, **yy**, **bbb**, **eee**, **hhh**, **lll**, **ooo**, **rrr**, **uuu**, **xxx**, **aaaa**, **dddd**, overlay. Images **j**, **nn**, **tt**, **ccc**, **zz**, **ppp**, **fff**, **sss**, and **yyy** were processed with a gamma value ɣ=0.8. Scale bars are corrected for the expansion factor, (**a-dddd**) 200 nm.



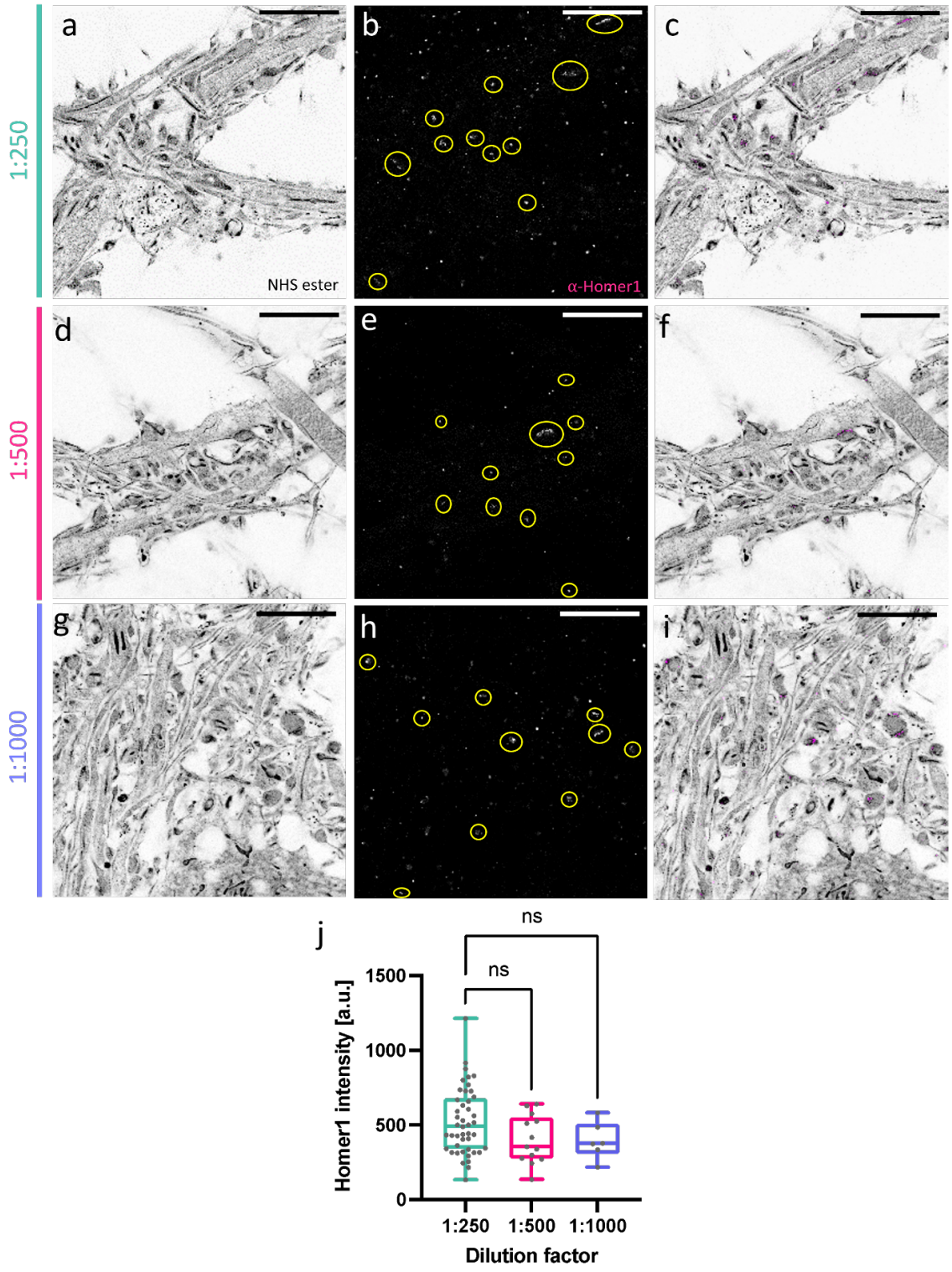

**Supplementary Figure 4: Gallery of PSD-95 immunolabeled and NHS ester pan-stained synapses in dissociated mouse hippocampal neurons. a**, **d**, **g**, **j**, **m**, **p**, **s**, **v**, **y**, **bb**, **ee**, **hh**, **kk**, **nn**, **qq**, axial or top views of synapses pan-stained with NHS ester. **b**, **e**, **h**, **k**, **n**, **q**, **t**, **w**, **z**, **cc**, **ff**, **ii**, **ll**, **oo**, **rr**, PSD-95 immunolabeling localized near dense projections. **c**, **f**, **i**, **l**, **o**, **r**, **u**, **x**, **aa**, **dd**, **gg**, **jj**, **mm**, **pp**, **ss**, overlay. Images **m** and **kk** were processed with a gamma value $\gamma$=0.7 and images **a**, **d**, **g**, **j**, **p**, **s**, **v**, **y**, **ee**, **hh,** and **nn** with $\gamma$=0.8. Scale bars are corrected for the expansion factor, (**a-pp**) 200 nm. (**qq-ss**) 1 µm.



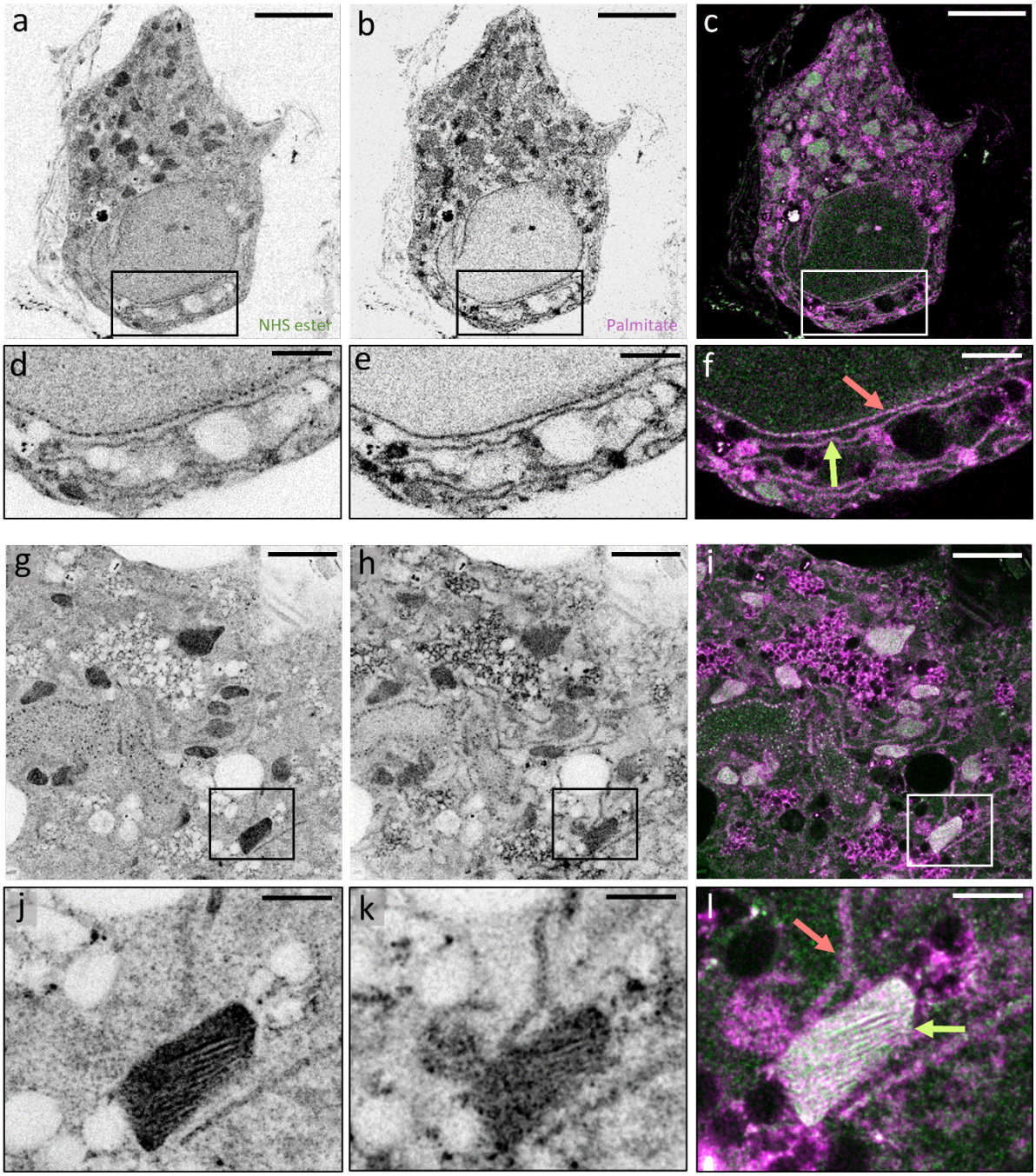

**Supplementary Figure 5: Gallery of Homer1- and Bassoon-immunolabeled and NHS ester pan-stained synapses in dissociated mouse hippocampal neurons. a**, **d**, **g**, **j**, **m**, **p**, axial or top views of synapses pan-stained with NHS ester. **b**, **e**, **h**, **k**, **n**, **q**, Homer1 and Bassoon immunolabeling. **c**, **f**, **i**, **l**, **o**, **r**, overlay. **s-u**, z-stack of a synapse (top view) spanning 276 nanometers and pan-stained with NHS ester. **z-ff**, Homer1 and Bassoon immunolabeling of the same areas as **s-u**. **gg-mm**, overlay. Images **a, d, j** and **s-y** were processed with a gamma value ɣ=0.7. Scale bars are corrected for the expansion factor, (**a-mm**) 200 nm.



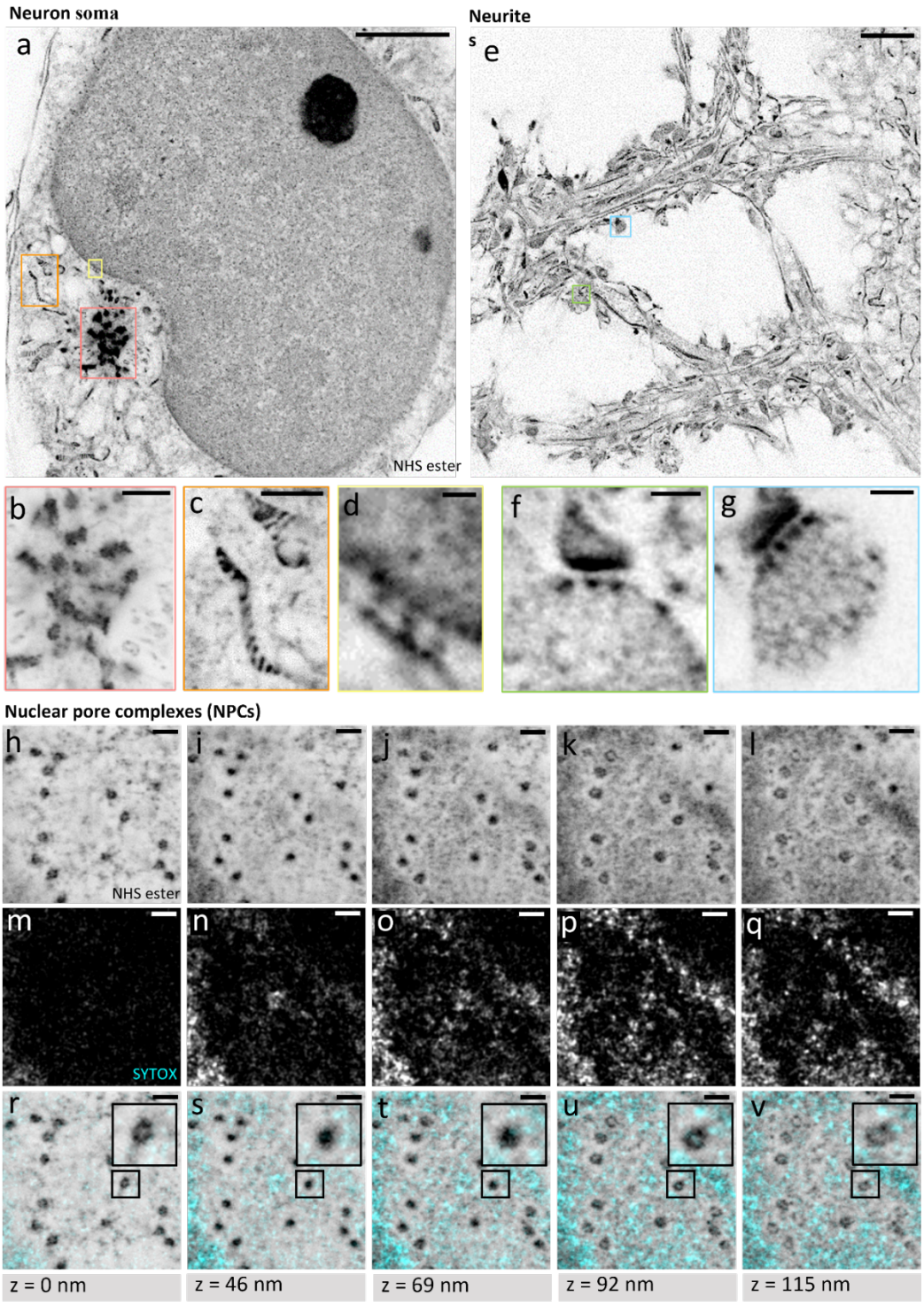

**Supplementary Figure 6: Ultrastructural features in neurons are not visible in non-expanded and ~5 fold expanded samples. a,** non-expanded neuron pan-stained with BDP-TR-ME. **b,** magnified view of the area outlined in the lavender box in **a** showing a neuron soma. **c,** magnified view of the area outlined by the salmon box in **a** showing neurites. **d**, ~5-fold expanded neurons pan-stained with NHS ester showing a neuron soma. **e**, ~5-fold expanded neurons pan-stained with NHS ester showing neurites. **f**, **i**, ~5-fold expanded neurons pan-stained with NHS ester showing synapses. **g**, **j**, Bassoon and Homer1 immunolabeling of the same areas shown in **f** and **i**. **h**, **k**, overlay. Images **d**, **e**, **f**, and **i** were processed with a gamma value ɣ=0.8. Scale bars are corrected for the expansion factor, (**a**) 20 µm, (**b**, **c**, **e-k**) 1 µm, (**d**) 10 µm.



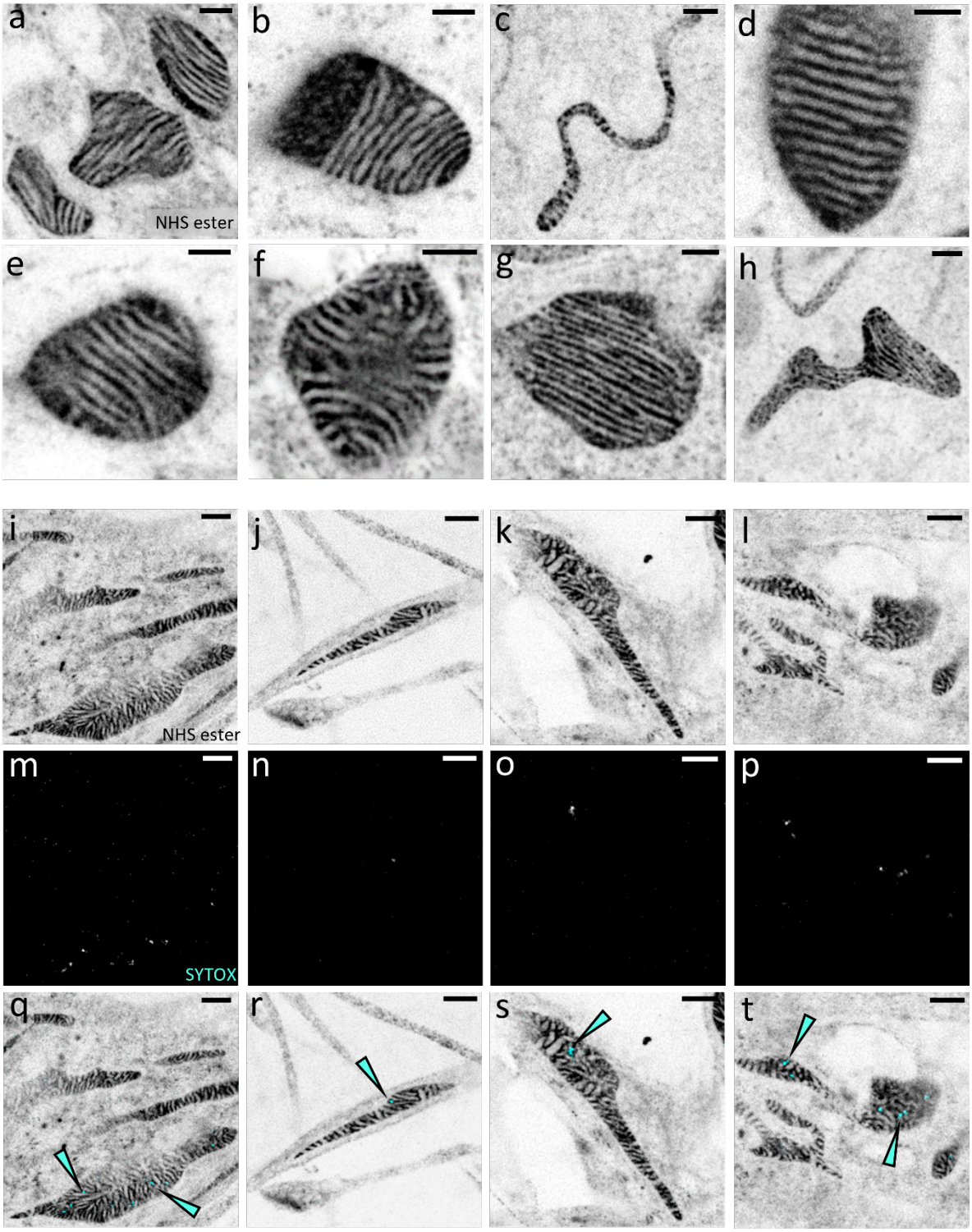

**Supplementary Figure 7: Effect of antibody dilution factor on background noise in expanded mouse neurons. a**, **d**, **g**, pan-ExM processed neurons pan-stained with NHS ester. **b**, **e**, **h**, Homer1 immunolabeling of the areas shown in **a**, **d**, and **g**, respectively. Yellow circles show 'true' Homer1 signal. **c**, **f**, **i**, overlay. **j**, intensity measurements of Homer1 peak signal according to the dilution factors of both primary and secondary antibodies (1:250: n = 45 measurements from 7 FOVs; 1:500: n = 13 measurements from 3 FOVs; 1:1000: n = 6 measurements from 1 FOV). ns: non-significant. Images **a**, **d**, and **g** were processed with a gamma value ɣ=0.8. Scale bars are corrected for the expansion factor, (**a-i**) 4 µm.



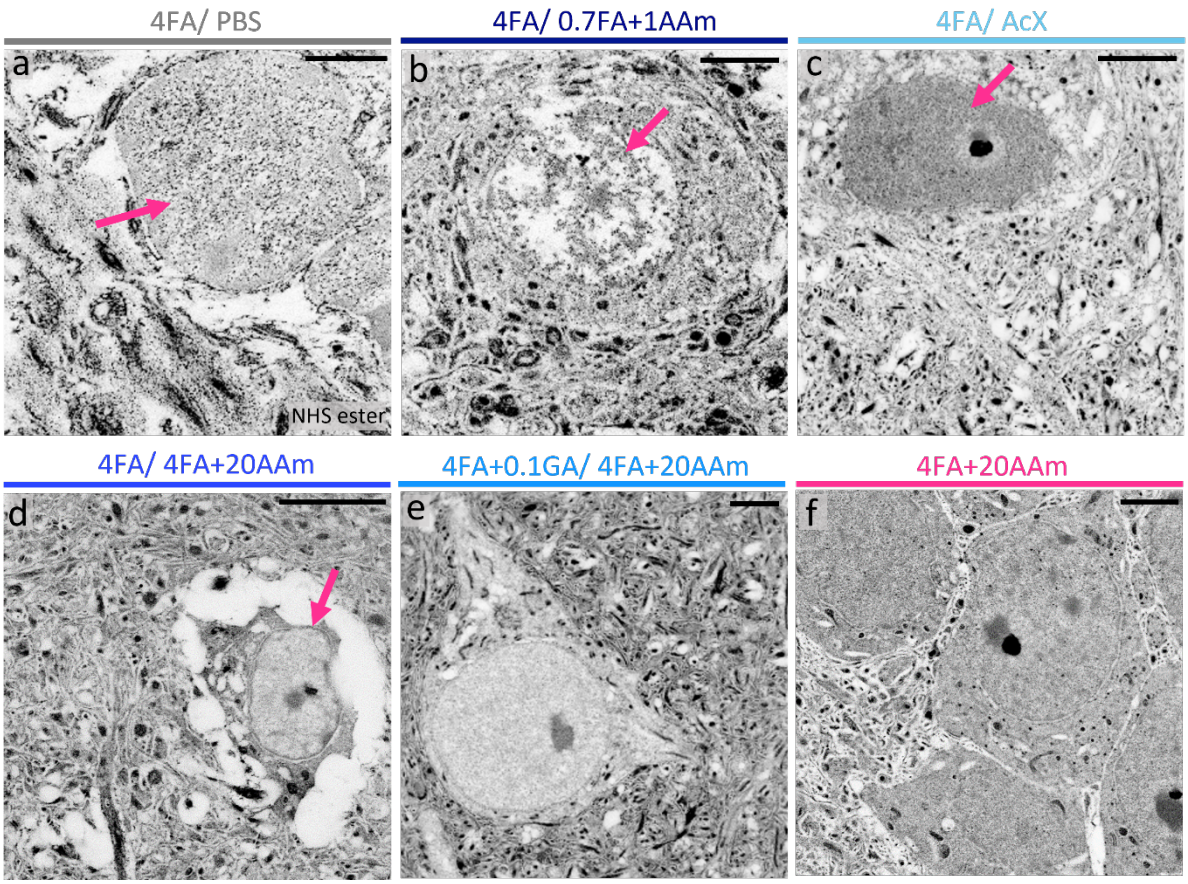

**Supplementary Figure 8: Palmitate and NHS ester differential pan-staining in dissociated mouse neurons.** **a**, NHS ester pan-stained neuron soma. **b**, palmitate pan-staining of the same area shown in **a**. **c**, overlay. **d-f**, magnified views of the areas outlined in the black boxes in **a-c**. Salmon arrow in f points to the nuclear envelope and lime arrow points to an ER tubule. **g**, NHS ester pan-stained neuron soma cytosol. **h**, palmitate pan-staining of the same area shown in **g**. **i**, overlay. **j-l**, magnified views of the areas outlined in the black boxes in **g-i.** Salmon arrow in **l** points to an ER tubule that is contacting a mitochondrion (lime arrow). Image **g** was processed with a gamma value ɣ=0.8. Scale bars are corrected for the expansion factor, (**a-c**) 5 µm, (**d-f**, **g-i**) 2 µm, (**j-l**) 500 nm.



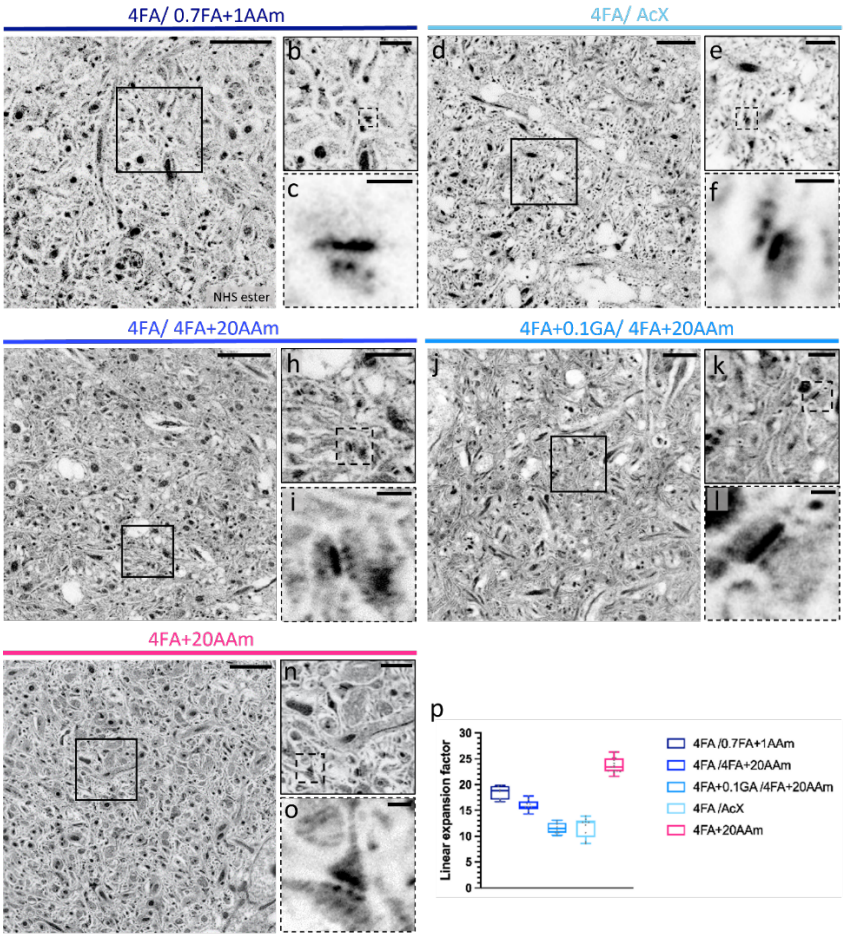

**Supplementary Figure 9: Gallery of subcellular features in dissociated mouse hippocampal neurons. a**, neuron soma processed with pan-ExM and pan-stained with NHS ester. **b**, **c**, **d**, magnified views of the areas in **a** outlined by the salmon, orange, and yellow boxes showing a centrosome, mitochondria and the side view of nuclear pore complexes (NPCs) respectively. **e**, neuron neurites processed with pan-ExM and pan-stained with NHS ester. **f**, **g**, magnified views of the areas in **e** outlined by the lime and light blue boxes showing synapses. **h-l**, z-stack of nuclear pore complexes pan-stained with NHS ester (top view) spanning 115 nanometers. **m-q**, SYTOX Green staining of the same areas as in **h-l**. **r-v**, overlay. Insets in **r** and **u** show hollow rings corresponding to the cytoplasmic and nuclear surface of the NPC respectively. Image **a** was processed with a gamma value ɣ=0.8 and image **e** with ɣ=0.7. Scale bars are corrected for the expansion factor, (**a**, **e**) 3 µm, (**b-c**) 500 nm, (**d**) 100 nm, (**f-v**) 200 nm.




**Supplementary Figure 10: Gallery of mitochondria in dissociated mouse and rat neurons. a-h**, NHS ester pan-stained mitochondria showing resolvable cristae. **i-l**, mitochondria in neuron somas (**i**, **k**, **l**) and a neurite (**j**) pan-stained with NHS ester. **m-p**, SYTOX Green staining of the same areas shown in **i-l**. **q-t**, overlay. Cyan arrows point at SYTOX Green-stained mtDNA. Images **a**, **b**, **d**, **e**, **i**, **j**, **k**, and **l** were processed with a gamma value ɣ=0.8. Scale bars are corrected for the expansion factor, (**a-h**) 200 nm, (**i-t**) 500 nm



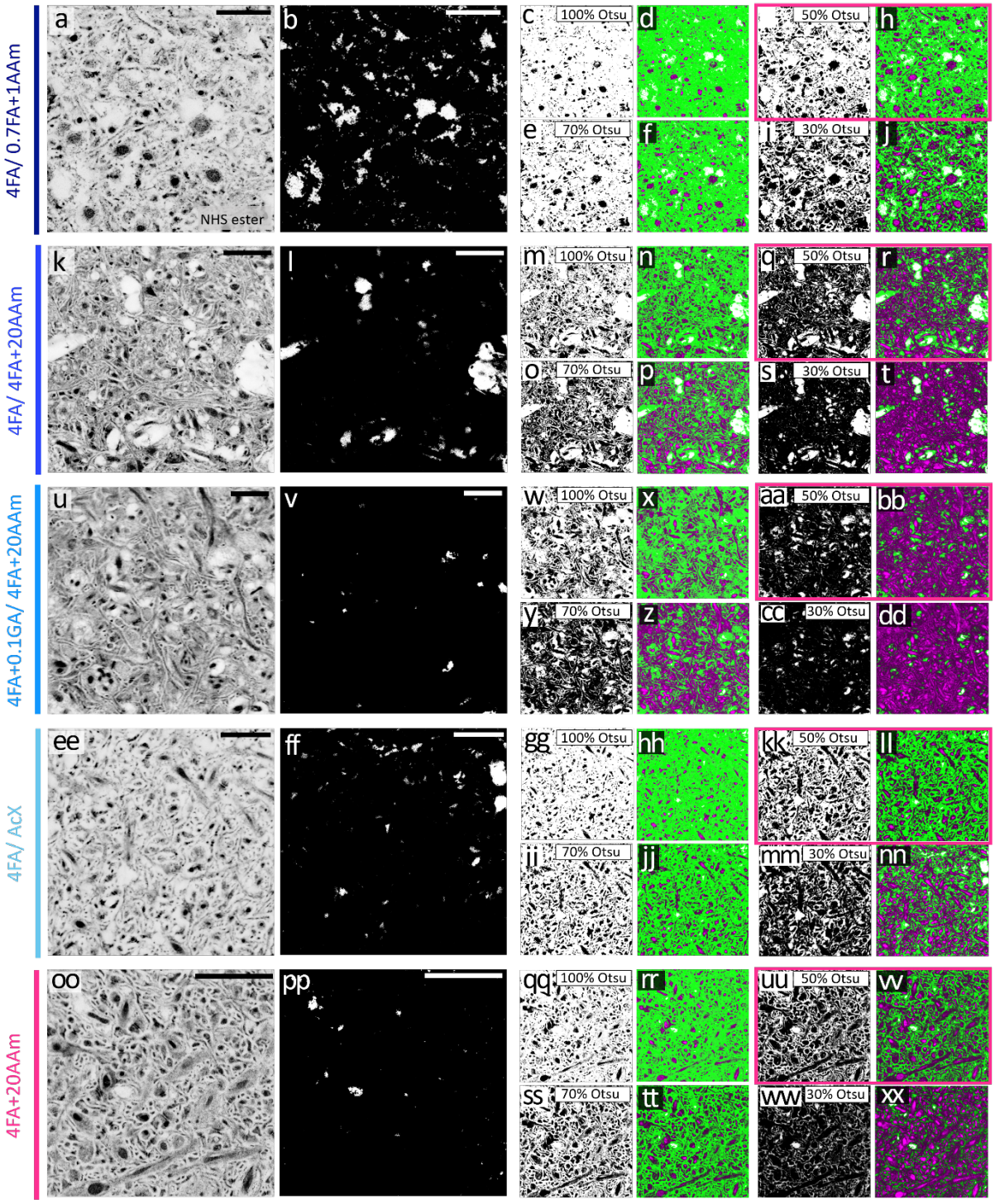

**Supplementary Figure 11: Effect of fixation and post-fixation on cell ultrastructure in expanded mouse brain tissue sections. a**, NHS ester pan-stained brain tissue fixed with 4% FA and not post-fixed (stored in PBS). Only the cell nucleus is discernable (pink arrow). **b**, NHS ester pan-stained brain tissue fixed with 4% FA and post-fixed with 0.7% FA + 1% AAm. Cell nucleus shows major extraction artifacts (pink arrow). **c**, NHS ester pan-stained brain tissue fixed with 4% FA and post-treated with 0.1 mg/mL AcX. Cell nucleus (pink arrow) appears highly stained, but cytosol and surrounding neuropil present extraction artifacts. **d**, NHS ester pan-stained brain tissue fixed with 4% FA and post-fixed with 4% FA + 20% AAm. Cell (pink arrow) is detached from surrounding tissue. **e**, NHS ester pan-stained brain tissue fixed with 4% FA + 0.1% GA and post-fixed with 4% FA + 20% AAm showing adequate cell preservation. **f**, NHS ester pan-stained brain tissue fixed with 4% FA + 20% AAm showing adequate cell preservation. Scale bars are not corrected for the expansion factor (**a-f**) 50 µm.




q

| Ref in text | Fix /Post-fix | Neuropil preservation | Cell body preservation | Expansion factor |
|---|---|---|---|---|
| *Fix-2* | 4FA /0.7FA+1AAm | + (low S/N) | + | ++ |
| *Fix-3* | 4FA /4FA+20AAm | ++ | + (detached) | ++ |
| *Fix-4* | 4FA+0.1GA /4FA+20AAm | +++ | +++ | + |
| *Fix-5* | 4FA /AcX | + | + | + |
| *Fix-6* | 4FA+20AAm | +++ | +++ | +++ |

**Supplementary Figure 12: Effect of fixation and post-fixation on neuropil ultrastructure in expanded mouse brain tissue sections. a**, NHS ester pan-stained brain tissue fixed with 4% FA and post-fixed with 0.7% FA + 1% AAm. **b**, magnified view of the area outlined in the black box in **a**. **c**, magnified view of the area outlined in the dotted black box in **b** showing a synapse. Neuropil in this condition has low signal to noise (difficult to distinguish neurites). **d**, NHS ester pan-stained brain tissue fixed with 4% FA and post-treated with 0.1 mg/mL AcX . **e**, magnified view of the area outlined in the black box in **d**. **f**, magnified view of the area outlined in the dotted black box in **e** showing a synapse. Neuropil in this condition is poorly preserved (presence of many artifactual gaps). **g**, NHS ester pan-stained brain tissue fixed with 4% FA and post-fixed with 4% FA + 20% AAm. **h**, magnified view of the area outlined in the black box in **g**. **i**, magnified view of the area outlined in the dotted black box in **h** showing a synapse. Neuropil in this condition is somewhat preserved (neurites distinguishable but presence of some artifactual gaps). **j**, NHS ester pan-stained brain tissue fixed with 4% FA + 0.1% GA and post-fixed with 4% FA + 20% AAm. **k**, magnified view of the area outlined in the black box in **j**. **l**, magnified view of the area outlined in the dotted black box in **k** showing a synapse. Neuropil in this condition is adequately preserved. **m**, NHS ester pan-stained brain tissue fixed with 4% FA + 20% AAm. **n**, magnified view of the area outlined in the black box in **m**. **o**, magnified view of the area outlined in the dotted black box in **n** showing a synapse. Neuropil in this condition is adequately preserved. **p**, plot of expansion factors (Fix-2: n = 38 measurements from 9 FOVs; Fix-3: n = 81 measurements from 9 FOVs; Fix-4: n = 77 measurements from 8 FOVs; Fix-5: 74 measurements from 10 FOVs; Fix-6: 254 measurements from 10 FOVs in 3 independent experiments). **q**, table outlining a qualitative assessment of mouse brain tissue ultrastructure preservation according to the different fixation schemes used. Black scale bars are corrected for the expansion factor (**a**, **d**, **g**, **f**, **m**) 3 µm, (**b**, **e**, **h**, **k**, **n**) 1 µm, (**c**, **f**, **i**, **l**, **o**) 200 nm.

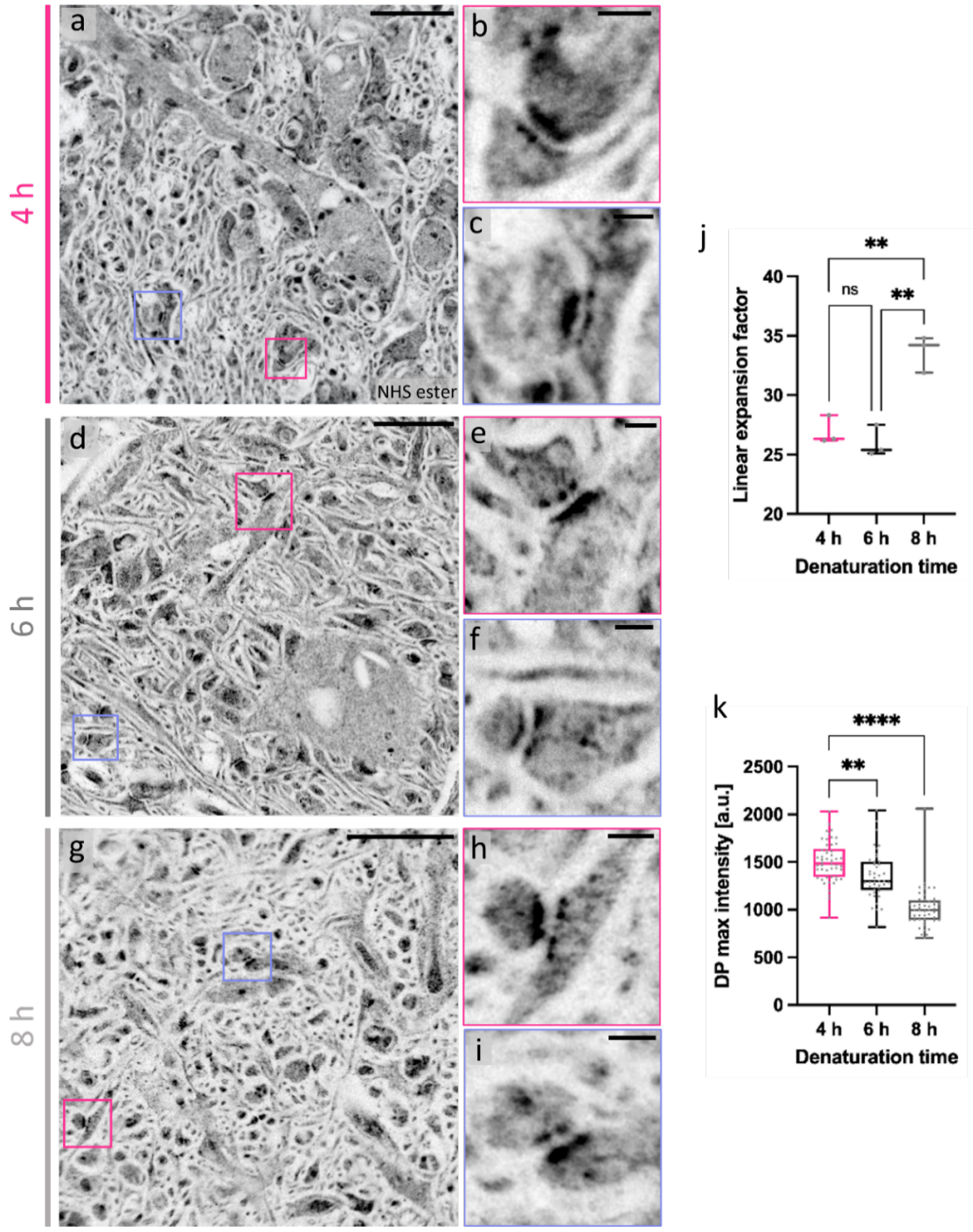



yy

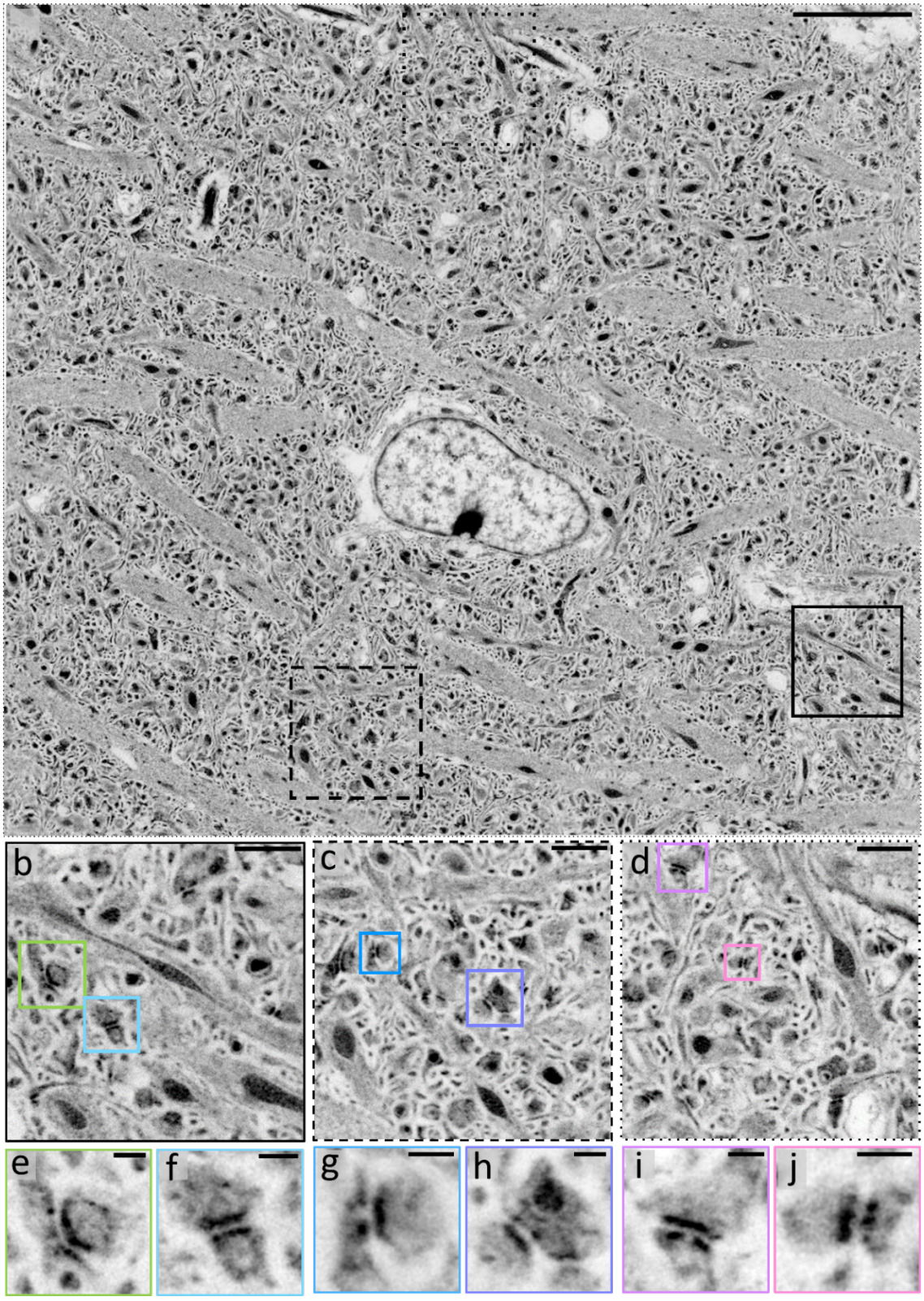
| Ref in text | Fix/Post-fix | ECS + lipid membrane fraction (ECS+) | | | |
|---|---|---|---|---|---|
| | | 100% Otsu | 70% Otsu | 50% Otsu | 30% Otsu |
| *Fix-2* | 4FA /0.7FA+1AAm | 92%± 1% | 84%± 2% | 73%± 3% | 50%± 4% |
| *Fix-3* | 4FA /4FA+20AAm | 75%± 2% | 53%± 2% | 32%± 1% | 12%± 1% |
| *Fix-4* | 4FA+0.1GA /4FA+20AAm | 75%± 5% | 50%± 9% | 29%± 9% | 10%± 6% |
| *Fix-5* | 4FA /AcX | 89%± 2% | 78%± 3% | 64%± 4% | 36%± 4% |
| *Fix-6* | 4FA+20AAm | 79%± 3% | 58%± 5% | 38%± 5% | 14%± 5% |

**Supplementary Figure 13: Effect of fixation and post-fixation on extracellular space (ECS) preservation in expanded mouse brain tissue sections. a**, **k**, **u**, **ee**, **oo**, NHS ester pan-stained neuropil-rich regions in brain tissue fixed with the different indicated fixation schemes. **b**, **l**, **v**, **ff**, **pp**, same areas as in **a**, **k**, **u**, **ee**, and **oo** showing pixels (white) that are excluded from the analysis ($A_{excl.}$). **c**, **m**, **w**, **gg**, **qq**, same areas as in **a**, **k**, **u**, **ee**, and **oo**, respectively, where black pixels represent the areas selected by applying 100% of the Otsu threshold. Here, white

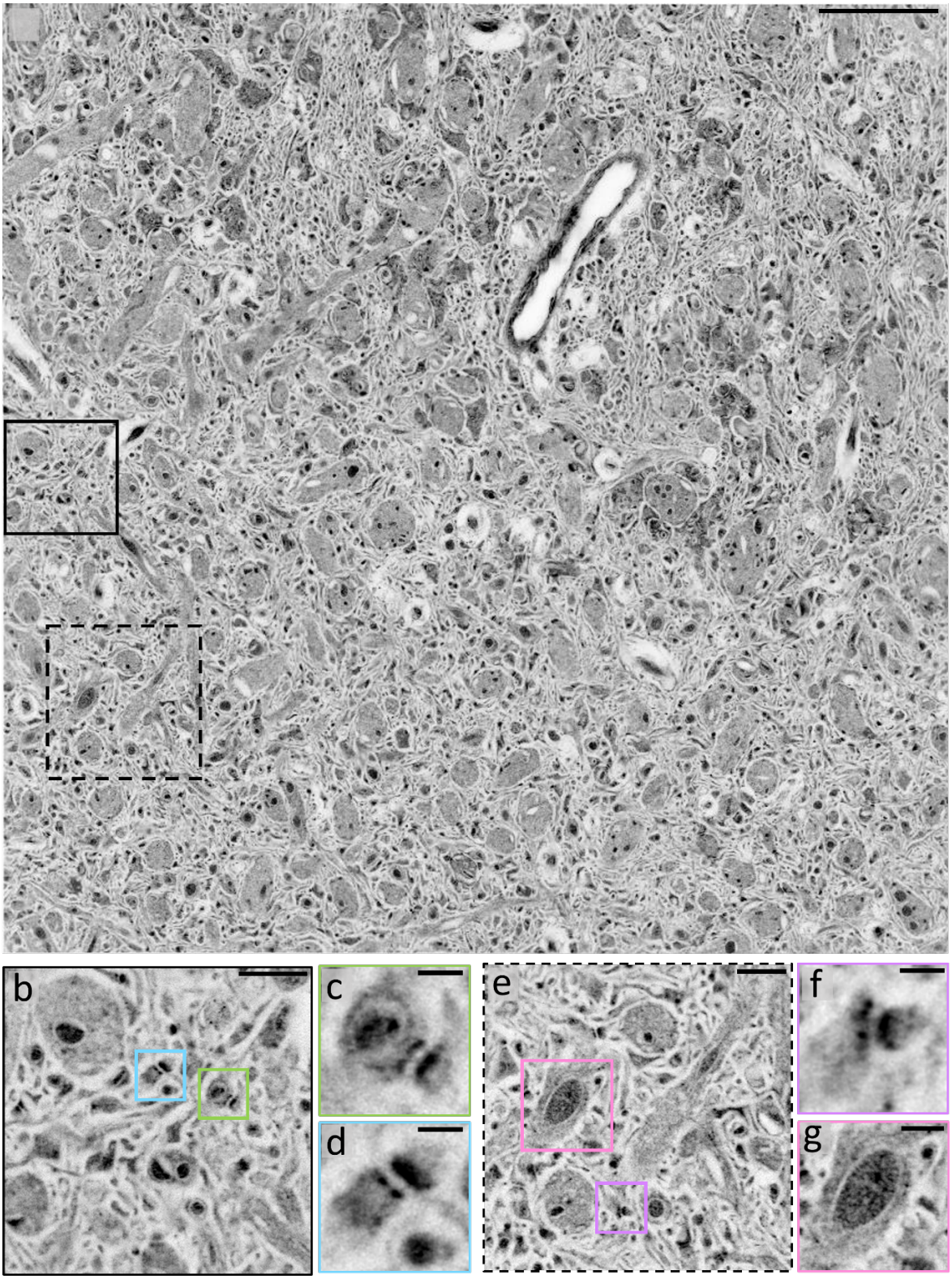
pixels correspond to the uncorrected ECS + lipid membrane fraction ($A_{ECS}$). **d**, **n**, **x**, **hh**, **rr**, overlay of **a**, **k**, **u**, **ee**, **oo** (magenta), **b**, **l**, **v**, **ff**, **pp** (white), and **c**, **m**, **w**, **gg**, **qq** (green), respectively. **e**, **o**, **y**, **ii**, **ss** same areas as in **a**, **k**, **u**, **ee**, **oo**, respectively, where black pixels represent the areas selected by applying 70% of the Otsu threshold. **f**, **p**, **z**, **jj**, **tt** overlay of **a**, **k**, **u**, **ee**, **oo** (magenta), **b**, **l**, **v**, **ff**, **pp** (white), and **e**, **o**, **y**, **ii**, **ss** (green), respectively. **g**, **q**, **aa**, **kk**, **uu**, same areas as in **a**, **k**, **u**, **ee**, and **oo**, respectively, where black pixels represent the areas selected by applying 50% of the Otsu threshold. **h**, **r**, **bb**, **ll**, **vv**, overlay of **a**, **k**, **u**, **ee**, **oo** (magenta), **b**, **l**, **v**, **ff**, **pp** (white), and **g**, **q**, **aa**, **kk**, **uu** (green), respectively. **i**, **s**, **cc**, **mm**, **ww**, same areas as in **a**, **k**, **u**, **ee**, and **oo**, respectively, where black pixels represent the areas selected by applying 30% of the Otsu threshold. **j**, **t**, **dd**, **nn**, **xx**, overlay of **a**, **k**, **u**, **ee**, **oo** (magenta), **b**, **l**, **v**, **ff**, **pp** (white), and **i**, **s**, **cc**, **mm**, **ww** (green), respectively. **yy**, table summarizing the corrected ECS + lipid membrane (ECS+) values obtained by dividing $A_{ECS}$ by ($A_{total}$-$A_{excl.}$), where $A_{total}$ is the total field of view area (Fix-2: n = 8 FOVs from N = 1 independent experiment; Fix-3: n = 8 FOVs from N = 1 independent experiment; Fix-4: n = 8 FOVs from N = 1 independent experiment; Fix-5: n = 8 FOVs from N = 1 independent experiment; Fix-6: n = 14 FOVs from N = 3 independent experiments). Values in pink report the chosen ECS+ values for this comparison. Scale bars are corrected for the expansion factor (**a**, **b**, **k**, **l**, **u**, **v**, **ee**, **ff**, **oo**, **pp**) 3 μm.



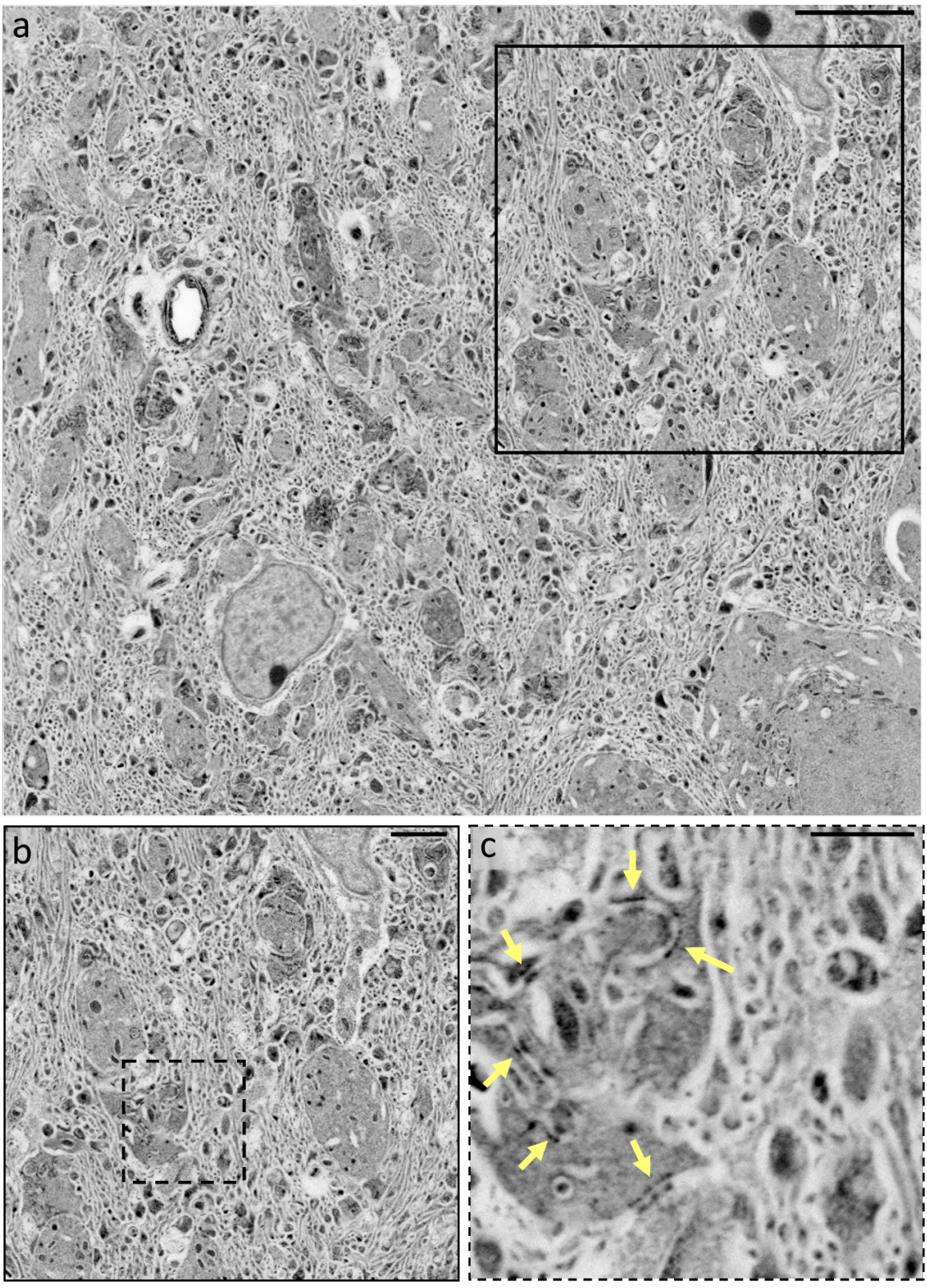

**Supplementary Figure 14: Effect of denaturation time on expansion factor and protein retention in expanded mouse brain tissue sections. a**, NHS ester pan-stained brain tissue denatured for 4 h. **b**, magnified view of the area outlined in the pink box in **a**. **c**, magnified view of the area outlined in the lavender box in **a**. **d**, NHS ester pan-stained brain tissue denatured for 6 h. **b**, magnified view of the area outlined in the pink box in **d**. **e**, magnified view of the area outlined in the lavender box in **d**. **g**, NHS ester pan-stained brain tissue denatured for 8 h. **h**, magnified view of the area outlined in the pink box in **g**. **i**, magnified view of the area outlined in the lavender box in **g**. **j,** plot of expansion factors (4 h: n = 50 measurements from 3 FOVs; 6 h: n = 42 measurements from 3 FOVs; 8 h: n = 100 from 3 FOVs). **k**, relative protein retention was measured by comparing the peak intensity of dense projection (DP) NHS ester signal (4 h: n = 50 measurements from 3 FOVs; 6 h: n = 42 measurements from 3 FOVs; 8 h: 48 measurements from 3 FOVs). Images were processed with a gamma value ɣ=0.8. Black scale bars are corrected for the expansion factor (**a**, **d**, **g**) 2 µm, (**c**, **d**, **e**, **f**, **h**, **i**) 200 nm.



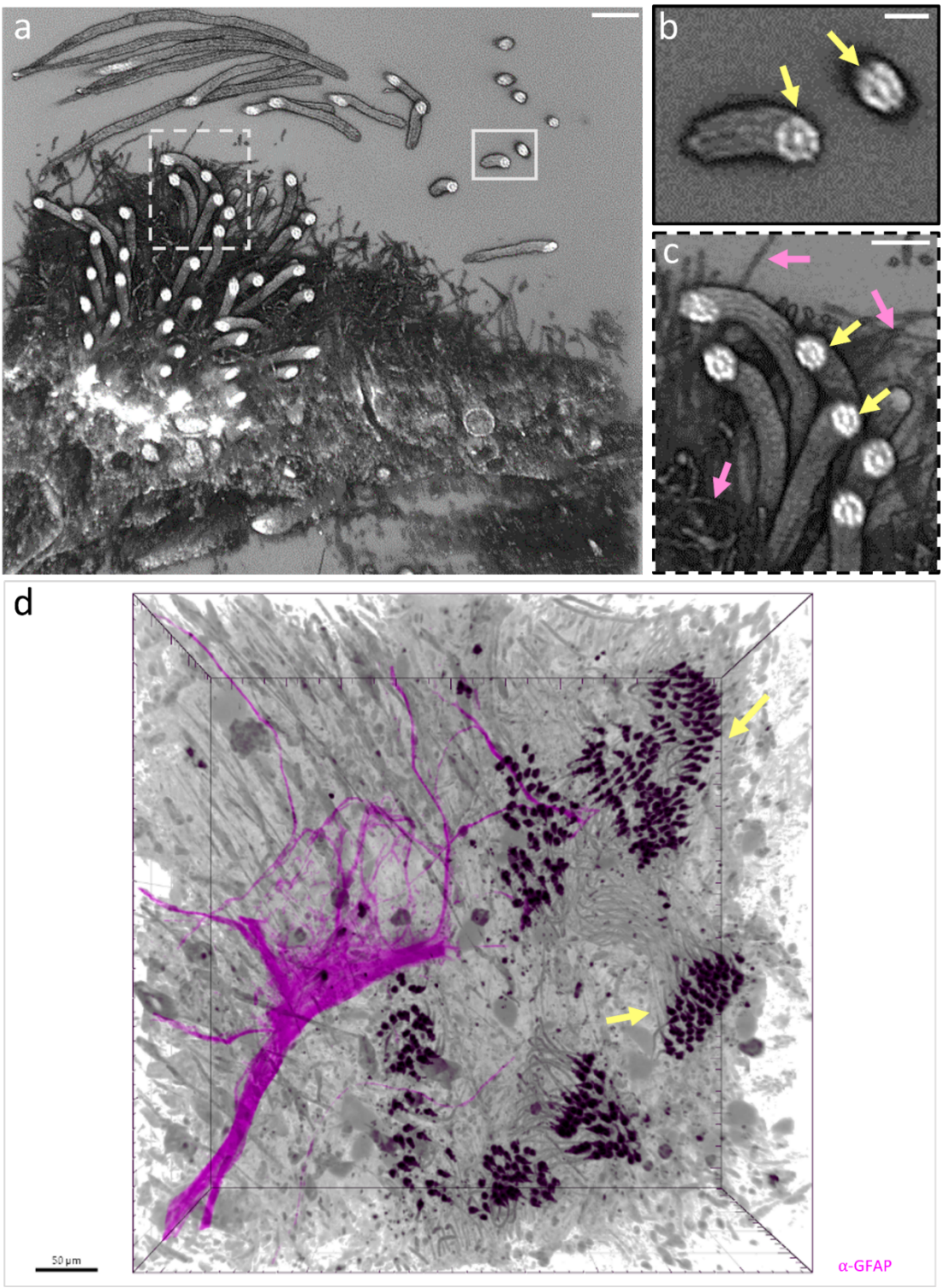

**Supplementary Figure 15: pan-ExM-t reveals mouse brain tissue ultrastructure (overview 1). a**, NHS ester pan-stained tissue section in the mouse hippocampus. **b-d**, magnified areas in the solid, dashed, and dotted black boxes in **a**, respectively, showing neuropil. **e**, **f**, magnified areas in the lime and light blue boxes in **b**, respectively, showing synapses. **g**, **h**, magnified areas in the blue and orchid boxes in **c**, respectively, showing synapses. **i**, **j**, magnified areas in the lavender and pink boxes in **d**, respectively, showing synapses. Images were acquired with a 25X/0.95 NA water objective. Images were processed with a gamma value ɣ=0.8. Black scale bars are corrected for the expansion factor (**a**) 5 µm, (**b-d**) 1 µm, (**e-j**) 200 nm.



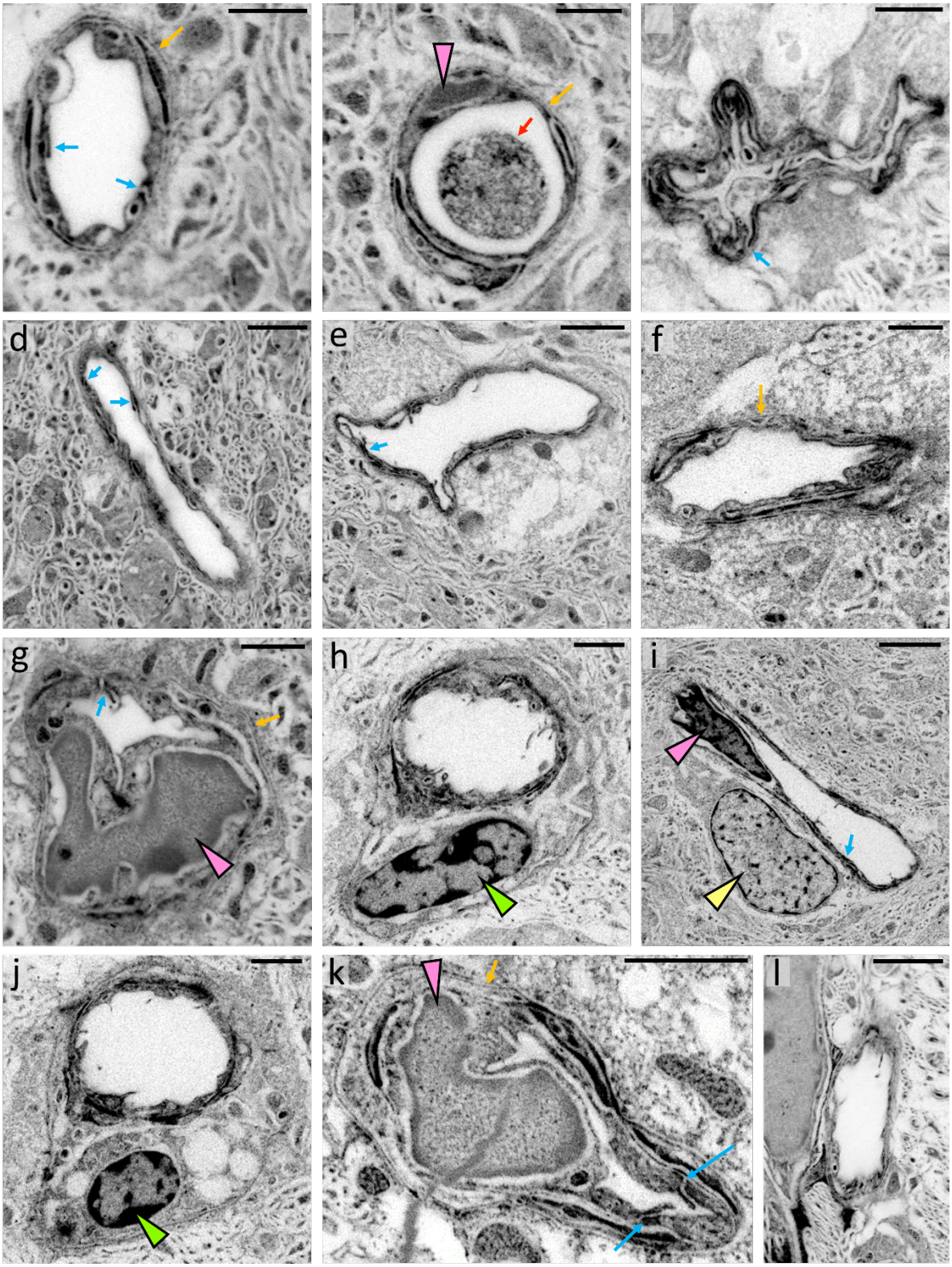

**Supplementary Figure 16: pan-ExM-t reveals mouse brain tissue ultrastructure (overview 2). a**, NHS ester pan-stained tissue section in the mouse cortex. **b**, **e**, magnified areas in the solid and dashed black boxes in **a**, respectively, showing neuropil. **c**, **d**, magnified areas in the lime and light blue boxes in **b**, respectively, showing synapses. **f**, **g**, magnified areas in the lavender and pink boxes in **e** showing a synapse and mitochondrion, respectively. Images were acquired with a 25X/0.95 NA water objective. Images were processed with a gamma value ɣ=0.7. Black scale bars are corrected for the expansion factor (**a**) 5 µm, (**b**, **e**) 1 µm, (**c**, **d**, **f**) 200 nm, (**g**) 500 nm.



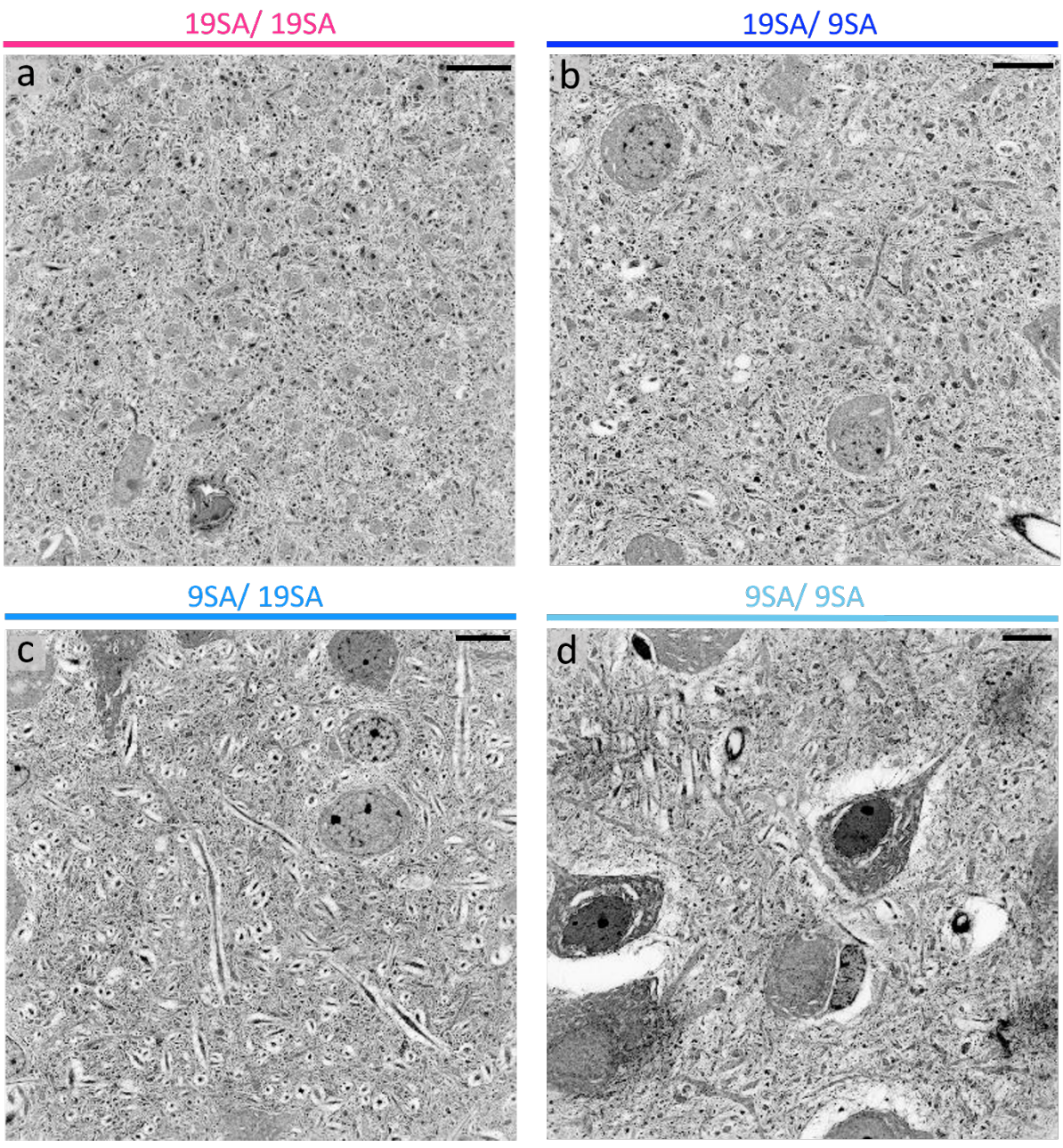

**Supplementary Figure 17: pan-ExM-t reveals mouse brain tissue ultrastructure (overview 3). a**, NHS ester pan-stained tissue section in the mouse cortex. **b**, magnified area in the black boxes in **a** showing neuropil. **c**, magnified area in the dotted black box in **b** showing multiple putative synapses (yellow arrows). Images were acquired with a 25X/0.95 NA water objective. Images were processed with a gamma value ɣ=0.7. Black scale bars are corrected for the expansion factor (**a**) 5 µm, (**b**) 2 µm, (**c**) 1 µm.



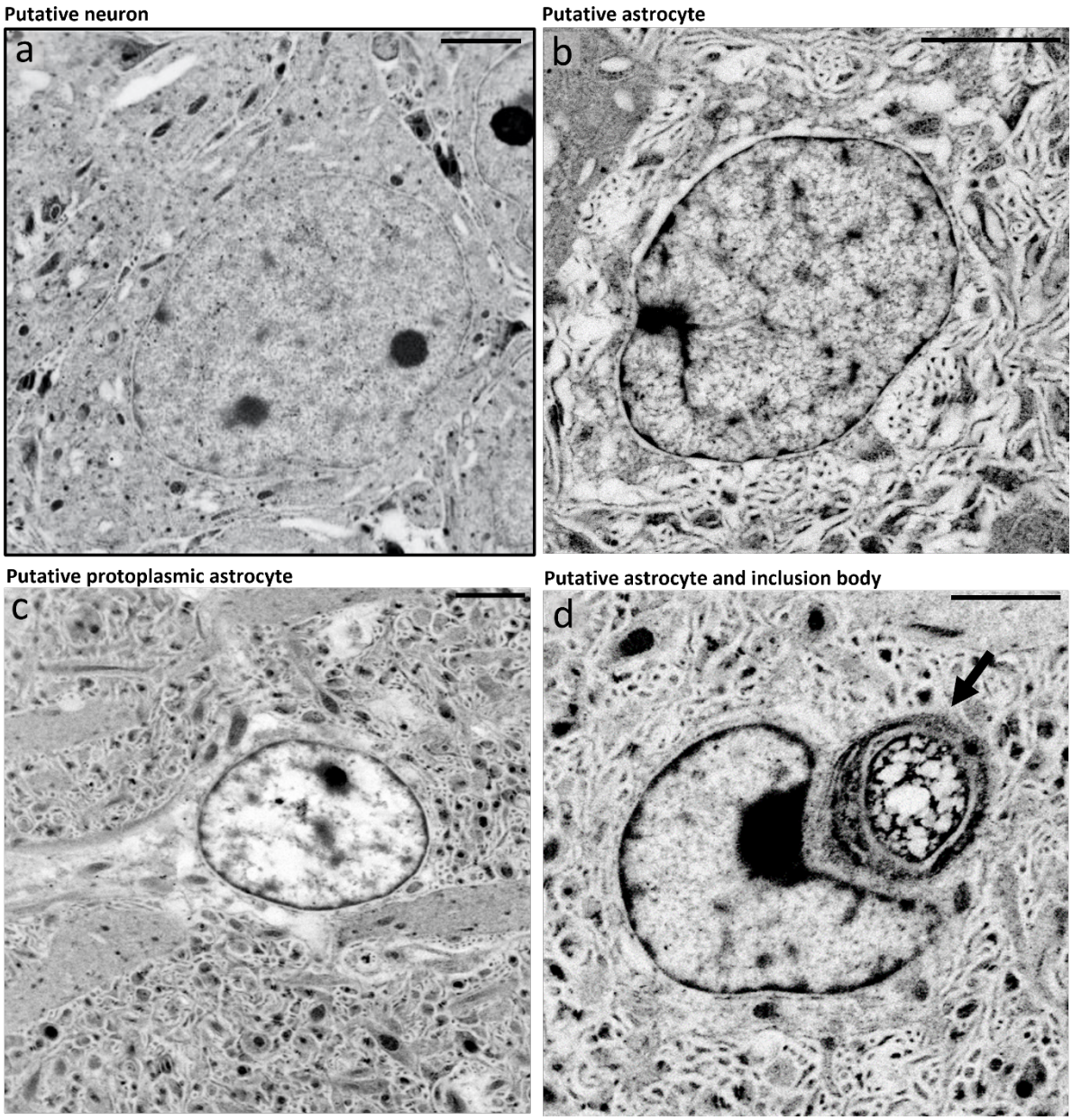

**Supplementary Figure 18: Multiciliated ependymal epithelia lining the lateral ventricles of the mouse brain**. **a**, 3D rendering of NHS ester pan-stained ependymal epithelia showing multiple cilia. **b**, **c**, magnified areas in the solid and dashed gray boxes in **a**, respectively, showing cilia with visible nine-fold microtubule symmetry (yellow arrows) and filopodia-like structures (pink arrows). **d**, 3D rendering of NHS ester pan-stained multi-ciliated ependymal epithelia (grayscale) and anti-GFAP immunolabeling (magenta). Yellow arrows point to cilia. 3D image processing details are described in the **Methods** section. Note that sample **a** was processed with *Fix-2* (4% FA fix and 0.7% FA + 1% AAm postfix). Image **a** was acquired with a 63X/1.2 NA water objective and image **d** was acquired with a 25X/0.95 NA water objective. Black scale bars are corrected for the expansion factor, (**a**, **d**) 1 µm, (**b**) 200 nm, (**c**) 400 nm.



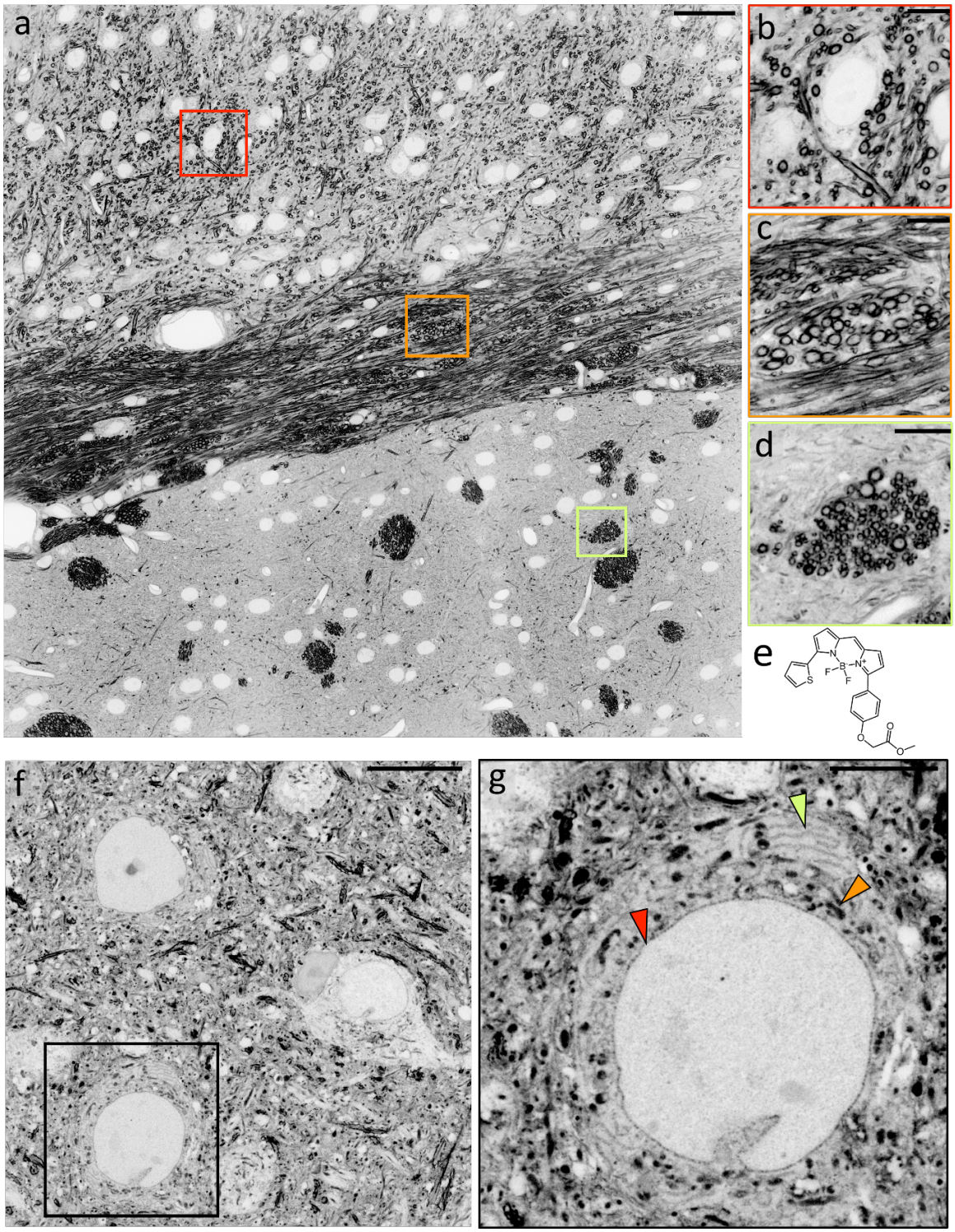

**Supplementary Figure 19: Gallery of mouse brain capillaries**. **a-l**, NHS ester pan-stained brain capillaries. Blue arrows point to tight junctions. Red arrow in **b** points to an erythrocyte. Tangerine arrow points to the basement membrane. Pink arrowheads in **b**, **g**, and **k** point to epithelial cell nuclei. Lime arrowheads in **h** and **j** point to pericyte nuclei. Yellow arrowhead in **i** points to a perivascular glial cell. All images were acquired with a 20X/0.95 NA water objective except for **f** and **k** which were acquired with a 86X/1.2 NA water objective. Images **a**, **b**, **c**, **d**, **e**, **g**, **i**, **j**, **k**, **l** were processed with a gamma value ɣ=0.7 and image **f** with ɣ=0.5. Black scale bars are corrected for the expansion factor, (**a**, **b**, **c**, **f**, **g**, **j**, **k**, **l**) 1 µm, (**d**, **e**, **i**) 2 µm.


19SA/ 19SA
19SA/ 9SA
a
b
9SA/ 19SA
9SA/ 9SA
c
d
e
****
***
****
Linear expansion factor
30
25
20
15
10
5
0
19SA /19SA
19SA /9SA
9SA /19SA
9SA /9SA

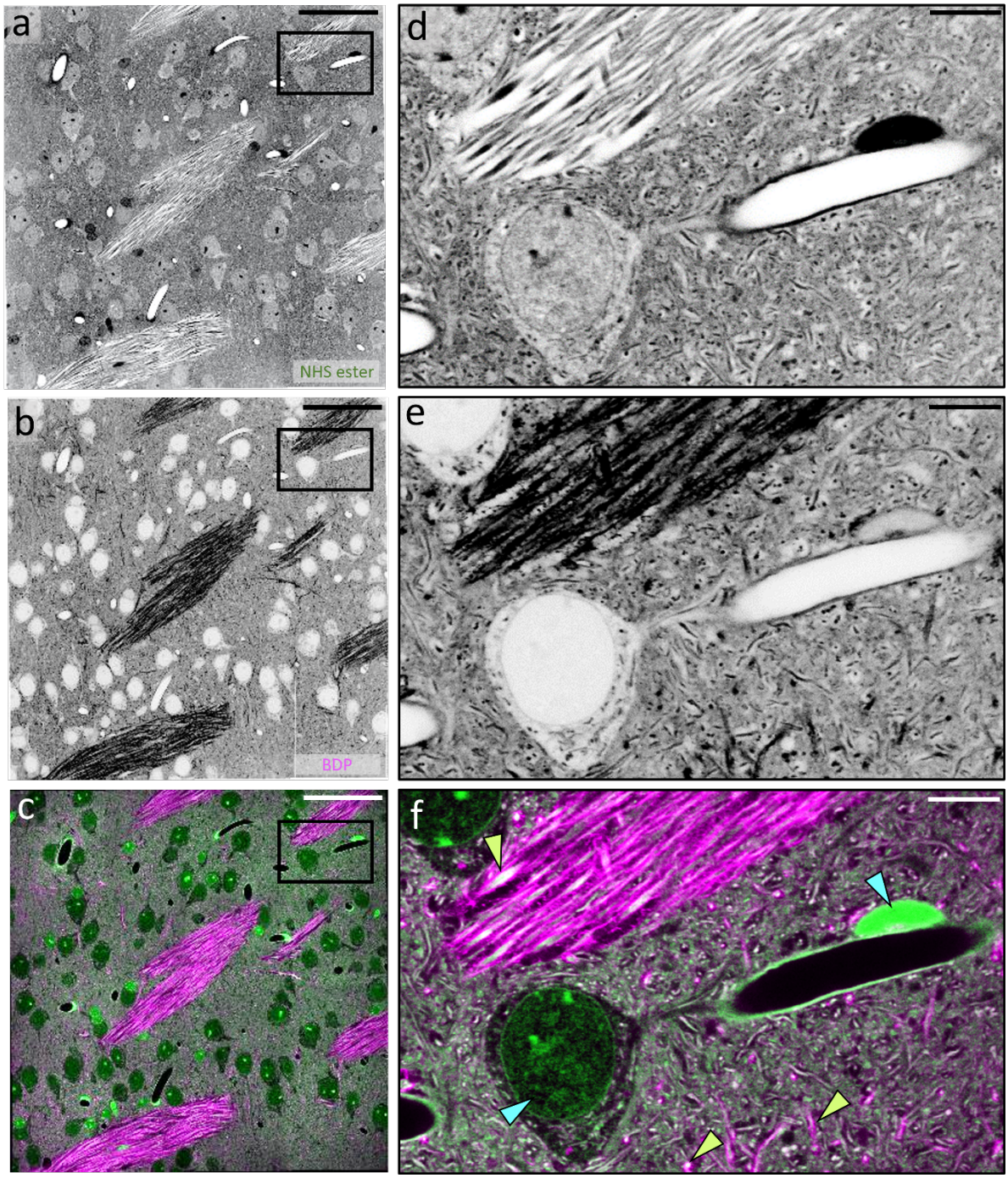
**Supplementary Figure 20: Effect of sodium acrylate (SA) monomer concentration on expanded mouse brain tissue integrity. a**, NHS ester pan-stained brain tissue gelled with 1st expansion gel monomer solution containing 19% (w/v) SA and 2nd expansion gel monomer gel monomer solution containing 19% (w/v) SA. **b**, NHS ester pan-stained brain tissue gelled with 1st expansion gel monomer solution containing 19% (w/v) SA and 2nd expansion gel monomer gel monomer solution containing 9% (w/v) SA. **c**, NHS ester pan-stained brain tissue gelled with 1st expansion gel monomer solution containing 9% (w/v) SA and 2nd expansion gel monomer gel monomer solution containing 19% (w/v) SA. **d**, NHS ester pan-stained brain tissue gelled with 1st expansion gel monomer solution containing 9% (w/v) SA and 2nd expansion gel monomer gel monomer solution containing 9% (w/v) SA. **a-c** show neuropil and cell bodies with satisfactory preservation, while **d** shows detached cell bodies and distorted neuropil. **e**, Plot of expansion factors (19SA/ 19SA: n = 254 measurements from 10 FOVs from 3 independent experiments; 19SA/ 9SA: n = 267 measurements from 12 FOVs from 2 independent experiments; 9SA/ 19SA: n = 88 measurements from 6 FOVs from 2 independent experiments; 9SA/ 9SA: n = 86 measurements from 2 independent experiments). Images were processed with a gamma value ɣ=0.7. Black scale bars are corrected for the expansion factor (**a-d**) 5 µm.



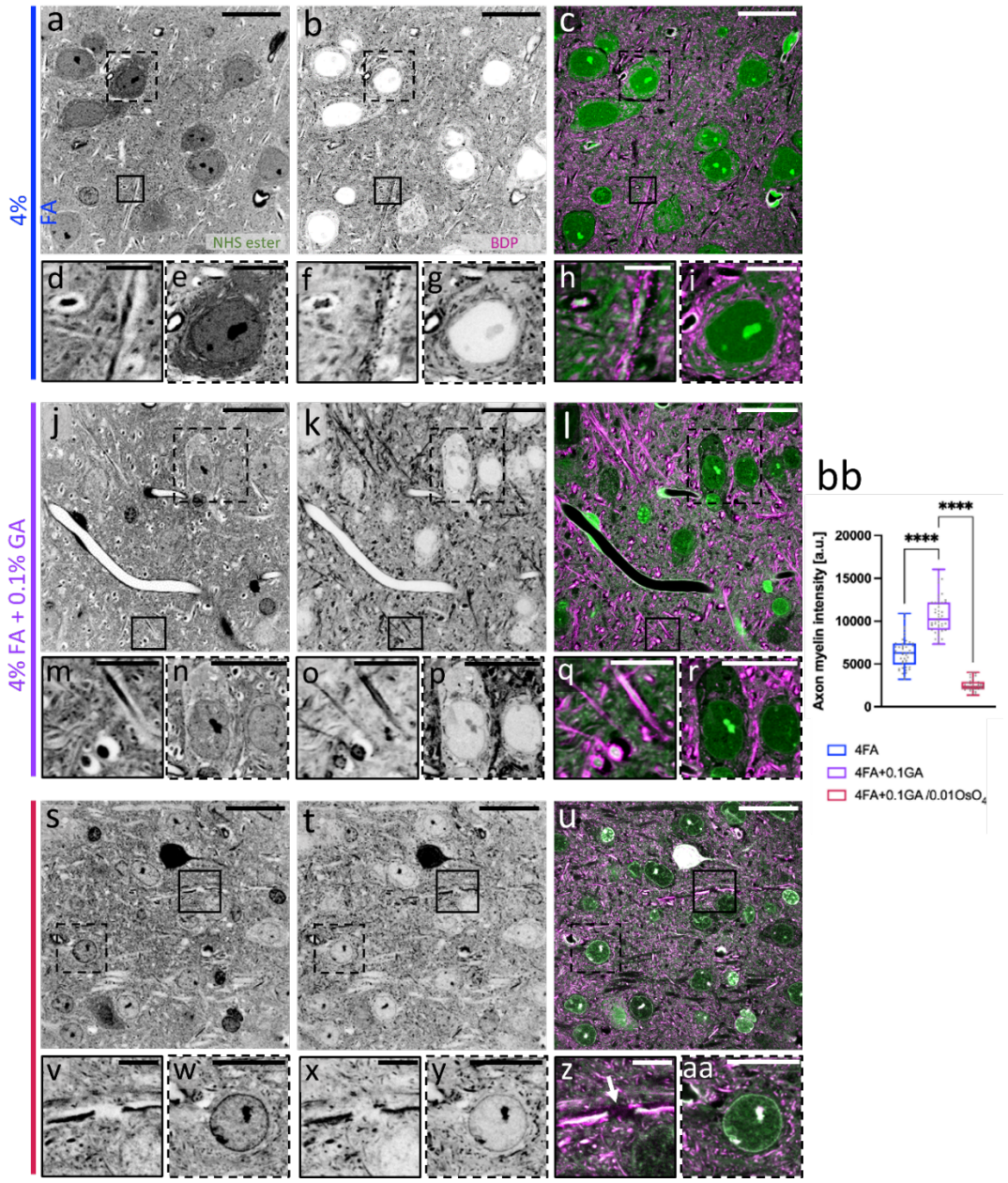

**Supplementary Figure 21: Astrocytes and neurons exhibit distinct NHS ester pan-staining patterns. a**, NHS ester pan-stained putative neuron showing a homogenous nuclear chromatin pattern. **b**, NHS ester pan-stained putative astrocyte showing a heterogeneous nuclear chromatin pattern and an irregular cytoplasm. **c**, NHS ester pan-stained putative protoplasmic astrocyte showing a pale nucleus with patches of chromatin, a pale cytoplasm, and triangular projections. **d**, NHS ester pan-stained putative astrocyte showing a heterogenous nuclear chromatin pattern, irregular cytoplasm, and an inclusion body (arrow). All images were processed with a gamma value of $\gamma$=0.7 Scale bars corrected for the expansion factor (**a-d**) 2 μm.



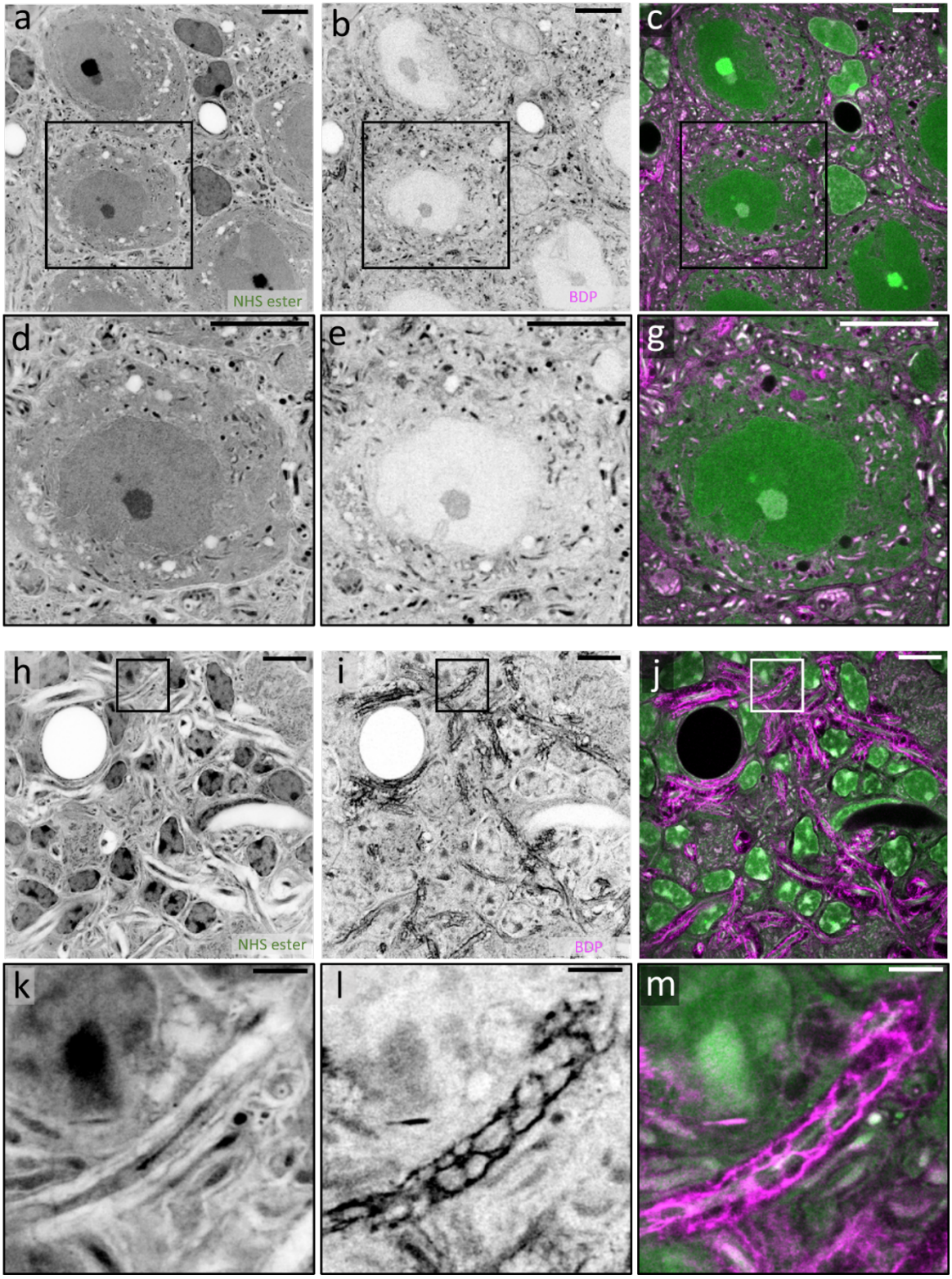

**Supplementary Figure 22: BODIPY-TR-Methyl Ester (BDP) pan-staining reveals lipophilic components in 4-fold expanded mouse brain tissue sections. a**, tiled image of a BDP pan-stained tissue section expanded ~4-fold. **b-d**, magnified images of the areas outlined by the red, orange, and lime boxes in **a**, showing highly pan-stained myelinated axons in top and lateral views. **e**, chemical structure of BODIPY-TR-Methyl Ester. **f**, BDP pan-stained tissue section expanded ~4-fold showing neurons. **g**, magnified image of the area outlined by the black box in **f** showing the nuclear envelope (red arrow), the endoplasmic reticulum (orange arrow), and mitochondria (lime arrow). Scale bars are not corrected for the expansion factor. (**a**) 100 µm, (**b-d**) 20 µm, (**f**) 50 µm, (**g**) 20 µm.



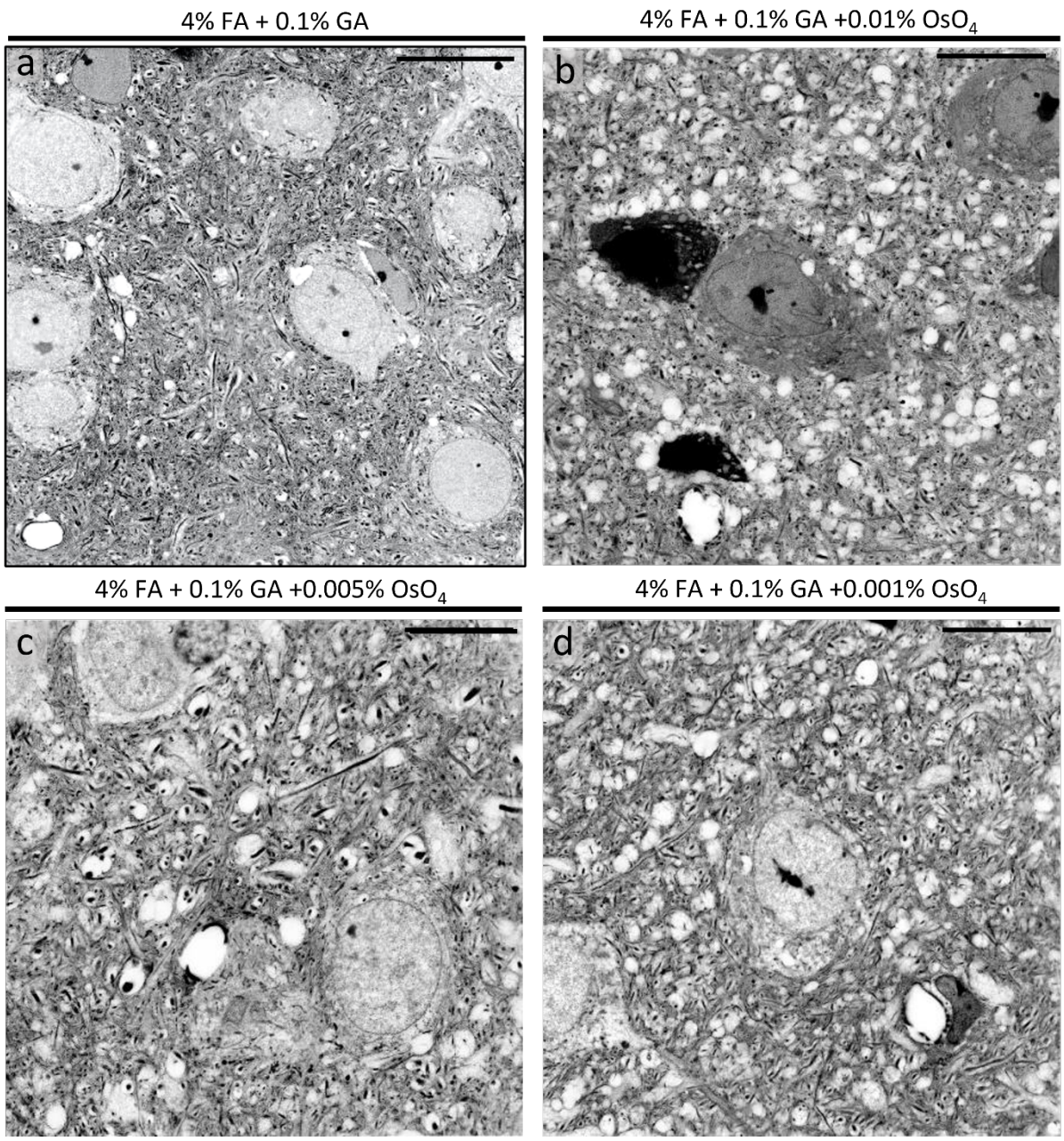

**Supplementary Figure 23: BODIPY-TR-Methyl Ester (BDP) and hydrophilic NHS ester differential pan-staining in a 4-fold expanded mouse brain tissue section. a**, tiled image of an NHS ester pan-stained tissue section expanded ~4-fold. **b**, BDP pan-staining corresponding to area shown in **a**. **c**, overlay of **a** and **b**. **d-f**, magnified images of the areas outlined by the black boxes in **a-c**. Lime arrows point to myelin in axons, cyan arrows point to nuclei stained exclusively by NHS ester. Scale bars are not corrected for the expansion factor. (**a-c**) 200 µm, (**d-f**) 20 µm.



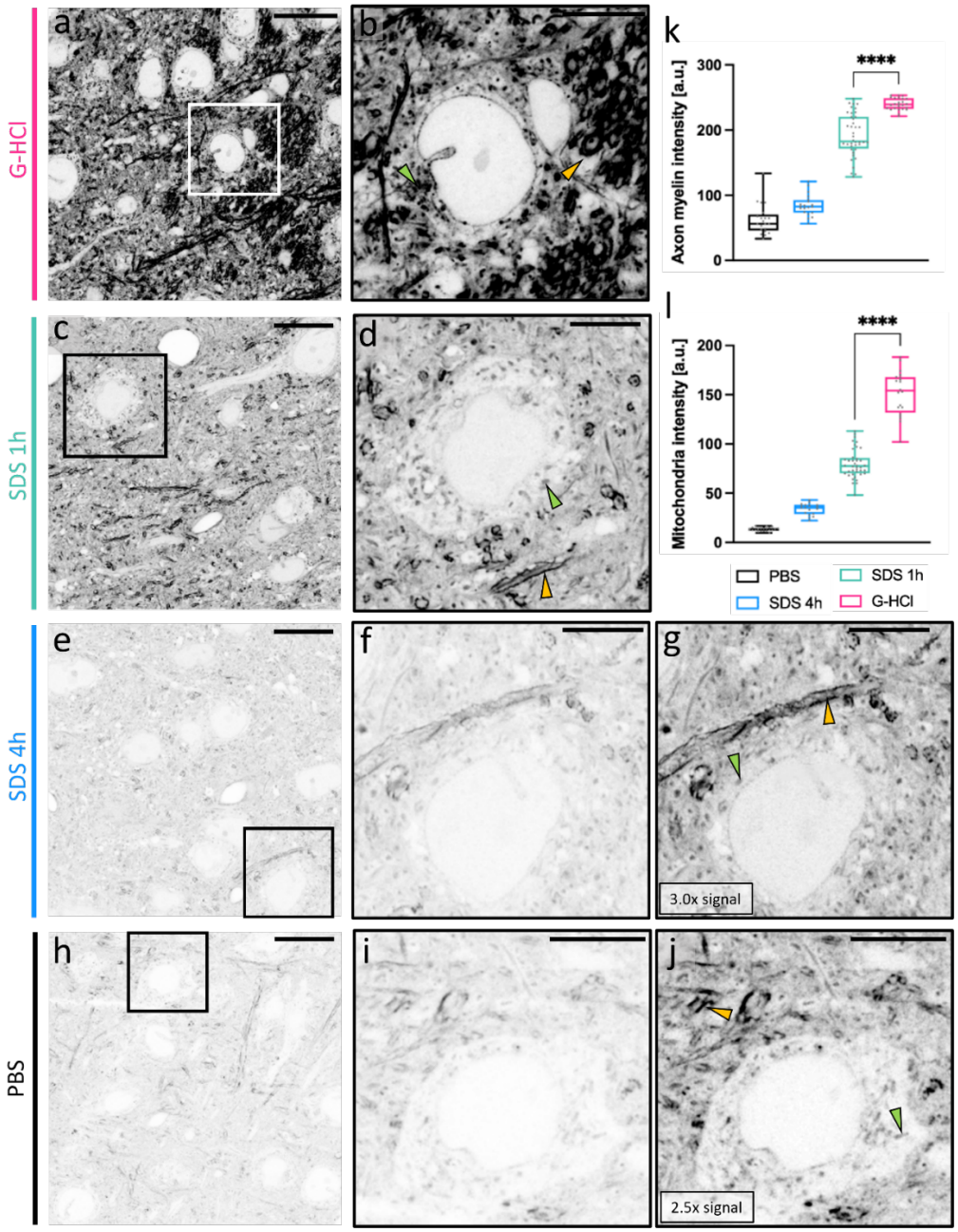

**Supplementary Figure 24: Effect of fixation on BODIPY-TR-Methyl Ester (BDP) pan-staining in 4-fold expanded mouse brain tissue sections. a**, NHS ester pan-stained tissue section expanded ~4-fold fixed with 4% FA. **b**, BDP pan-staining of the same area shown in **a**. **c**, overlay. **d**, **f**, **h**, magnified images of the areas outlined by the black boxes in **a**, **b**, and **c**, respectively, showing myelinated axons. **e**, **g**, **i**, magnified images of the areas outlined by the dashed black boxes in **a**, **b**, and **c**, respectively, showing a cell body. **j**, NHS ester pan-stained tissue section expanded ~4-fold fixed with 4% FA + 0.1% GA. **k**, BDP pan-staining of the same area shown in **j**. **l**, overlay. **m**, **o**, **q**, magnified images of the areas outlined by the black boxes in **j**, **k**, and **l**, respectively, showing myelinated axons. **n**, **p**, **r**, magnified images of the areas outlined by the dashed black boxes in **j**, **k**, and **l**, respectively, showing a cell body. **s**, NHS ester pan-stained tissue section expanded ~4-fold fixed with 4% FA. **t**, BDP pan-staining of the same area shown in **s**. **u**, overlay. **v**, **x**, **z**, magnified images of the areas outlined by the black boxes in **s**, **t**, and **u**, respectively, showing myelinated axons. **w**, **y**, **aa** magnified images of the areas outlined by the dashed black boxes in **s**, **t**, and **u**, respectively, showing a cell body. **bb**, plot comparing axon myelin BDP intensity across the indicated fixation conditions (4% FA: n = 46 measurements from 5 FOVs; 4% FA + 0.1% GA: n = 46 measurements from 5 FOVs; 4% FA + 0.1% GA + 0.01 % $OsO_4$: n = 38 measurements from 5 FOVs). ****: $p<0.0001$. Scale bars are not corrected for the expansion factor. (**a-c**, **j-l**, **s-u**), 100 µm, (**d**, **f**, **h**, **m**, **o**, **q**, **v**, **x**, **z**) 20 µm, (**e**, **g**, **h**, **n**, **p**, **r**, **w**, **y**, **aa**) 50 µm.



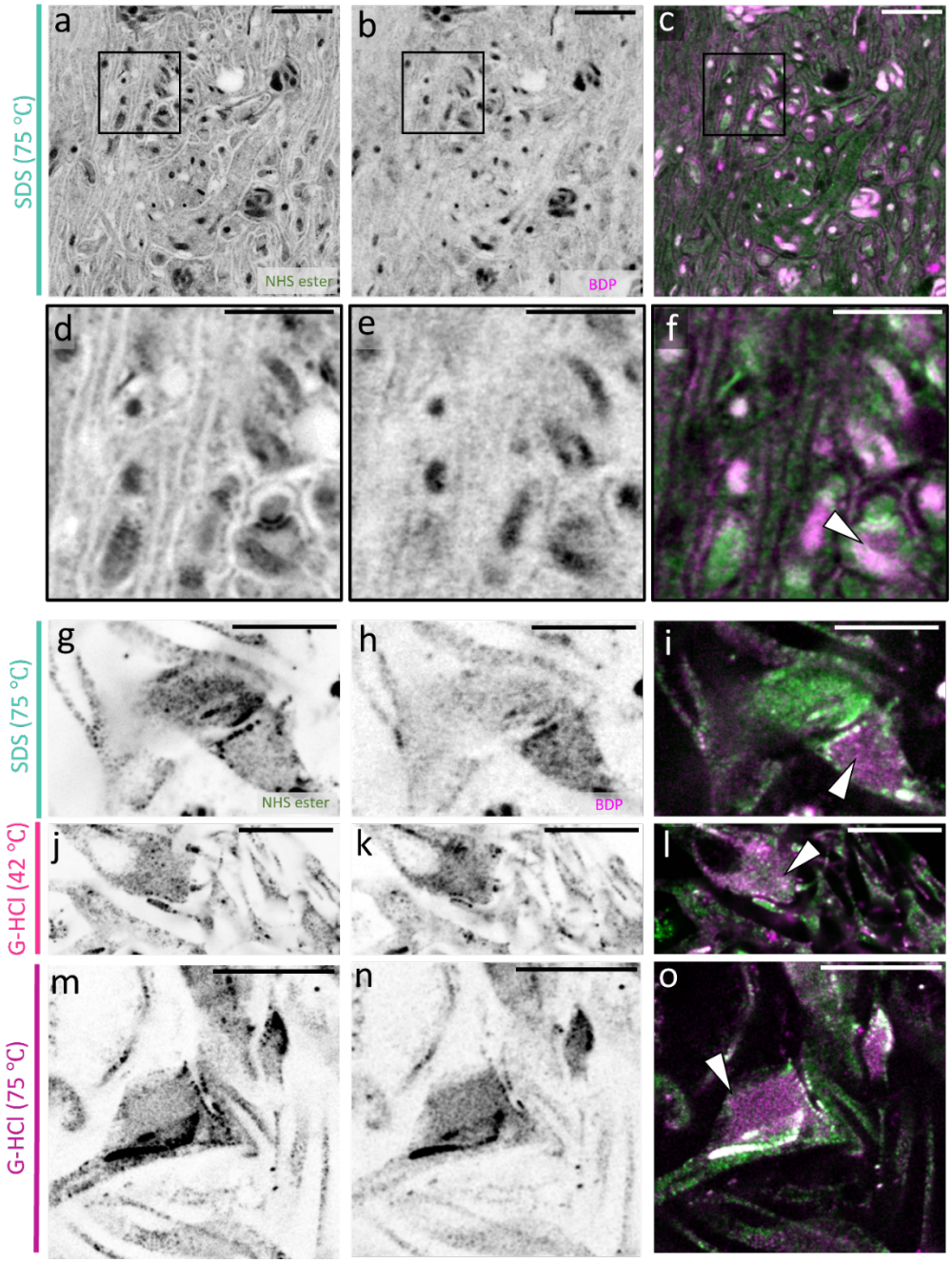

**Supplementary Figure 25: BODIPY-TR-Methyl Ester (BDP) and hydrophilic NHS ester differential pan-staining in pan-ExM-t expanded mouse brain tissue sections. a**, NHS ester pan-stained tissue section fixed with 4% FA + 0.1% GA and expanded 13-fold showing neuron somas. **b**, BDP pan-staining corresponding to area shown in **a**. **c**, overlay of **a** and **b**. **d-g,** magnified images of the areas outlined by the boxes in **a-c**. **h**, NHS ester pan-stained tissue section fixed with 4% FA + 0.1% GA and expanded 13-fold showing myelinated axons. **i**, BDP pan-staining corresponding to area shown in **h. j**, overlay of **h** and **i. k-m**, magnified images of the areas outlined by the boxes in **h-j**. Scale bars are corrected for the expansion factor. (**a-j**) 5 µm, (**k-m**) 1 µm.



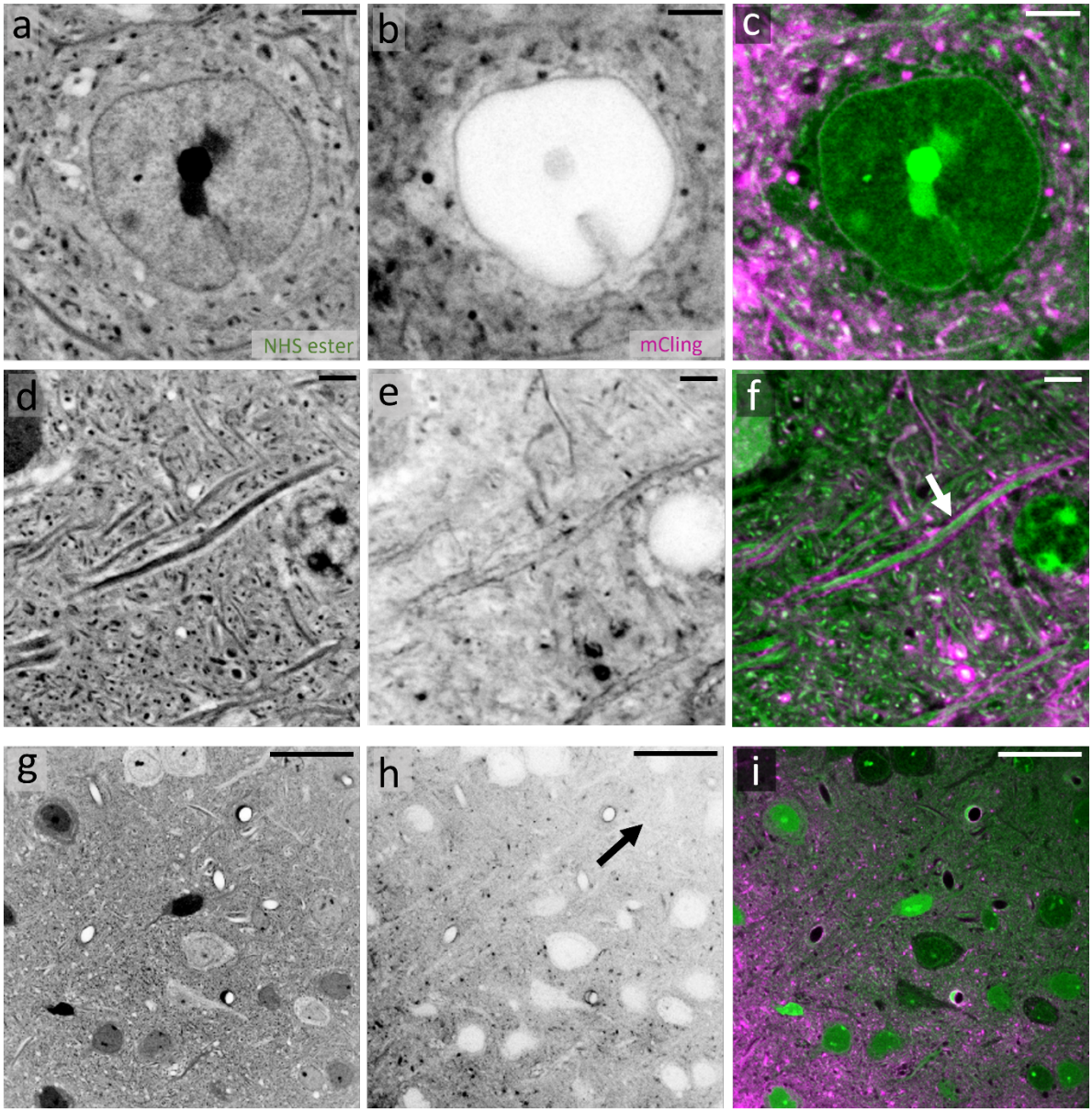

**Supplementary Figure 26: Effect of osmification on pan-ExM-t expanded brain tissue integrity. a**, NHS ester pan-stained brain tissue fixed with 4% FA + 0.1% GA. **b**, NHS ester pan-stained brain tissue fixed with 4% FA + 0.1% GA + 0.01% $OsO_4$. **c**, NHS ester pan-stained brain tissue fixed with 4% FA + 0.1% GA + 0.005% $OsO_4$. **d**, NHS ester pan-stained brain tissue fixed with 4% FA + 0.1% GA + 0.001% $OsO_4$. Very dark neuron perikarya (**a**) and multiple tissue perforations (**b-d**) appear to be artifactual. Images **b-d** were processed with a gamma value $\gamma$=0.7. Scale bars are not corrected for the expansion factor (**a-d**) 200 µm.



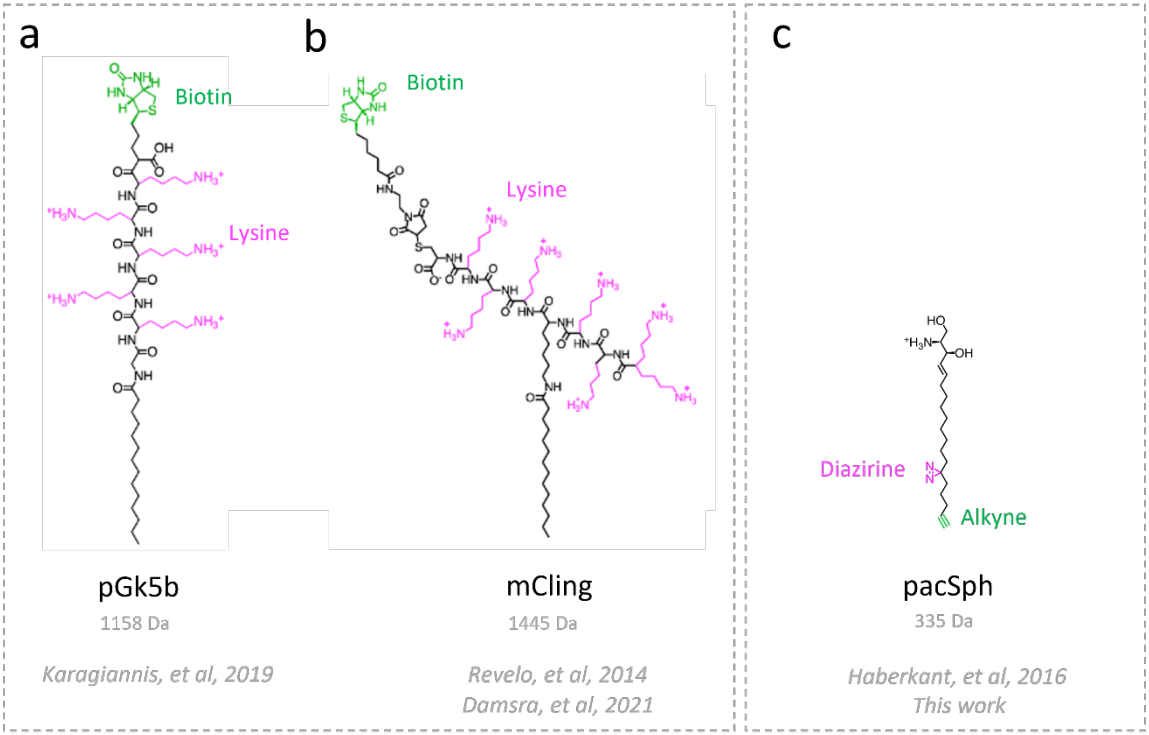

**Supplementary Figure 27: BODIPY-TR-Methyl Ester (BDP) signal is higher in G-HCl-denatured than in SDS- and non-denatured ~4-fold expanded mouse brain tissue sections. a,** BDP pan-stained tissue section denatured with G-HCl. **b**, magnified image of the area outlined by the black box in **a**. **c**, BDP pan-stained tissue section denatured with SDS for 1 h. **d**, magnified image of the area outlined by the black box in **c**. **e**, BDP pan-stained tissue section denatured with SDS for 4 h. **f**, magnified image of the area outlined by the black box in **e**. **g**, same area as in **f** with signal increased 2.5-fold. **e**, BDP pan-stained tissue section non-denatured. **i**, magnified image of the area outlined by the white box in **h**. **j**, Same area as in **I** with signal increased 3-fold. Samples in **a-j** were all expanded ~4-fold. Orange arrows point to myelinated axons. Green arrows point to mitochondria in neuron somas. **k**, comparison of BDP intensities in axons across different denaturation conditions (PBS: n = 41 measurements, N = 2 FOVs; SDS 4h: n = 20 measurements, N = 1 FOV; SDS 1h: n = 40 measurements, N = 4 FOVs; G-HCl: n = 24 measurements, N = 1 FOV). **l**, comparison of BDP intensities in mitochondria across different denaturation conditions (PBS: : n = 41 measurements, N = 2 FOVs; SDS 4h: n = 18 measurements, N = 1 FOV; SDS 1h: n = 40 measurements, N = 4 FOVs; G-HCl: n = 20 measurements, N = 1 FOV). Means ± standard deviations are reported. An ANOVA with post-hoc Tukey test was used to analyze the data. ****: $p<0.0001$. Scale bars are not corrected for the expansion factor. (**a**, **c**, **e**, **h**) 50 µm, (**b**, **d**, **f**, **g**, **i**, **j**) 20 µm .



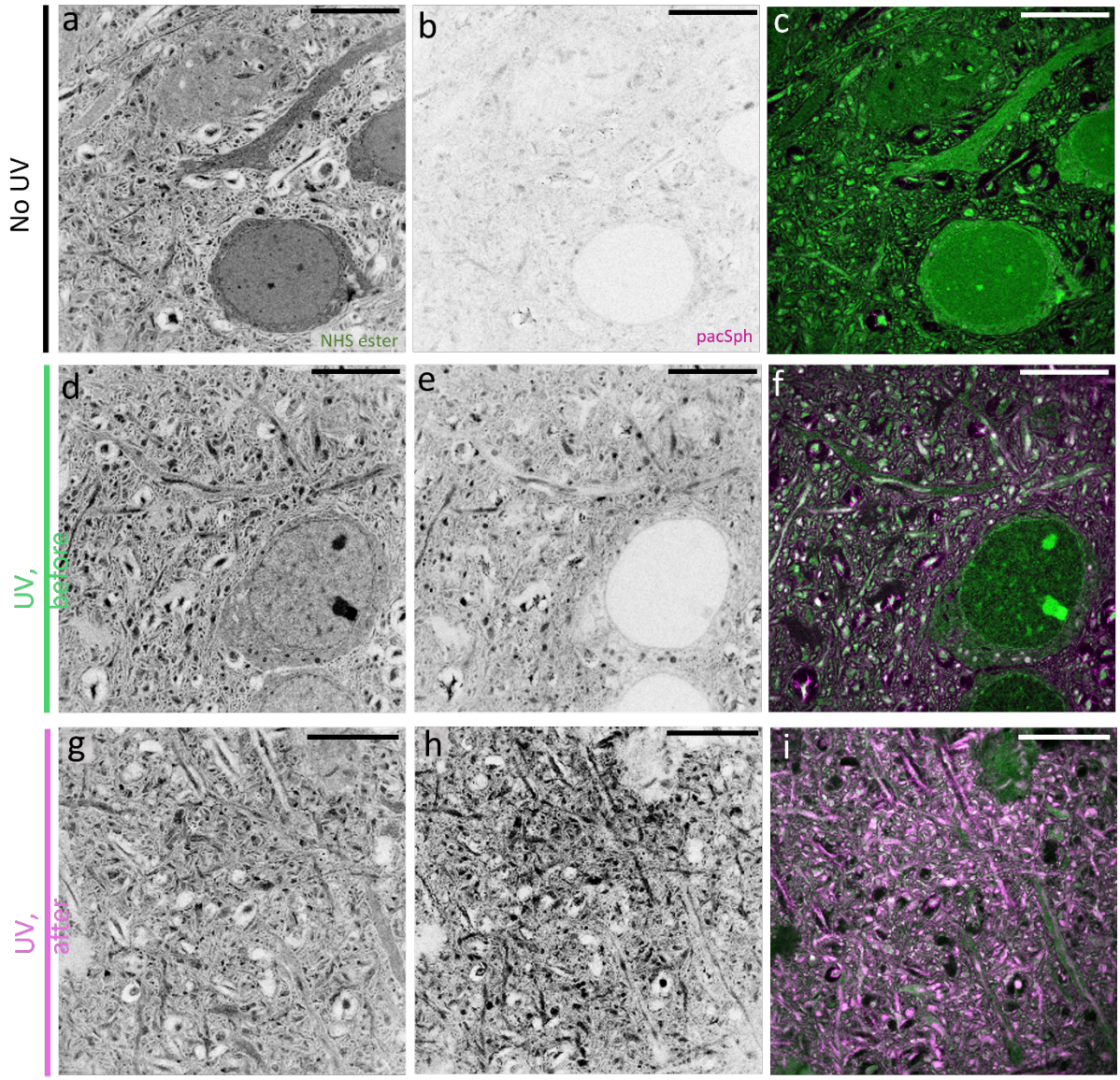

**Supplementary Figure 28: BODIPY-TR-Methyl Ester (BDP) does not label neurite boundaries specifically.** **a**, NHS ester pan-stained tissue section fixed with 4% FA + 0.1% GA and denatured with SDS. **b**, BDP pan-staining of the same area as in **a**. **c**, overlay of **a** and **b**. **d-f**, magnified images of the areas outlined by the black boxes in **a-c** showing BDP pan-stained mitochondria, including a mitochondrion in a synapse (white arrow). **g**, NHS ester pan-stained synapse in a dissociated neuron sample fixed with 3% FA + 0.1% GA and denatured with SDS at 75°C. **h**, BDP pan-staining of the same area as in **g**. **i**, overlay of **g** and **h**. **j**, NHS ester pan-stained synapse in a dissociated neuron sample fixed with 3% FA + 0.1% GA and denatured with guanidium hydrochloride (G-HCl) at 42°C. **k**, BDP pan-staining of the same area as in **j**. **l**, overlay of **j** and **k**. **m-o**, same as **j-l** but in a dissociated neuron sample denatured with G-HCl at 75°C. White arrows in **i**, **l**, and **o** point at the presynaptic bouton which is differentially pan-stained with BDP. It is worth noting that BDP does not appear to stain cellular membranes at the boundary of neurites regardless of whether the detergent SDS is used. BDP however appears to stain hydrophobic compartments such as mitochondria and the presynaptic compartment (likely because of the abundance of synaptic vesicles). Scale bars are not corrected for the expansion factor. (**a-c**) 20 µm, (**d-f**) 10 µm, (**g-o**) 20 µm.



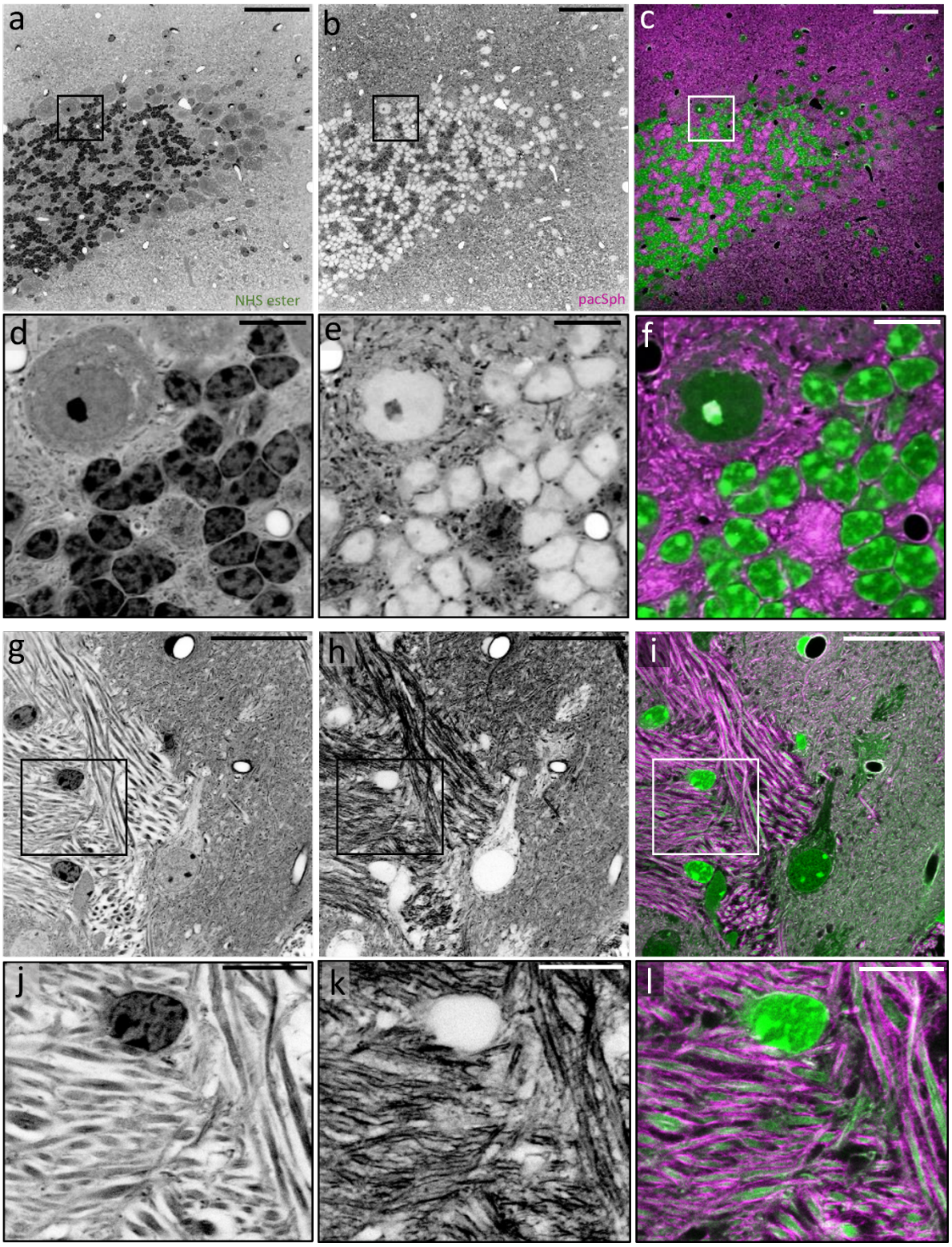

**Supplementary Figure 29: mCling only labels the surface of 4-fold expanded mouse brain tissue sections fixed with 3% FA + 0.1% GA. a**, NHS ester pan-stained tissue section expanded ~4-fold showing a neuron soma. **b**, mCling staining of the same area shown in **a**. **c**, overlay. **d**, NHS ester pan-stained tissue section expanded ~4-fold showing a myelinated axon. **e**, mCling staining of the same area shown in **d**. **f**, overlay. White arrow points to myelinated axon. **g**, Large FOV image of an NHS ester pan-stained tissue section expanded ~4-fold. **h**, mCling pan-staining of the same area shown in **a** showing uneven labeling which is indicative of poor ligand penetration. Black arrow points to region of low mCling staining. **i**, overlay. Scale bars are not corrected for the expansion factor. (**a-f**), 10 μm, (**g-i**) 100 μm.



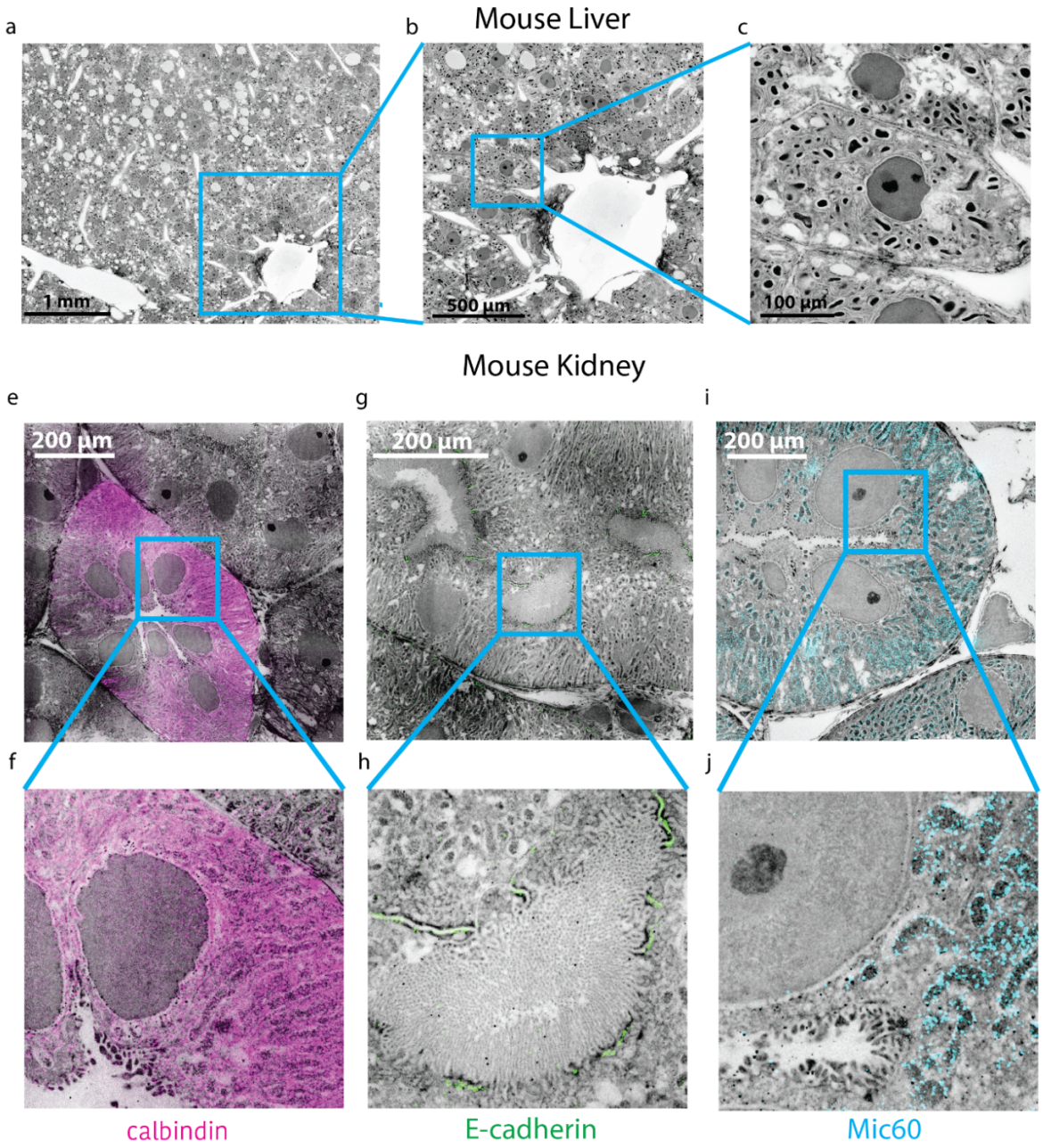

**Supplementary Figure 30: Chemical structures of pGk5b, mCling, and pacSph. a**, chemical structure of palmitoyl-glycine-(penta)lysine-biotin (pGk5b). pGk5b is 1158 Da in size. It has 5 reactive primary amine groups, a palmitoyl group for lipid membrane intercalation, a glycine for mechanical flexibility, and a biotin reporter group. **b**, chemical structure of membrane-binding fluorophore-cysteine-(hepta)lysine-palmitoyl group (mCling). mCling (biotin) is 1445 Da in size. It has 7 reactive primary amine groups, a palmitoyl group for lipid membrane intercalation, and a biotin (or fluorophore) reporter group. **c**, chemical structure of photoactivatable and clickable sphingosine (pacSph). pacSph is 335 Da in size. It is a sphingosine that intercalates lipid membranes. It has a diazirine UV photocrosslinkable group and an alkyne reporter group.



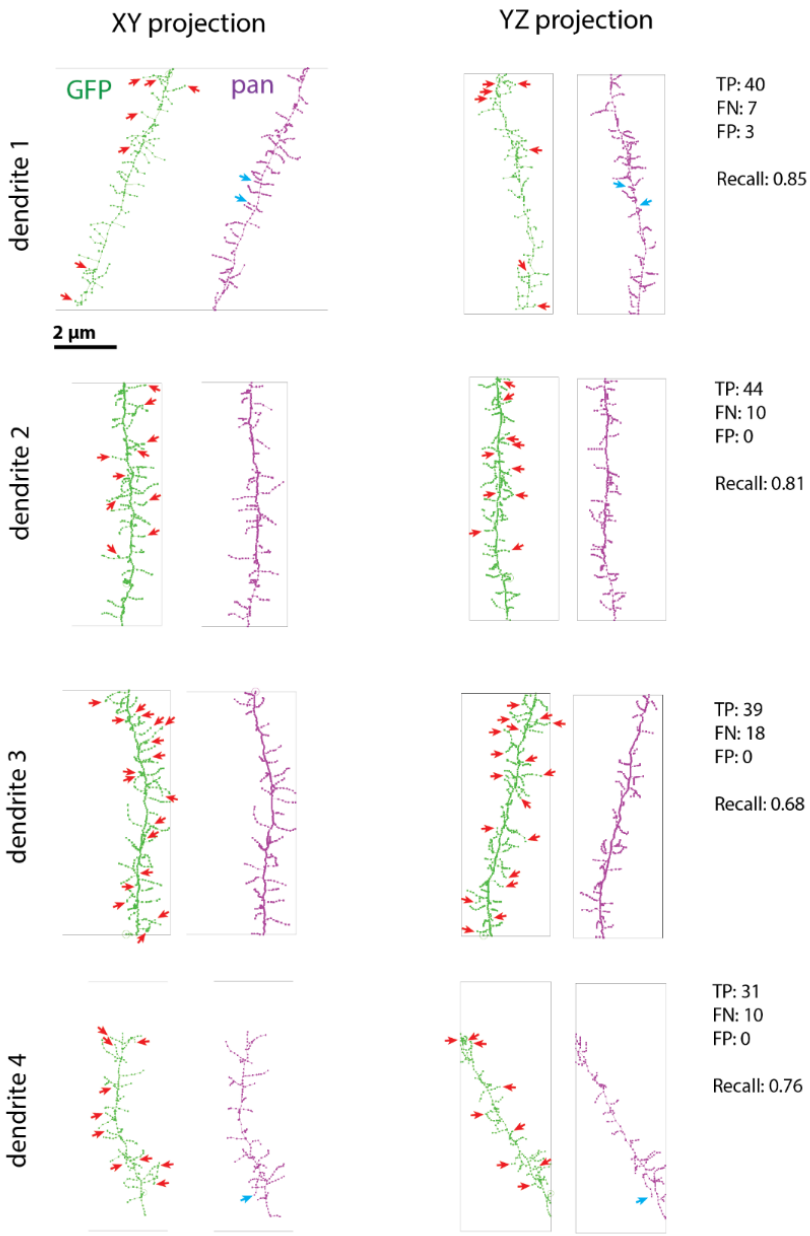

**Supplementary Figure 31: Effect of UV irradiation on pacSph pan-staining in pan-ExM-t expanded mouse brain tissue sections.** **a**, NHS ester pan-stained neuropil. **b**, pacSph pan-staining of the same area shown in **a** without UV irradiation. **c**, overlay. **d**, NHS ester pan-stained neuropil. **e**, pacSph pan-staining of the same area shown in **d** with UV irradiation before hydrogel embedding. **f**, **o**verlay. **g**, NHS ester pan-stained neuropil. **h**, pacSph pan-staining of the same area shown in **g** with UV irradiation after hydrogel embedding and before denaturation. **i**, overlay. Scale bars are corrected for the expansion factor. (**a-i**), 5 µm




**Supplementary Figure 32: Examples of pacSph and NHS ester differential pan-staining in 4-fold expanded mouse brain tissue sections.** **a**, **g**, NHS ester pan-stained tissue section expanded ~4-fold. **b**, **h**, pacSph pan-staining of the same area shown in **a** and **g**, respectively. **c**, **i**, overlay. **d**, **e**, **f**, magnified images of the areas outlined by the boxes in **a**, **b**, and **c**, respectively, showing cell bodies. **j**, **k**, **l**, magnified images of the areas outlined by the boxes in **g**, **h**, and **l**, respectively, showing myelinated axons. Scale bars are not corrected for the expansion factor. (**a-c**) 200 µm, (**d-f**, **j-l**) 30 µm, (**g-i**) 100 µm.




**Supplementary Figure 33: | pan-ExM-t data from non-brain tissue**. **a-c,** pan-ExM-t image of mouse liver. Progressive zoom-ins reveal structure of a bile duct (b) and hepatocyte (c). **e-l,** pan-ExM images of mouse kidney tissue with various antibody labels. **e-f,** calbindin; **g-h,** CALHM2; **i-j,** Mic60. All scale bars: not corrected for the expansion factor.




**Supplementary Figure 34: Quantification of tracing accuracy from pan-ExM-t data.** Comparisons on skeleton-based tracings of hippocampal dendrites within pan-ExM-t image volumes. Dendrites were traced based on either the anti-GFP channel (green, ground truth) or the pan channel (purple, blind to the ground truth). XY and YZ projections are shown to make all dendritic spines visible. True Positives (TP) correspond to spines found on both skeletons. False Negatives (FN, missed spines) are indicated by red arrows. False Positives (FP, erroneous spines) are indicated by cyan arrows. The quantification of recall (TP/(TP+FN)) is reported for each dendrite. The overall recall was 0.77 ± .07.

# Supplementary Tables

**Supplementary Table 1**: Polymerization, buffer, and fixative reagents used

| Step | Product | Acronym | Storage | Catalog # | Vendor |
|---|---|---|---|---|---|
| **Polymerizations** | 40% Acrylamide | AAm | 4°C | A9099 | Sigma-Aldrich |
| | N,N'-(1,2-Dihydroxyethylene) bisacrylamide | DHEBA | 4°C | 294381 | Sigma-Aldrich |
| | N,N'-(1,2-Dihydroxyethylene) bisacrylamide | DHEBA | 4°C | sc-215503 | SCBT* |
| | Sodium acrylate | SA | -20°C desiccated | 408220 | Sigma-Aldrich |
| | Sodium acrylate | SA | -20°C desiccated | sc-236893C | SCBT* |
| | N,N′-Methylenebis (acrylamide) | BIS | RT | 146072 | Sigma-Aldrich |
| | Ammonium persulfate | APS | RT desiccated | AB00112 | American Bio |
| | Ammonium persulfate | APS | RT desiccated | A3678 | Sigma-Aldrich |
| | N,N,N',N'-Tetramethylethylenediamine | TEMED | RT desiccated | AB02020 | American Bio |
| **Buffers** | 10X Phosphate buffered saline (Gibco) | 10X PBS | RT | 70011044 | Thermofisher |
| | Sodium hydroxide | NaOH | RT | S8045 | Sigma-Aldrich |
| | 20% Sodium dodecyl sulfate solution | SDS | RT | AB01922 | American Bio |
| | 5 M NaCl solution | NaCl | RT | AB1915 | American Bio |
| | Sodium Chloride | NaCl | RT | 3624-01 | J.T. Baker |
| | 1 M Tris solution, pH 8 | Tris | RT | AB14043 | American Bio |
| | Tris [hydroxymethyl] aminomethane | Tris | RT | AB02000 | American Bio |
| | Triton X-100 | TX-100 | RT | T8787 | Sigma-Aldrich |
| | Tween 20 | Tween 20 | RT | P7949 | Sigma-Aldrich |
| | NP-40 | NP-40 | RT | I8896 | Sigma-Aldrich |
| | 1X Phosphate buffered saline (Gibco) | 1X PBS | RT | 10010023 | Thermofisher |
| | Sodium Bicarbonate | - | RT | S5761 | Sigma-Aldrich |
| | Bovine Serum Albumin | BSA | 4°C | 001-000-162 | Jackson IR |
| | Normal Goat Serum | NGS | 4°C | 005-000-121 | Jackson IR |
| | Guanidine hydrochloride | G-HCl | RT | G3272 | Sigma-Aldrich |
| **Fixatives** | 16% Paraformaldehyde | FA | RT | 15710 | EMS** |
| | 8% Glutaraldehyde | GA | 4°C | 16019 | EMS** |

* Santa Cruz Biotechnology; ** Electron Microscopy Sciences

**Supplementary Table 2**: Materials used

| Materials | Vendor | Catalog number |
|---|---|---|
| No. 1.5 12-mm round glass coverslips | Electron Microscopy Sciences | 72230-01 |
| Glass microscope slide | Sigma-Aldrich | S8400 |
| No. 1.5 22 x 22 mm square cover glass coverslips | Fisher Scientific | 12-541B |
| No. 1.5 18-mm round coverslip | Marienfeld | 0117580 |
| 50mm MatTekdish, No. 1.5 coverslip 30-mm diameter | MatTek Life Sciences | P50G-1.5-30-F |
| Picodent Twinsil | Picodent | 1300 1000 |

**Supplementary Table 3:** Primary antibodies used to immunolabel neuron and brain tissue samples

| Primary antibody | Target | Host species | Dilution | Catalog number | Vendor |
|---|---|---|---|---|---|
| Recombinant anti-Homer1 antibody [EPR15309] | Homer1 | Rb mAb | 1:500 (**N**); 1:250 (**B**) | ab184955 | abcam |
| Anti-Bassoon/BSN antibody [SAP7F407] | Bassoon | Ms mAb | 1:500 (**N**); 1:250 (**B**) | ab82958 | abcam |
| Anti-PSD-95 antibody [K28/43] | PSD-95 | Ms mAb | 1:500 (**N**); 1:250 (**B**) | 75-028 | antibodiesinc |
| Anti-Synaptophysin antibody (D8F6H) | Synaptophysin | Rb mAb | 1:250 (**N**) | 36406 | CST |
| Anti-Synaptophysin antibody | Synaptophysin | Rb pAb | 1:250 (**B**) | 17785-1-AP | protein tech |
| Anti-Synaptophysin 1 antibody | Synaptophysin | Ms mAb | 1:250 (**N**) | 101 011 | SYSY |
| Anti-GFAP polyclonal antibody | GFAP | Rb pAb | 1:500 (**B**) | PA1-10019 | Thermofisher |
| Purified anti-Myelin Basic Protein antibody | MBP | Ms mAb | 1:500 (**B**) | 808401 | BioLegend |
| Anti-GFP polyclonal antibody | GFP | Rb pAb | 1:500 (**B**) | A-11122 | Thermofisher |

**N:** cultured neuron samples**, B:** brain tissue section samples

**Supplementary Table 4:** Secondary antibodies used to immunolabel neuron and brain tissue samples

| Secondary dye | Species reactivity | Host | Dilution | Ex/Em [nm] | Catalog number | Vendor |
|---|---|---|---|---|---|---|
| ATTO594 | Mouse | Goat | 1:250-1:500 | 603/626 | 76085 | Sigma-Aldrich |
| ATTO594 | Rabbit | Goat | 1:250-1:500 | 603/626 | 77671 | Sigma-Aldrich |
| ATTO647N | Mouse | Goat | 1:250-1:500 | 646/664 | 50185 | Sigma-Aldrich |
| ATTO647N | Rabbit | Goat | 1:250-1:500 | 646/664 | 40839 | Sigma-Aldrich |
| CF568 | Rabbit | Donkey | 1:250 | 562/583 | 20098 | Biotium |

**Supplementary Table 5:** Fluorescent pan-stains and lipid probes used

| Stain/Pan-stain | Concentration | Ex/Em [nm] | Catalog number | Vendor |
|---|---|---|---|---|
| ATTO532, NHS ester | 20 µg/mL (**N**); 30 µg/mL (**B**) | 532/552 | 88793 | Sigma-Aldrich |
| ATTO532, NHS ester | 20 µg/mL (**N**); 30 µg/mL (**B**) | 532/552 | AD 532-31 | ATTO-TEC |
| ATTO594, NHS ester | 20 µg/mL (**N**); 30 µg/mL (**B**) | 603/626 | 08741 | Sigma-Aldrich |
| ATTO594, NHS ester | 20 µg/mL (**N**); 30 µg/mL (**B**) | 603/626 | AD 594-31 | ATTO-TEC |
| ATTO488, NHS ester | 20 µg/mL (**N**) | 500/520 | 41698 | Sigma-Aldrich |
| SYTOX Green | 1 µM (**N**); 1.7 µM (**B**) | 504/523 | S7020 | Thermofisher |
| BODIPY TR Methyl Ester | 10 µM (**B**) | 588/621 | C34556 | Thermofisher |
| ATTO590, alkyne | 5 µM (**N**) | 594/624 | 93990 | Sigma-Aldrich |
| ATTO590, azide | 5 µM (**N**) | 593/622 | AD 590-101 | ATTO-TEC |
| Palmitic acid azide | 50 µM (**N**) | NA | C10265 | Thermofisher |
| PhotoClick Sphingosine (pacSph) | 50 µM (**B**) | NA | 900600 | Avanti Polar Lipids |
| Click-IT Cell Reaction Buffer Kit | NA | NA | C10269 | Thermofisher |

**N:** cultured neuron samples**, B:** brain tissue section samples

**Supplementary Table 6**: Overview of Labeling Conditions.

**Cultured Hippocampal Neurons**

| Target or Stain | Fixative, Duration | Primary (catalog #, host) | Dilution, Incubation | Secondary and Dilution | Notes |
|---|---|---|---|---|---|
| Homer1 | 4% FA, 15 min @ RT | ab184955, mouse mAb | 1:500, overnight (~15 h) @ 4 °C | ATTO594 anti-mouse, 1:500 O/N @ 4 °C | Uses pan-ExM; detergent-light buffer (0.05% TX-100 + 0.05% NP-40 + 0.2% BSA) |
| Bassoon | same as above | ab82958, mouse mAb | 1:500, ON @ 4 °C | same as above | Dual-label with Homer1 possible (add both primaries together) |
| PSD-95 | same as above | 75-028, mouse mAb | 1:500, ON @ 4 °C | same as above | — |
| Synaptophysin | 3% FA + 0.1% GA, 15 min @ RT | CST 36406, rabbit pAb | 1:250, 36–40 h @ 37 °C | CF568 anti-rabbit, 1:250, 16–20 h @ 37 °C | Higher temp improves penetration; GA stabilizes vesicles |
| Metabolic azido-palmitate | Live label 5 h @ 37 °C → 3% FA + 0.1% GA fix @ RT | Click after expansion with ATTO590-alkyne | 50 µM palmitate | — | Reveals ER-mitochondria contacts; works with NHS-ester protein pan-stain |

**Mouse Brain Tissue Sections**

| Target or Stain | Fixative (all overnight @ 4 °C) | Hydrogel combo* | Primary (dilution × time @ 4 °C) | Secondary and Dilution | Notes |
|---|---|---|---|---|---|
| Homer1 | 4% FA + 20% AAm | 19SA / 9SA | 1:250 × 30 h | ATTO594 anti-mouse 1:250 | Synaptic protein panel; long incubations for thick tissue |
| Bassoon | same as above | 19SA / 9SA | 1:250 × 30 h | ATTO594 anti-mouse 1:250 | — |
| PSD-95 | same as above | 19SA / 9SA | 1:250 × 30 h | ATTO594 anti-mouse 1:250 | — |
| Synaptophysin | same as above | 19SA / 9SA | 1:250 × 30 h | ATTO594 anti-rabbit 1:250 | — |
| GFAP (astrocytes) | same as above | 19SA / 19SA | Rabbit PA1-10019, 1:500 × 30 h | ATTO594 anti-rabbit 1:500 | Stiffer gel preserves filamentous processes |
| MBP (myelin) | same as above | 19SA / 19SA | Mouse 808401, 1:500 × 30 h | ATTO594 anti-mouse 1:500 | Myelinated axons appear as protein-void tubes |
| GFP (Thy1-EGFP) | same as above | 19SA / 19SA | Rabbit A-1122, 1:500 × 30 h | ATTO594 anti-rabbit 1:500 | Sparse neuron tracing; GFP excluded from mitochondria |
| PacSph (lipid membrane) | Pre-label 50 µM pacSph o/n 4 °C, UV 365 nm 30 min each side after first gelation | Standard gels | Click with 5 µM ATTO590-azide post-expansion | — | "UV-after" gives highest retention; delineates bilayers |

# Supplementary Methods

### Neuron culture

Rat and mouse neuron cultures used to generate pan-ExM images shown in **Figures 1** NHS ester, anti-Homer1, anti-Bassoon, and anti-PSD-95 images were cultured as described previously [1] and detailed in **Supplementary Methods**. In short, primary neuron cultures were prepared from hippocampal regions dissected from E18 Sprague Dawley Rat pups (Charles River Laboratories). The brains were removed, and hippocampi were isolated on ice in HBS medium (Sigma; catalog no. H2387) containing 10 mM HEPES (Gibco; catalog no. 15630-080). The hippocampal neurons were then dissociated via incubation at 37°C for 30 minutes in 2% papain solution (Worthington; catalog no. LS003127). Following incubation, hippocampi were washed and triturated in Neurobasal medium (Gibco; catalog no. 21103-049) supplemented with 5% fetal bovine serum (Atlanta; S11150), 2% B27 (Invitrogen; catalog no. 17504-044), 1% Glutamax (Invitrogen; catalog no. 35050-061) and gentamycin 1ng/ul (Gibco; catalog no. 1570060). The cells were plated at a density of 20,000 cells per Poly-DL-Ornithine (Sigma; catalog no. P0421-100MG) and Laminin (Corning; catalog no. #354232) coated 12-mm glass coverslip (Assistant; catalog no. 633009). To reduce glia growth, cultures were treated with 10 μM 5-Fluoro-2'-deoxyuridine (Sigma; catalog no. F0503). After 14 days in vitro, neurons were fed with Neurobasal medium (Gibco; catalog no. 21103-049) supplemented with 2% B27 (Invitrogen; catalog no. 17504-044), 1% Glutamax (Invitrogen; catalog no. 35050-061), 10 μM 5-Fluoro-2'-deoxyuridine (Sigma; catalog no. F0503) and gentamycin 1ng/ul (Gibco; catalog no. 1570060). Experiments were performed on 15–21 DIV cultures.

Rat neuron cultures used to generate NHS ester and anti-Synaptophysin images were cultured as follows: hippocampal CA3-CA1 regions were isolated and dissected from E18 Sprague Dawley Rats (Charles River Laboratories) in the presence of chilled hibernate E media (BrainBits). Hippocampal neurons were then incubated at 37°C for 25 minutes in 0.25% trypsin (Corning; catalog no. 25–053 CI) and immediately washed with DMEM (Thermofisher; catalog no. 11965–118) containing 10% fetal bovine serum (Thermofisher; catalog no. 16000044). Following trypsinization, hippocampi were triturated and immediately plated in DMEM containing 10% fetal bovine serum on poly-D-lysine (Thermofisher; catalog no. ICN10269491) coated 18 mm glass coverslips (Warner instruments; catalog no. 64–0734 [CS-18R17]). After 1 hour of incubation at 37°C, DMEM was removed and replaced with Neurobasal-A (Thermofisher; catalog no. 10888–022) medium containing 2% B-27 (Thermofisher; catalog no. 17504001) and 2 mM Glutamax (Gibco; catalog no. 35050061). Experiments were performed 15-17 days after plating.

Mouse hippocampal cultures used to generate NHS ester images were performed on C57BL/6 E17-E18 embryos, in accordance with IACUC protocol number 2019-07912. Pregnant animals were sacrificed with CO2 asphyxiation. The embryos were isolated from uterus horns through Cesarean section, followed by decapitation and hippocampal dissection. Hippocampi were dissociated using papain dissociation kit (Worthington LK003176) for 10 minutes at 30°C. Neurons were triturated and plated onto 12 mm Poly-D-lysine coated coverslips in a 24 well dish at a density of 150,000 cells per well in Neurobasal Plus media (Thermo-Fisher; catalog no. A3653401) supplemented with 2% B27 plus (Thermo-Fisher; catalog no. A3582801), and 50ug/ml of gentamicin (Thermo-Fisher; catalog no. 15750060). Fixation was performed at DIV 14-15.

Mouse hippocampal cultures used to generate 5-fold expansion images were performed on BalbC P0 pups, in accordance with IACUC protocol number 2019-07912. Hypothermia was

induced in pups using ice, followed by decapitation and hippocampal dissection. Hippocampi were dissociated using 200 units Papain (Worthington LS003124, 200 units) for 40 minutes at 37°C. Neurons were triturated and plated onto 12 mm Poly-D-lysine coated coverslips in a 24 well dish at a density of 150,000 cells per well in Neurobasal/B27 Plus media (Thermo-Fisher; catalog no. A3653401) supplemented with 10% FBS and 1% Penicillin/Streptomycin (Thermo-Fisher; catalog no. 15140163). Following 3 hours of incubation at 37°C and 5% CO2, the media was replaced with Neurobasal/B27 Plus media (Thermo-Fisher; catalog no. A3653401) supplemented with 1% Penicillin/Streptomycin (Thermo-Fisher; catalog no. 15140163)). Fixation was performed at DIV 14-15.

**First round of expansion for dissociated neurons**

Neurons, previously fixed as described in the **Neuron culture** section, were incubated in post-fixation solution (0.7% FA + 1% AAm (w/v) in 1× PBS) for 6–7 h at 37 °C. Next, the neurons were washed twice with 1× PBS for 10 min each on a rocking platform and embedded in the first expansion gel solution (18.5% (w/v) SA + 10% AAm (w/v) + 0.1% (w/v) DHEBA + 0.25% (v/v) TEMED + 0.25% (w/v) APS in 1× PBS). Gelation proceeded for 10-15 min at room temperature (RT) and then for 1.5 h at 37 °C in a humidified chamber. Coverslips with hydrogels were then incubated in ~4 mL denaturation buffer (200 mM SDS + 200 mM NaCl + 50 mM Tris in MilliQ water, pH 6.8) in 6-well plates for 45 min at 37 °C. Gels were then transferred to denaturation buffer-filled 1.5 mL Eppendorf tubes and incubated at 73 °C for 1 h. Next, the gels were washed twice with PBS for 20 min each and stored in PBS overnight at 4 °C. Gels were then cut and placed in 6-well plates filled with MilliQ water for the first expansion. Water was exchanged twice every 30 min and once for 1 h. Gels expanded between 4.0× and 4.5× according to SA purity (see **pan-ExM-t reagents**).

**Re-embedding in neutral hydrogel**

Expanded hydrogels (of both dissociated neuron and tissue samples) were incubated in fresh re-embedding neutral gel solution (10% (w/v) AAm + 0.05% (w/v) DHEBA + 0.05% (v/v) TEMED + 0.05% (w/v) APS) two times for 20 min each on a rocking platform at RT. Immediately after, the residual gel solution was removed by gentle pressing with Kimwipes. Each gel was then sandwiched between one no. 1.5 coverslip and one glass microscope slide. Gels were incubated for 1.5 h at 37 °C in a nitrogen-filled and humidified chamber. Next, the gels were detached from the coverslips and washed two times with 1× PBS for 20 min each on a rocking platform at RT. The samples were stored in 1× PBS at 4 °C. No additional post-fixation of samples after the re-embedding step was performed.

**Second round of expansion**

Re-embedded hydrogels (of both dissociated neuron and tissue samples) were incubated in fresh second hydrogel gel solution (19% (w/v) SA + 10% AAm (w/v) + 0.1% (w/v) BIS + 0.05% (v/v) TEMED + 0.05% (w/v) APS in 1× PBS) two times for 15 min each on a rocking platform in 4 °C. Each gel was then sandwiched between one no. 1.5 coverslip and one glass microscope slide. Gels were incubated for 1.5 h at 37 °C in a nitrogen-filled and humidified chamber. Next, to dissolve DHEBA, gels were detached from the coverslips and incubated in 200 mM NaOH for 1 h on a rocking platform at RT. Gels were afterwards washed three to four times with 1× PBS for 30 min each on a rocking platform at RT or until the solution pH reached 7.4. The gels were optionally stored in 1× PBS at 4 °C. Subsequently, the gels were labeled with antibodies and pan-stained with NHS ester dyes. Finally, the gels were placed in 6-well plates filled with MilliQ water for the second expansion. Water was exchanged at least three times every 1 h at RT. Gels expanded ~ 4.5× according to SA purity (see **pan-ExM-t**

**reagents**) for a final expansion factor of ~16× (dissociated neurons) and ~24× (brain tissue). Expanded samples show a remarkable stability: when stored in the refrigerator and prevented from drying out, we did not observe any obvious structural degradation or a substantial change in expansion factor over a 7-month time span (CA3 region of hippocampus; expansion factor 20 ± 3 for a freshly prepared sample vs. 19 ± 3 after ~7 months).

**Antibody labeling of neurons post-expansion**

Samples immunolabeled with Homer1, Bassoon, and PSD-95 were fixed with 4% FA in 1× PBS for 15 min as described in the **Neuron Culture** section~~**Neuron fixation** section~~, processed with pan-ExM, and incubated overnight (~15 h) with monoclonal anti-Homer1 antibody (abcam, catalog no. ab184955), monoclonal anti-Bassoon antibody (abcam, catalog no. ab82958), or monoclonal anti-PSD-95 antibody (antibodiescinc, catalog no. 75-028) diluted 1:500 in antibody dilution buffer (0.05% TX-100 + 0.05% NP-40 + 0.2% BSA in 1× PBS). All primary antibody incubations were performed on a rocking platform at 4 °C. Gels were then washed with 0.1% (v/v) TX-100 in 1× PBS twice for 20 min each on a rocking platform at RT and once overnight (~15 h) at 4 °C. Next, samples were incubated overnight with ATTO594-conjugated anti-mouse antibodies (Sigma-Aldrich, catalog no. 76085) or ATTO594-conjugated anti-rabbit antibodies (Sigma-Aldrich, catalog no. 77671) diluted 1:500 in antibody dilution buffer. All secondary antibody incubations were performed on a rocking platform at 4 °C. The gels were subsequently washed in 0.1% (v/v) TX-100 in 1× PBS twice for 20 min each at RT and once overnight at 4 °C. Gels were stored in PBS at 4 °C until subsequent treatments. Bovine serum albumin (BSA; catalog no. 001-000-162) was purchased from Jackson ImmunoResearch and NP-40 (catalog no. T8786) and Triton X-100 (TX-100; catalog no. T8787) was purchased from Sigma-Aldrich.

Samples immunolabeled with both Homer1 and Bassoon simultaneously were fixed with 4% FA in 1× PBS for 15 min as described in the **Neuron Culture** section, processed with pan-ExM, and incubated overnight (~15 h) with both monoclonal anti-Homer1 antibody (abcam, catalog no. ab184955) and monoclonal anti-Bassoon antibody (abcam, catalog no. ab82958) diluted 1:500 in antibody dilution buffer (0.05% TX-100 + 0.05% NP-40 + 0.2% BSA in 1× PBS). Primary antibody incubations were performed on a rocking platform at 4 °C. Gels were then washed with 0.1% (v/v) TX-100 in 1× PBS twice for 20 min each on a rocking platform at RT and once overnight (~15 h) at 4 °C. Next, samples were incubated overnight (~15 h) with both ATTO594-conjugated anti-rabbit antibodies (Sigma-Aldrich, catalog no. 77671) and ATTO647N-conjugated anti-mouse antibodies (Sigma-Aldrich, catalog no. 50185) diluted 1:500 in antibody dilution buffer. Secondary antibody incubations were performed on a rocking platform at 4 °C. The gels were subsequently washed in 0.1% (v/v) TX-100 in 1× PBS twice for 20 min each at RT and once overnight at 4 °C. Gels were stored in PBS at 4 °C until subsequent treatments.

Samples immunolabeled with Synaptophysin were fixed with 3% FA + 0.1% GA 1× PBS as described in the **Neuron Culture** section, processed with pan-ExM, and incubated for ~36-40 h at 37° C with rabbit anti-synaptophysin (Cell signaling technology, catalog no. 36406) diluted 1:250 in antibody dilution buffer (2% (w/v) BSA in 1× PBS). Gels were then washed in PBS-T (0.1% (v/v) Tween 20 in 1× PBS) three times for 20 min each on a rocking platform at RT. Next, samples were incubated for ~16-20 h at 37°C with donkey anti-rabbit CF568 (Biotium, catalog no. 20098) diluted 1:250 in antibody dilution buffer. The gels were washed in PBS-T three times for 20 min each at RT each before subsequent pan-staining.

**NHS ester pan-staining of neurons**

After antibody labeling, gels were incubated for 1.5 h with 20 µg/mL NHS ester-ATTO532 (Sigma-Aldrich, catalog no. 88793) (Homer1, Bassoon, PSD-95, centriole, and NPC samples), or 20 µg/mL NHS ester-ATTO488 (Sigma-Aldrich, catalog no. 41698) (Synaptophysin samples), or 20 µg/mL NHS ester-ATTO594 (Sigma-Aldrich, catalog no. 08741) (mitochondria samples), dissolved in 100 mM sodium hydrogencarbonate solution (Sigma-Aldrich, catalog no. SLBX3650) on a rocking platform at RT. The gels were subsequently washed four to six times in either 1× PBS or PBS-T for 20 min each on a rocking platform at RT.

**Palmitate pan-staining of neurons**

Live and dissociated 80%-confluent hippocampal neurons were incubated with 50 µM azide-functionalized palmitate (Thermofisher, catalog no. C10265) diluted in delipidated medium (DMEM + 10% charcoal-stripped FBS; Thermofisher, catalog no. A3382101) for 5 h at 37 °C and 5% CO2. Next, the neurons were fixed with 3% FA + 0.1% GA in 1× PBS for 15 min at RT and processed according to the pan-ExM protocol. Prior to NHS ester pan-staining with ATTO532 , CuAAC (Copper(I)-catalyzed Azide-Alkyne Cycloaddition) was performed using the Click-iT Cell Reaction Buffer Kit (Thermo Fisher, catalog no. C10269) according to manufacturer instructions. Alkyne-functionalized ATTO590 dye (Sigma-Aldrich, catalog no. 93990) was used at a concentration of 5 µM. After CuAAC, the gels were washed twice with 2% (w/v) delipidated BSA (Sigma Aldrich, catalog no. A4612) in 1× PBS for 20 min each on a rocking platform at RT and twice with 1× PBS for 20 min each at RT.

**SYTOX Green staining post-expansion**

pan-ExM and pan-ExM-t processed gels were incubated with SYTOX Green (Invitrogen, catalog no. S7020) diluted 1:5,000 (dissociated neuron samples) and 1:3,000 (brain tissue samples) in 1× PBS for 30 min on a rocking platform at RT. The gels were then washed three times with PBS-T for 20 min each on a rocking platform at RT.

**Mouse Brain Tissue**

Brain tissue experiments were conducted in 2 wild-type (C57BL/6) adult male mice purchased from the Charles River Laboratories and 2 wild-type (C57BL/6) adult male mice and 1 Thy1-EGFP mouse (strain Tg(Thy1-EGFP)MJrs/J, 4-8 weeks), purchased from the Jackson Laboratory.

All experiments were carried out in accordance with National Institutes of Health (NIH) guidelines and approved by the Yale IACUC.

All wild-type (C57BL/6) adult male mice were between P21 and P35 and maintained in the vivarium with a 12-h light–dark cycle, stable temperature at 22 ± 1 °C and humidity between 20 and 50%. The mice were anesthetized by a mixture of Ketamine (ketaset, Zoetis Inc, Cat # 010177) and Xylazine (Anased Injection, Akorn Animal health, NDC: 59399-110-20) with a 4:1 ratio. This mixture was then diluted 5x in saline, and administered IP. Mice were transcardially perfused first with ice-cold 1× PBS and then with either 4% FA, 4% FA + 0.1% FA, or 4% FA + 20% acrylamide (AAm; Sigma; catalog no. A9099) (all in 1× PBS, pH 7.4). Brains were isolated and post-fixed overnight in the same perfusion solution at 4 °C. Brains were subsequently washed and stored in PBS at 4 °C. Brains were mounted in ice-cold PBS and coronally sectioned at 70 µm using a vibrating microtome (Vibratome 1500, Harvard Apparatus). Medial hippocampal slices were selected and washed four times for 15 min in PBS at room temperature. Sections were stored in PBS at 4 °C for up to 3 months.

Thy1-EGFP mouse was anesthetized with ketamine (100 mg/kg, Butler Schein: 9952949) and xylazine (10 mg/kg, Akorn: NDC 59399-110-20) in saline (Hudson RCI: 200-59) soon after delivery. The mouse was transcardially perfused first with ice cold 1× PBS (Fisher; BP2944-100) and then with 4% FA (J.T. Baker; S898-07) + 20% AAm in 1× PBS, pH 7.4. The brain was isolated and postfixed overnight in 4% FA + 20% AAm in 1× PBS at 4°C. The brain was then washed in PBS and coronally sectioned at 70 µm using vibrating microtome (Leica VT1000, Leica Biosystems, Nussloch, Germany). Sections were stored in 1× PBS with 0.01% sodium azide (Sigma-Aldrich, St. Louis, MO) at 4°C for up to 7 months.

**pan-ExM gelation chamber for dissociated neurons**

The gelation chamber was constructed using a glass microscope slide (Sigma-Aldrich, catalog no. S8400) and two spacers, each consisting of a stack of two no. 1.5 22 × 22 mm coverslips (Fisher Scientific, catalog no. 12-541B). The spacers were superglued to the microscope slide on both sides of the neuron-adhered coverslip, with this latter coverslip glued in between. A no. 1.5 22 × 22 mm coverslip was used as a lid after addition of the gel solution. This geometry yielded an initial gel thickness size of ~170 µm.

**pan-ExM-t gelation chamber for brain tissue sections**

The gelation chamber was constructed using a glass microscope slide (Sigma-Aldrich, catalog no. S8400) and two spacers, each consisting of one no. 1.5 22 × 22 mm coverslip (Fisher Scientific, catalog no. 12-541B). The spacers were superglued to the microscope slide spaced ~ 1 cm from one another. After incubation in activated first expansion gel solution (as described below in **First round of expansion for brain tissue sections**), the 70 µm-thick brain tissue section was placed and flattened on an additional no. 1.5 22 × 22 mm coverslip which was used as a chamber lid after addition of more activated first expansion gel solution on the microscope slide in-between the spacers. This geometry yielded an initial gel thickness size of ~170 µm.

Optimizing antibody-labeling parameters to achieve efficient and specific staining is critical for pan-ExM imaging. Because the hydrogels used in pan-ExM are entangled and dense (~30% w/v monomer concentration), we suspect that many antibodies can become entrapped within this hydrogel matrix when used in high concentrations, often producing a granular background (**Supplementary Fig. 7b**). We found, for example, that lowering the concentrations of both Homer1 primary and dye-conjugated secondary antibodies from ~4 µg/mL to ~2 µg/mL strongly reduced the background without compromising signal levels (**Supplementary Fig. 7j**).

**Assessment of fixation effects in brain tissue ultrastructural preservation**

Ultrastructural analysis of brain tissue sections in EM has typically relied on formaldehyde (FA) and glutaraldehyde (GA) fixation to best preserve fine structures [2,3]. Because pan-ExM is an ultrastructural imaging method, structural preservation at the 10-nm scale is of utmost importance [4]. However, compatibility with immunolabeling is equally important to the core concept of our technique, and antigens are known to be masked by glutaraldehyde fixation [5]. To examine the effects of fixation and post-fixation on tissue preservation, we expanded 70 µm-thick mouse brain tissue sections that were fixed with 4% FA and not post-fixed (*Fix-1*), fixed with 4% FA and post-fixed with 0.7% FA + 1% acrylamide (AAm) (*Fix-2*; similar to [6]), fixed with 4% FA and post-fixed with 4% FA + 20% AAm (*Fix-3*), fixed with 4% FA + 0.1% GA and post-fixed with 4% FA + 20% AAm (*Fix-4*), and fixed with 4% FA and post-treated with 0.1 mg/mL acryloyl-X SE (AcX) (*Fix-5*), a common acryloylated and amine-reactive reagent used in ExM [7]. **Supplementary Figs. 11-12** show that tissue treated with *Fix-1* has no

distinguishable structural features beyond the outline of cell nuclei, suggesting little protein retention; tissue treated with *Fix-2* expands 18.5 ± 1.3-fold (mean ± s.d.; N = 6 fields of view; n = 38 synaptic profiles, **Supplementary Fig. 12p**) and shows resolved synapses and cell bodies, but no distinguishable neurites; tissue treated with *Fix-3* expands 16.0 ± 1.0-fold (mean ± s.d.; N = 9 fields of view; n = 81 synaptic profiles) and shows distinguishable neurites, but many detached cell bodies; tissue treated with *Fix-4* expands 11.6 ± 1.1-fold (mean ± s.d.; N = 8 fields of view; n = 77 synaptic profiles) and exhibits adequate neuropil and cell body preservation, and finally; tissue treated with *Fix-5* expands 11.8 ± 1.9-fold (mean ± s.d.; N = 9 fields of view; n = 74 synaptic profiles) and shows poor cell body preservation and multiple artifactual gaps in neuropil. These results suggest that the expansion factor increases with lower post-fixation strength and decreases with the addition of GA in the fixative. They also suggest that use of AcX results in lower expansion factors as well as multiple extraction artifacts in tissue ultrastructure (but see [8]).

To examine tissue preservation further, we determined the extracellular space and lipid membrane (ECS+) fraction of neuropil across the different fixation schemes presented using Otsu's method, an automatic image thresholding algorithm [9] (see **Methods**). The ECS fraction in live organotypic brain slices, determined by STED microscopy, ranges from 5% to 36% [10]. We therefore expect the ECS+ fraction to be within that range or higher by ~10% to account for unlabeled lipid membrane boundaries. **Supplementary Fig. 13** shows that indeed lowering the strength of the post-fixative (*Fix-2*) or using AcX (*Fix-5*) result in large ECS gaps (ECS+>60%) that are likely artifactual, while using stronger post-fixatives (*Fix-3* and *Fix-4*) result in an ECS+ fraction within an acceptable range (~30%). It is worth noting that in EM of chemically fixed tissue, the ECS fraction is notoriously underestimated because of tissue shrinkage from excessive fixation (ECS shrinkage is ~6 fold), giving the misleading impression that neurites are tightly apposed to one another [11,12].

We conclude based on our assessment of fixation effects on ultrastructural preservation in expanded brain tissue that strong post-fixation with FA and AAm (*Fix-3* and *Fix-4*) is necessary for good neuropil and ECS preservation. However, these still cause artifactual gaps in neuropil, and in the case of FA+GA-fixed tissue, result in a low expansion factor of ~11 fold. Therefore, we hypothesized that excessive interprotein crosslinking occurs in the initial fixation stage and predicted that transcardial perfusion with both FA and AAm along with post-fixation in the same fixative would result in a more uniform expansion. Inspired by CLARITY and MAP [13,14] where FA is combined with acrylamide to simultaneously quench inter-protein crosslinking and functionalize proteins with an AAm group, we used 4% FA + 20% AAm in both the transcardial perfusion and overnight post-fixation solutions (*Fix-6*). We obtained an expansion factor of 24.1 ± 1.4-fold (mean ± s.d.; N = 10 fields of view from 3 independent experiments; n = 254 synaptic profiles, **Fig. 2i**; **Supplementary Fig. 12p**) as well as good neuropil preservation, very little artifactual tissue perforations (**Fig. 2a-c**; **Supplementary Figs. 11-12**), and an acceptable ECS+ fraction of ~38% (**Fig. 2j-l**; **Supplementary Fig. 13**). We therefore decided to use this fixation strategy for all subsequent experiments. Comparison of pan-ExM images with EM images from tissue sections prepared using this pan-ExM-t perfusion protocol *(Fix-6)* further confirmed the preservation of ultrastructural features, including cellular membranes, synaptic vesicles, mitochondrial cristae, and Golgi apparatus (**Extended Data Fig. 4**).

*Fix-1* brain tissue samples were previously fixed with 4% FA in 1× PBS overnight at 4 °C and sectioned to 70 µm as described in the **Brain perfusion** section. Next, they were washed three times with 1× PBS for 30 min each on a rocking platform at RT and processed with the pan-ExM-t protocol. *Fix-2* brain tissue samples were previously fixed with 4% FA in 1× PBS

overnight at 4 °C and sectioned to 70 µm as described in the **Brain perfusion** section. Next, they were post-fixed in 0.7% FA + 1% AAm in 1× PBS for 7 h at 37 °C, washed three times with 1× PBS for 30 min each on a rocking platform at RT, and processed with the pan-ExM-t protocol. *Fix-3* brain tissue samples were previously fixed with 4% FA in 1× PBS overnight at 4 °C and sectioned to 70 µm as described in the **Brain perfusion** section. Next, they were post-fixed in 4% FA + 20% AAm in 1× PBS for 7 h at 37 °C, washed three times with 1× PBS for 30 min each on a rocking platform at RT, and processed with the pan-ExM-t protocol. *Fix-4* brain tissue samples were previously fixed with 4% FA + 0.1% GA in 1× PBS overnight at 4 °C and sectioned to 70 µm as described in the **Mouse Brain Tissue** section. Next, they were post-fixed in 4% FA + 20% AAm in 1× PBS for 12 h at 4°C, washed three times with 1× PBS for 30 min each on a rocking platform at RT, and processed with the pan-ExM-t protocol. *Fix-5* brain tissue samples were previously fixed with 4% FA in 1× PBS overnight at 4 °C and sectioned to 70 µm as described in the **Brain perfusion** section. Next, they were treated with 0.1 mg/mL acryloyl-X, SE (AcX; Thermofisher, catalog no. A20770) in 1× PBS for 3 h at RT, washed three times with 1× PBS for 30 min each on a rocking platform at RT, and processed with the pan-ExM-t protocol. *Fix-6* brain tissue was previously fixed with 4% FA + 20% AAm in 1× PBS overnight at 4 °C and sectioned to 70 µm as described in the **Brain perfusion** section. Next, they were washed three times with 1× PBS for 30 min each on a rocking platform at 4°C and processed with the pan-ExM-t protocol.

Expansion factors were calculated as described in the **General neuron and brain tissue expansion factor calculation** section. For *Fix-2* DP-PSD measurements, 38 line profiles were drawn from 6 FOVs. For *Fix-3* DP-PSD measurements, 81 line profiles were drawn from 9 FOVs. For *Fix-4* DP-PSD measurements, 77 line profiles were drawn from 8 FOVs. For *Fix-5* DP-PSD measurements, 74 line profiles were drawn from 9 FOVs. For *Fix-6* DP-PSD measurements, 254 line profiles were drawn from 10 FOVs in 3 independent experiments. Results are summarized in **Supplementary Fig. 12**.

To calculate the ECS + lipid membrane (ECS+) fraction, ~250 x 250 µm$^2$ large-FOV images that show predominantly neuropil pan-stained with NHS ester, were processed with a Gaussian blur of 1 sigma (*Fix-1*, *Fix-2* and *Fix-5*) or 0.5 sigma (*Fix-3*, *Fix-4* and *Fix-6*) in FIJI. A mask created with manual thresholding was used to exclude large gaps in the image that do not represent neurites. The images were then thresholded using Otsu's method [9], an automatic image thresholding algorithm widely used in microscopy image analysis [15], with 100%, 70%, 50%, and 30% of the automatically determined threshold. The ECS+ fraction was calculated by dividing the total thresholded pixels by the total area represented by the masked pixels. The segmentation based on 50% of the automatically determined threshold was most consistent with the dense segmentation results from manual annotation used for neuron tracing (see Synaptic circuit analysis section below and Discussion). For *Fix-2*, 8 FOVs from 1 independent experiment were processed. For *Fix-3*, 8 FOVs from 1 independent experiment were processed. For *Fix-4*, 8 FOVs from 1 independent experiment were processed. For *Fix-5*, 8 FOVs from 1 independent experiment were processed. For *Fix-6*, 14 FOVs from 3 independent experiments were processed. Results are summarized in **Supplementary Fig. 13**.

**Assessment of denaturation effects in brain tissue ultrastructural preservation**

In the process of optimizing protein denaturation conditions, we found that increasing the denaturation temperature above 90 °C or using alkaline buffers resulted in hydrogel disintegration, possibly because of the lability of the DHEBA crosslinker molecule [16]. We therefore adopted the pH 6.8 SDS buffer of pan-ExM and used 75 °C as the temperature for denaturation, similar to 73 °C used in the original protocol [4]. We also found that tissue-hydrogel hybrids denatured for 4 h were macroscopically flat, while gels denatured for fewer than 4 h

exhibited crumbled macrostructures, signifying incomplete mechanical homogenization. We therefore assessed denaturation times of 4 h (*Denat-4*), 6 h (*Denat-6*), and 8 h (*Denat-8*) for both expansion factor and relative protein retention (measured by reporting peak DP intensity). We found that *Denat-4* results in an expansion factor of 26.9 ± 1.2 (mean ± s.d.; N = 3 fields of view; n = 50 synaptic profiles, **Supplementary Fig. 14j**) and DP peak intensity of 1500 ± 200 (mean ± s.d.; N = 3 fields of view; n = 50 intensity measurements, **Supplementary Fig. 14k**), *Denat-6* yields a similar expansion factor of 26.0 ± 1.3 (mean ± s.d.; N = 3 fields of view; n = 42 synaptic profiles) and slightly lower DP peak intensity of 1400 ± 200 (mean ± s.d.; N = 3 fields of view; n = 42 intensity measurements), and finally *Denat-8* shows an increase in expansion factor to 33.7 ± 1.6 (mean ± s.d.; N = 3 fields of view; n = 100 synaptic profiles) and partial protein loss with DP peak intensity of 1000 ± 200 (mean ± s.d.; N = 2 fields of view; n = 48 intensity measurements). Since we prioritize protein retention and argue that expansion factors of ~24 fold are sufficient to resolve ultrastructural features of interest, we denatured our samples for 4 h at 75 °C in all subsequent experiments.

*Denat-4, Denat-6,* and *Denat-8* brain tissue samples were previously fixed with 4% FA + 20% AAm in 1× PBS overnight at 4 °C and sectioned to 70 µm as described in the **Brain perfusion** section. Next, they were washed three times with 1× PBS for 30 min each on a rocking platform at RT and processed with the pan-ExM-t protocol with these modifications: *Denat-6* samples were denatured for 6 h and *Denat-8* samples were denatured for 8 h.

Expansion factors were calculated as described in the **General neuron and brain tissue expansion factor calculation section**. For *Denat-4* DP-PSD measurements, 50 line profiles were drawn from 3 FOVs. For *Denat-6* DP-PSD measurements, 42 line profiles were drawn from 3 FOVs. For *Denat-8* DP-PSD measurements, 100 line profiles were drawn from 3 FOVs. Results are summarized in **Supplementary Fig. 14**.

Relative protein retention was measured by comparing the peak intensity of DP NHS ester signal from 2-pixel thick line profiles in FIJI. For *Denat-4* measurements, 50 DP peak intensities were recorded from 3 FOVs. For *Denat-6* measurements, 42 DP peak intensities were recorded from 3 FOVs. For *Denat-8* measurements, 48 DP peak intensity measurements were recorded from 3 FOVs. The intensity values were multiplied by the cube of the expansion factor determined for every denaturation condition. Results are summarized in **Supplementary Fig. 14**.

**Assessment of SA monomer concentration effects in brain tissue preservation**

We assessed both antibody-labeling efficiency and ultrastructural preservation in hydrogels synthesized with different sodium acrylate (SA) monomer concentrations. We hypothesized that lowering this concentration would allow for larger effective hydrogel mesh sizes and therefore better antibody penetration. In summary, we used four different hydrogel monomer combinations with either 19% (w/v) or 9% (w/v) SA in the first and second expansion hydrogels, referred to as *19SA/19SA*, *19SA/9SA*, *9SA/19SA*, and *9SA/9SA*. Comparing expansion factors, we found that *19SA/19SA* gels expand as we previously reported 24.1± 1.4-fold (mean ± s.d.; N = 10 fields of view from 3 independent experiments; n = 254 synaptic profiles, **Supplementary Fig. 20e**), *19SA/9SA* gels expand 20.3± 1.2-fold (mean ± s.d.; N = 12 fields of view from 2 independent experiments; n = 267 synaptic profiles), *9SA/19SA* gels expand 20.5± 1.8-fold (mean ± s.d.; N = 6 fields of view from 2 independent experiments; n = 88 synaptic profiles), and *9SA/9SA* gels expand 18.5± 1.7-fold (mean ± s.d.; N = 6 fields of view from 2 independent experiments; n = 86 synaptic profiles). While expansion factors are not radically affected by variations in SA monomer concentrations, we noticed visible ultrastructural differences. Judging tissue preservation by the frequency of gaps in neuropil and

detachments of cell bodies from the underlying tissue, we observe equally good tissue integrity in *19SA/19SA*, *19SA/9SA*, and *9SA/19SA* gels (**Supplementary Fig. 20a-c)**, but significantly distorted neuropil and dissociated cell bodies in *9SA/9SA* gels (**Supplementary Fig. 20d**). We suspect that this distortion effect is due to a decrease in hydrogel mechanical sturdiness when hydrogels of lower monomer concentrations, like the ones in ExR [17], are used. We therefore caution against synthesizing hydrogels that are mechanically too brittle to properly preserve the integrity of biological structures. As for antibody-staining efficiency, we observed equally efficient labeling in *19SA/19SA*, *19SA/9SA*, and *9SA/19SA* hydrogels for most antigens, with reduced background following synaptic protein immunolabeling in *19SA/9SA* hydrogels. Therefore, in all subsequent immunoassays, we used *19SA/9SA* gels for synaptic protein immunolabeling and *19SA/19SA* gels in immunolabeling structural markers.

*19SA/19SA, 19SA/9SA, 9SA/19SA,* and *9SA/9SA* brain tissue samples were previously fixed with 4% FA + 20% AAm in 1× PBS overnight at 4 °C and sectioned to 70 µm as described in the **Brain perfusion** section. Next, they were washed three times with 1× PBS for 30 min each on a rocking platform at RT and processed with the pan-ExM-t protocol with these modifications: the monomer composition of the second expansion hydrogel in *19SA/9SA* samples was 10% (w/v) AAm + 9% SA (w/v); the monomer composition of the first expansion hydrogel in *9SA/19SA* samples was 10% (w/v) AAm + 9% SA (w/v); and the monomer composition of the first and second expansion hydrogels in *9SA/9SA* samples was 10% (w/v) AAm + 9% SA (w/v).

Expansion factors were calculated as described in the **General neuron and brain tissue expansion factor calculation section**. For *19SA/19SA* DP-PSD measurements, 254 line profiles were drawn from 10 FOVs in 3 independent experiments. For *19SA/9SA* DP-PSD measurements, 267 line profiles were drawn from 12 FOVs in 2 independent experiments. For *9SA/19SA* DP-PSD measurements, 88 line profiles were drawn from 6 FOVs in 2 independent experiments. For *9SA/9SA* DP-PSD measurements, 86 line profiles were drawn from 6 FOVs in 2 independent experiments. All results are summarized in **Supplementary Fig. 20e**.

**Measurements of synaptic protein distributions in brain tissue**

Using 2-pixel thick line profiles in FIJI, the peak-to-peak distances between the intensity distributions between Homer1 and PSD, PSD-95 and DP, and Bassoon and PSD were measured and divided by the determined experiment expansion factor. For Homer1-DP measurements in brain tissue, 120 line profiles were drawn from 5 FOVs in 2 independent experiments. For PSD-95-DP measurements in brain tissue, 113 line profiles were drawn from 3 FOVs in one independent experiment. For Bassoon-PSD measurements in brain tissue, 74 line profiles were drawn from 3 FOVs in one independent experiment. Results are summarized in **Fig. 3ooo-rrr**.

**Measurement of BDP signal in 4-fold expanded brain tissue across fixation conditions**

To compare the effect of fixation on lipid retention, brain tissue was fixed with either 4% FA in 1× PBS (*FA-fix*) or 4% FA+ 0.1% GA in 1× PBS (*FA/GA-fix*) overnight at 4 °C and sectioned to 70 µm as described in the **Brain perfusion** section. Several *FA/GA-fix* tissue sections were post-fixed with 0.01% osmium tetroxide (4% osmium solution; EMS, catalog no. 19150) in 1× PBS for 1h at RT (*FA/GA/OsO4-fix*), washed three times with 1× PBS at RT, and stored in 4 °C until subsequent treatment. All tissue sections were post-fixed in 4% FA + 20% AAm in 1× PBS for 15 h at 4 °C, washed three times with 1× PBS for 30 min each on a rocking platform at 4°C, and processed only with the **First round of expansion for brain tissue** protocol with this modification: tissue sections were denatured in SDS buffer for 1 h. For NHS ester pan-staining, gels were incubated with 10 µg/mL NHS ester ATTO532 (Sigma-Aldrich, catalog no.

88793) in 1× PBS for 30 min on a rocking platform at RT and washed three times with 1× PBS for 30 min each. For BDP pan-staining, gels were incubated with 10 µM BODIPY TR Methyl Ester (Thermofisher, catalog no. C34556) in 1× PBS for 1 h on a rocking platform at RT and washed three times with 1× PBS for 30 min each. Gels were subsequently expanded in MilliQ water and imaged.

BDP pan-staining signal in axons was measured by recording the peak intensity of BDP signal from 10-pixel thick line profiles drawn across the width of axons in FIJI. For *FA-fix* measurements, 46 peak intensities were recorded from 5 FOVs. For *FA/GA-fix* measurements, 46 peak intensities were recorded from 5 FOVs. For *FA/GA/OsO4-fix* measurements, 38 peak intensities were recorded from 5 FOVs. Results are summarized in **Supplementary Fig. 24bb**.

**Measurement of BDP signal in 4-fold expanded brain tissue across denaturation conditions**

To compare the effect of fixation on lipid retention, brain tissue was fixed with 4% FA+ 0.1% GA in 1× PBS overnight at 4 °C and sectioned to 70 µm as described in the **Brain perfusion** section. All tissue sections were post-fixed in 4% FA + 20% AAm in 1× PBS for 15 h at 4 °C, washed three times with 1× PBS for 30 min each on a rocking platform at 4°C, and processed only with the **First round of expansion for brain tissue** protocol with this modification: tissue sections were denatured with either SDS buffer at 75°C for 1 h (*SDS-1h*), or SDS buffer at 75°C for 4 h, (*SDS-4h*), non-denatured (*PBS*), or denatured with guanidine hydrochloride (*G-HCl*) buffer (6 M G-HCl + 5 mM DTT + 50 mM Tris in MilliQ water, pH 7.5) at 42°C overnight. For NHS ester pan-staining, gels were incubated with 10 µg/mL NHS ester ATTO532 (Sigma-Aldrich, catalog no. 88793) in 1× PBS for 30 min on a rocking platform at RT and washed three times with 1× PBS for 30 min each. For BDP pan-staining, gels were incubated with 10 µM BODIPY TR Methyl Ester (Thermofisher, catalog no. C34556) in 1× PBS for 1 h on a rocking platform at RT and washed three times with 1× PBS for 30 min each. Gels were subsequently expanded in MilliQ water and imaged.

BDP pan-staining signal in axons was measured by recording the peak intensity of BDP signal from 10-pixel thick line profiles drawn across the width of axons in FIJI. For *SDS-1h* measurements, 40 peak intensities were recorded from 4 FOVs. For *SDS-4h* measurements, 20 peak intensities were recorded from 1 FOV. For *PBS* measurements, 41 peak intensities were recorded from 2 FOVs. For *G-HCl* measurements, 24 peak intensities were recorded from 1 FOV. Results are summarized in **Supplementary Fig. 27k**.

BDP pan-staining signal in mitochondria was measured by recording the peak intensity of BDP signal from 10-pixel thick line profiles drawn across the width of mitochondria in FIJI. For *SDS-1h* measurements, 40 peak intensities were recorded from 4 FOVs. For *SDS-4h* measurements, 18 peak intensities were recorded from 1 FOV. For *PBS* measurements, 41 peak intensities were recorded from 2 FOVs. For *G-HCl* measurements, 20 peak intensities were recorded from 1 FOV. Results are summarized in **Supplementary Fig. 27l.**

**Lipid staining with pacSph** Since there are roughly 5 million lipids per 1 µm$^2$ of membrane surface and 150-times more lipids than proteins on a typical cell membrane [18], we expect that even following detergent extraction with SDS, a fraction of these lipids would remain in the hydrogel. Interestingly, when we labeled SDS-denatured and ~4-fold expanded brain tissue with BODIPY TR Methyl Ester (BDP), we achieved a distinct pan-staining (**Supplementary Fig. 22**). Here, BDP highlights the nuclear envelope, organelles like mitochondria, the Golgi complex, the ER, as well as myelinated axons. All these structures resemble those shown in

mExM [19], but were acquired without using any specialized probes. Overlaid with sulfonated NHS ester dye pan-staining, we observe a striking differential hydrophilic-lipophilic pan-staining pattern (**Supplementary Fig. 23**), with significantly higher BDP staining levels achieved in tissue fixed with 4% FA + 0.1% GA than in tissue fixed with 4% FA (**Supplementary Fig. 24**). Similarly, in pan-ExM-t expanded tissue, we achieve distinctive and bright BDP labeling in tissue fixed with 4% FA + 0.1% GA (**Supplementary Fig. 25**), but almost no staining in tissue fixed with 4% FA. We also see major structural artifacts when supplementing the fixatives with 0.01% osmium tetroxide, known to better preserve lipids [20,21] (**Supplementary Fig. 24s-aa**; **Supplementary Fig. 26**). These results confirm that GA plays a major role in stabilizing and crosslinking the lipid content [2].

Next, we asked whether replacing the anionic detergent SDS in our denaturation buffer with the chaotropic reagent guanidine hydrochloride (G-HCl) would better preserve the lipid content and enable superior lipid staining in 4% FA + 0.1% GA-fixed, pan-ExM-t expanded tissue. Unlike SDS, hyperhydration with urea or guanidine HCl is known to disrupt hydrogen bonding in proteins without solubilizing lipids [22]. EM images of brain tissue samples fixed with only 4% FA and chemically cleared with the functionally similar chaotropic molecule urea show intact membrane ultrastructure and up to 70% lipid retention [23,24]. We chose to work with G-HCl and not urea, because the latter is known to decompose and carbamylate proteins at the elevated temperatures required for efficient denaturation [25]. **Supplementary Fig. 27** shows that BDP signal is in fact higher in G-HCl-denatured neuron and tissue samples, giving credence to this approach. However, our data also show that BDP does not exclusively stain cell membranes and subjecting samples to no denaturation at all results in lower BPD signal. This observation is more evident in ~20-fold expanded samples where easily distinguishable neurite boundaries are not specifically stained with BDP (**Supplementary Fig. 28**). All these results suggest that lipophilic dyes like BDP do not exclusively label lipid membranes in denatured samples, but also label the hydrophobic core of proteins exposed following denaturation. In fact, in thermal denaturation assays, environmentally sensitive fluorescent dyes that bind to the hydrophobic core of proteins are commonly used to determine the temperature at which proteins denature (e.g., in differential scanning fluorimetry (DSF)) [26–28]. Protein denaturation, however, is a necessary step in enzyme-free ExM methods, since electrostatic interactions between proteins must be nulled for isotropic sample expansion.

Since strategies to preserve the lipid content for post-homogenization lipophilic labeling do not result in exclusive cell membrane delineation and require antigen-masking GA fixation [29], we decided to capitalize on pre-denaturation lipid labeling strategies. Here, proteins are not unfolded, and the lipid content may require less harsh fixation since we do not need to preserve it after the homogenization process. To label lipid membranes in ExM, all approaches have so far used trifunctional lipid probes in either live or fixed samples. In these probes, one functional group is a membrane-intercalating lipid, the second is hydrogel-anchorable, and the third is a reporter molecule. In the live-labeling approaches, cells have been labeled with acryolated and fluorescent 1,2-distearoyl-sn-glycero-3-phosphoethanolamine (DSPE) [30], clickable palmitic acid [4], aminated α-NH2-ω-N3-C6-ceramide [31], or clickable choline [32]. The only strategy available to stain lipids in tissue with ExM after it is fixed is to use aminated (poly-lysine) membrane-intercalating probes such as pG5kb [19] and mCling [8,33]. These survive detergent disruption by covalent attachment to the hydrogel matrix and contain a biotin group available for conjugation with dye-labeled streptavidin after expansion. When we tested mCling in 5-fold expanded brain tissue sections, we found that although it labeled tissue hydrophobic components, this labeling was limited to the tissue surface, likely because of diffusion limitations or depletion (**Supplementary Fig. 29**). When we tested mCling in pan-ExM-t samples, we observed little to no labeling. mCling [33] as well as an ExM-optimized version of

it, pG5kb [19], have 5 to 7 lysine groups making them relatively highly charged and bulky (**Supplementary Fig. 30a-b**). mCling and pG5kb also require that the tissue is fixed with GA, which we previously found decreases synaptic protein antigenicity as well as limits the expansion factor to ~12 fold, and so we did not explore this avenue any further.

We therefore developed a new pan-ExM-t lipid labeling strategy where we use a commercially available photocrosslinkable and clickable sphingosine pacSph [34] as a lipid intercalating reagent in tissue fixed only with 4% FA + 20% AAm (to preserve antigenicity) (**Fig. 6n, Methods**). In our protocol, we (1) label 70 µm-thick tissue sections with pacSph prior to hydrogel embedding; (2) irradiate the sample with UV light (365 nm) to photo-crosslink the probes onto neighboring proteins (from both directions to compensate for depth-dependent UV light absorption in the 70-µM thick tissue); and (3) probe the ligands with fluorescent dyes after homogenization and expansion. It is worth noting that pacSph is smaller (335 Da) than mCling (1445 Da) or pG5kb (1158 Da), polar, and partially positively charged (amine pKa ~6.6), allowing for high probe packing and sampling. Sphingosines are also membrane bilayer-rigidifying: they stabilize gel domains in membranes, raise their melting temperature, and induce membrane permeabilization without micellar extraction of proteins or lipids [35,36]. We therefore expect sphingosine to diffuse efficiently in thick tissue. Furthermore, pacSph has a photoactivatable diazirine group that forms reactive carbene intermediates capable of insertion in C-H or N-H, and O-H bonds of tissue components upon UV irradiation [37,38]. Since diazirine is on the lipid chain (**Fig. 6n**, pink diazirine), we expect that two pacSph lipids located on opposing sides of a membrane bilayer will photo-crosslink the embedded hydrogel polymer chains at the center of the hydrophobic phase of the bilayer, minimizing the linker error. This error is inevitable if we were to photo-crosslink the probes at the polar head group. Finally, retained lipids are conjugated with a hydrophobic azido dye at the lipid tail extremity (**Fig. 6n**, green alkyne). We believe all these factors make pacSph ideally suited for membrane delineation in pan-ExM-t. Additionally, pacSph reagents are inexpensive enough that large quantities can be applied to ensure robust labeling over large volumes.

To compare the effect of fixation on lipid retention, brain tissue was fixed with 4% FA+ 20% AAm in 1× PBS overnight at 4 °C and sectioned to 70 µm as described in the **Brain perfusion** section. Sections were incubated in 50 µM pacSph (PhotoClick Sphingosine; Avanti Polar Lipids, catalog no. 900600) in 1× PBS overnight at 4 °C, washed three times in 1× PBS for 1 h each at 4 °C, and either stored at 4 °C (*noUV*) or photo-crosslinked. Samples that were photo-crosslinked were kept on ice and irradiated with an 8 Watt, 365 nm UV light source (Analytik Jena, UVL-18) 1 cm away from a lamp surface for 30 min on both section surface sides, either before hydrogel embedding (*UV-before*) or immediately after **First round of expansion for brain tissue** while the tissue-hydrogel hybrid was still sandwiched between a glass microscope slide and glass coverslip (*UV-after*). Samples were processed with the remaining steps of the pan-ExM-t protocol with this modification: before NHS ester pan-staining, CuAAC was performed using the Click-iT Protein Reaction Buffer Kit (Thermo Fisher, catalog no. C10276) according to manufacturer instructions. Azide-functionalized ATTO590 dye (ATTO-TEC, catalog no. AD 590-101) was used at a concentration of 5 µM. After CuAAC, the gels were washed once with 2% (w/v) delipidated BSA (Sigma Aldrich, catalog no. A4612) in 1× PBS for 20 min each and three times with 1× PBS for 20 min each on a rocking platform at RT.

pacSph pan-staining signal in mitochondria was measured by recording the peak intensity of ATTO590 signal from 10-pixel thick line profiles drawn across the width of mitochondria in FIJI. For *noUV* measurements, 35 peak intensities were recorded from 5 FOVs in one independent experiment. For *UV-before* measurements, 37 peak intensities were recorded from 5 FOVs in one independent experiment. For *UV-after* measurements, 39 peak intensities were

recorded from 5 FOVs in one independent experiment. Results are summarized in **Fig. 6m**.

**Phosphotungstic acid (PTA) staining and electron microscopy**

For samples shown in Fig. 1l, brain tissue was fixed in 2.5% GA in phosphate buffer (pH 7.4) for one hour at room temperature, it was then cut into 100-µm thick slices by a vibratome and dehydrated in a graded series of ethanol to 95%. tissue sections were incubated in 1% phosphotungstic acid (Sigma, catalog no. P6395) in 0.5% ethanol for 2 hours at room temperature. After rinsing with propylene oxide (Electron Microscopy Sciences (EMS), catalog no. 75569), the sections embedded in EMbed 812 resin (EMS, catalog no. 14120), polymerized in a 60 °C oven overnight. Thin sections (65 nm) were cut by a Leica ultramicrotome (UC7) and directly collected on the sample grids without further metal staining. EM images were acquired by a FEI Tecnai transmission electron microscope at an accelerating voltage of 80 kV, an Olympus Morada CCD camera and iTEM imaging software.

For samples shown in Extended Data Fig. 4, brain tissue was fixed according to the pan-ExM-t protocol (4% FA + 20% acrylamide; without GA), then cut into 200-µm thick slices using a compresstome tissue slicer. Samples were thereafter prepared using standard electron microscopy protocols. Briefly, samples were stained in 1% osmium tetroxide / 1.5% potassium ferrocyanide in cacodylate buffer at room temperature for 1 hour, then washed with de-ionized water, stained in 1% uranyl acetate in maleate buffer overnight, washed with de-ionized water again, dehydrated with an ethanol series, and infiltrated with propylene oxide, then embedded in EMbed 812 resin and polymerized in a 60 °C oven overnight. Thin sections (65 nm) were cut by a Leica ultramicrotome (UC7) and directly collected on the sample grids without further post-staining. EM images were acquired on an FEI Talos TEM (120 kV).

**Neuron expansion factor calculation**

Images of hippocampal mouse and rat neuron cell nuclei in non-expanded and pan-ExM expanded samples stained with SYTOX Green (1:5,000) were acquired with a Leica SP8 STED 3X microscope using a HCX PL Fluotar 10×/0.30 dry objective. Average nuclear cross-sectional areas were determined using FIJI/ImageJ software. To calculate the expansion factor, the average nuclear cross-sectional area in pan-ExM samples was divided by the average nuclear cross-sectional area of non-expanded samples. The square root of this ratio represents an estimate of the linear expansion factor. For nuclei cross-section measurements in pan-ExM samples, 38 nuclei were analyzed from 4 independent experiments. For nuclei cross-section measurements in non-expanded samples, 279 nuclei were analyzed from 4 independent experiments.

Using 2-pixel thick line profiles in FIJI, the peak-to-peak distances between the intensity distributions of the dense projection (DP) and postsynaptic density (PSD) NHS ester signals in the same samples were measured and divided by the nuclear expansion factor determined above. For this measurement, 44 line profiles were drawn from 4 independent experiments. The DP-PSD value was determined to be 81.9 nm and was used to convert DP-PSD measurements to expansion factors in all subsequent experiments. Results are summarized in **Fig. 1n**. More generally, we quantified the expansion factor for datasets corresponding to each figure. We quantified 40-521 synapses total from at least 4-26 FOVs, and reported the mean and standard deviation across FOVs.

**Distance between individual DPs calculation**

Using 2-pixel thick line profiles in FIJI, the peak-to-peak distances between the intensity

distributions of individual dense projections (DPs) were measured and divided by the determined expansion factor. For this measurement, 78 line profiles were drawn from 41 synapses in 6 independent experiments. Results are summarized in **Fig. 1o**.

**Measurements of synaptic protein distributions in neurons**

Using 2-pixel thick line profiles in FIJI, the peak-to-peak distances between the intensity distributions between Homer1 and PSD, PSD-95 and DP, and Bassoon and PSD were measured and divided by the determined experiment expansion factor. For Bassoon-PSD measurements in neurons, 50 line profiles were drawn from 3 independent samples. For Homer1-DP measurements in neurons, 85 line profiles were drawn from 4 independent samples. For PSD95-DP measurements in neurons, 25 line profiles were drawn from 2 independent samples. Results are summarized in **Fig. 1p-s**.

**Measurement of anti-Homer1 signal across dilution factors**

Neuron samples were labeled with anti-Homer1 primary antibody and ATTO594-conjugated anti-rabbit antibodies as described in **Antibody labeling of neurons post-expansion** with this modification: Samples were labeled with primary and secondary antibodies both diluted 1:250 or 1:500 or 1:1000.

Relative protein retention was measured by comparing the peak intensity of Homer1 ATTO504 signal from 2-pixel thick line profiles in FIJI drawn across the punctate signal. For *1:250* measurements, 45 peak intensities were recorded from 7 FOVs. For *1:500* measurements, 13 peak intensities were recorded from 3 FOVs. For *1:1000* measurements, 6 peak intensity measurements were recorded from 1 FOV. Results are summarized in **Supplementary Fig. 7j**.

**Simulations of non-expanded sample images**

MATLAB was used to convolve the raw pan-ExM-t images with the theoretical point spread function (PSF) of a spinning-disk confocal microscope (lateral FWHM = 288 nm; axial FWHM = 844 nm) to simulate a conventional confocal microscope's resolution on pan-ExM-t samples. The background was subtracted using a rolling-ball algorithm with a radius of 50 px. The 3D stacks were smoothed using a Gaussian blur where $\sigma = 28$ px in XY and $\sigma = 21$ px in Z for Thy1eGFP and $\sigma = 24$ px in XY and $\sigma = 23$ px in Z for PSD-95. The processed image (**Supp. Extended Data Fig. 2 a-f**, **Extended Data Fig. 2 m-r**) directly demonstrates how nanoscale structures, which are clearly resolved in the unprocessed, Thy1-ExF and 20 ± 4, respectively, expanded pan-ExM-t images (**Extended Data Fig. 2 g-l**, **Extended Data Fig. 2 s-x**) would appear under standard confocal imaging conditions.

**Quantification of imaging resolution**

Image metadata was used to obtain voxel dimensions and the number of slices to convert pixel measurements into physical distances. Fifty point-like ROIs were selected for both the lateral and axial dimensions, and for each ROI, a rectangle that was ≥ 25 px (horizontal for lateral, and vertical for axial) was drawn, averaging over three pixels to generate an intensity profile. Each profile was fit to a Gaussian in MATLAB, which was used to compute full-width half-maximum (FWHM) values for lateral (290±60 nm) and axial (840±180 nm) resolution (**Extended Data Fig. 5**).

# Supplementary References

1. Biederer, T. & Scheiffele, P. Mixed-culture assays for analyzing neuronal synapse

formation. *Nat. Protoc.* **2**, 670–676 (3/2007).
2. Hayat, M. A. *Fixation for Electron Microscopy*. (Academic Press, San Diego, CA, 1982).
3. Sabatini, D. D., Bensch, K. & Barrnett, R. J. Cytochemistry and electron microscopy. The preservation of cellular ultrastructure and enzymatic activity by aldehyde fixation. *J. Cell Biol.* **17**, 19–58 (1963).
4. Ons M'Saad, M'Saad, O., Joerg Bewersdorf & Bewersdorf, J. Light microscopy of proteins in their ultrastructural context. *bioRxivorg* (2020) doi:10.1101/2020.03.13.989756.
5. Migneault, I., Dartiguenave, C., Bertrand, M. J. & Waldron, K. C. Glutaraldehyde: Behavior in Aqueous Solution, Reaction with Proteins, and Application to Enzyme Crosslinking. *Biotechniques* **37**, 790–802 (11/2004).
6. Gambarotto, D. *et al.* Imaging cellular ultrastructures using expansion microscopy (U-ExM). *Nature Methods 2018 16:1* **16**, 71–74 (2018).
7. Tillberg, P. W. *et al.* Protein-retention expansion microscopy of cells and tissues labeled using standard fluorescent proteins and antibodies. *Nat. Biotechnol.* **34**, 987–992 (9/2016).
8. Damstra, H. G. J. *et al.* Visualizing cellular and tissue ultrastructure using Ten-fold Robust Expansion Microscopy (TREx). *bioRxiv* (2021) doi:10.1101/2021.02.03.428837.
9. Otsu, N. A threshold selection method from gray-level histograms. *IEEE Trans. Syst. Man Cybern.* **9**, 62–66 (1979).
10. Jan Tønnesen *et al.* Super-Resolution Imaging of the Extracellular Space in Living Brain Tissue. *Cell* **172**, 1108–1121 (2018).
11. Vanharreveld, A., Crowell, J. & Malhotra, S. K. A study of extracellular space in central nervous tissue by freeze-substitution. *J. Cell Biol.* **25**, 117–137 (1965).
12. Natalya Korogod *et al.* Ultrastructural analysis of adult mouse neocortex comparing aldehyde perfusion with cryo fixation. *eLife* **4**, (2015).
13. Kwanghun Chung *et al.* Structural and molecular interrogation of intact biological systems. *Nature* **497**, 332–337 (2013).
14. Ku, T. *et al.* Multiplexed and scalable super-resolution imaging of three-dimensional protein localization in size-adjustable tissues. *Nat. Biotechnol.* **34**, 973–981 (9/2016).
15. Sankur, B. Survey over image thresholding techniques and quantitative performance evaluation. *J. Electron. Imaging* **13**, 146 (2004).
16. O'Connell, P. B. H. & Brady, C. J. Polyacrylamide gels with modified cross-linkages. *Anal. Biochem.* **76**, 63–73 (1976).
17. Deblina Sarkar *et al.* Expansion Revealing: Decrowding Proteins to Unmask Invisible Brain Nanostructures. *bioRxivorg* (2020) doi:10.1101/2020.08.29.273540.
18. Quinn, P., Griffiths, G. & Warren, G. Density of newly synthesized plasma membrane proteins in intracellular membranes II. Biochemical studies. *J. Cell Biol.* **98**, 2142–2147 (1984).
19. Karagiannis, E. D. *et al.* Expansion Microscopy of Lipid Membranes. *Bioengineering* (2019) doi:10.1101/829903.
20. Palade, G. E. A study of fixation for electron microscopy. *J. Exp. Med.* **95**, 285–298 (1952).
21. Litman, R. B. & Barrnett, R. J. The mechanism of the fixation of tissue components by osmium tetroxide via hydrogen bonding. *J. Ultrastruct. Res.* **38**, 63–86 (1972).
22. Adriana Huerta-Viga, Huerta-Viga, A., Sander Woutersen & Woutersen, S. Protein Denaturation with Guanidinium: A 2D-IR Study. *Journal of Physical Chemistry Letters* **4**, 3397–3401 (2013).
23. Hama, H. *et al.* ScaleS: an optical clearing palette for biological imaging. *Nat. Neurosci.*

**18**, 1518–1529 (10/2015).
24. Shimrit Oz *et al.* Tissue expansion of 'cleared' whole brains reduces contrast in ex vivo MRI. (2021) doi:10.21203/rs.3.rs-877945/v1.
25. Jon W. Poulsen *et al.* Using Guanidine-Hydrochloride for Fast and Efficient Protein Digestion and Single-step Affinity-purification Mass Spectrometry. *J. Proteome Res.* **12**, 1020–1030 (2013).
26. Senisterra, G., Chau, I. & Vedadi, M. Thermal denaturation assays in chemical biology. *Assay Drug Dev. Technol.* **10**, 128–136 (2012).
27. Vedadi, M. *et al.* Chemical screening methods to identify ligands that promote protein stability, protein crystallization, and structure determination. *Proc. Natl. Acad. Sci. U. S. A.* **103**, 15835–15840 (2006).
28. Lukas Hofmann *et al.* An effective thiol-reactive probe for differential scanning fluorimetry with a standard real-time polymerase chain reaction device. *Anal. Biochem.* **499**, 63–65 (2016).
29. Passagot, J. *et al.* Effect of glutaraldehyde on the antigenicity and infectivity of hepatitis A virus. *J. Virol. Methods* **16**, 21–28 (1987).
30. Wen, G. *et al.* Evaluation of Direct Grafting Strategies *via* Trivalent Anchoring for Enabling Lipid Membrane and Cytoskeleton Staining in Expansion Microscopy. *ACS Nano* **14**, 7860–7867 (2020).
31. Roland Götz *et al.* Nanoscale imaging of bacterial infections by sphingolipid expansion microscopy. *Nat. Commun.* **11**, 1–9 (2020).
32. De-en Sun *et al.* Click-ExM enables expansion microscopy for all biomolecules. *Nat. Methods* **18**, 107–113 (2020).
33. Natalia H. Revelo *et al.* A new probe for super-resolution imaging of membranes elucidates trafficking pathways. *J. Cell Biol.* **205**, 591–606 (2014).
34. Per Haberkant *et al.* Bifunctional Sphingosine for Cell-Based Analysis of Protein-Sphingolipid Interactions. *ACS Chem. Biol.* **11**, 222–230 (2016).
35. Contreras, F.-X., Sot, J., Alonso, A. & Goñi, F. M. Sphingosine increases the permeability of model and cell membranes. *Biophys. J.* **90**, 4085–4092 (2006).
36. Noemi Jiménez-Rojo *et al.* Membrane Permeabilization Induced by Sphingosine: Effect of Negatively Charged Lipids. *Biophys. J.* **106**, 2577–2584 (2014).
37. Gomes, A. F. & Gozzo, F. C. Chemical cross-linking with a diazirine photoactivatable cross-linker investigated by MALDI- and ESI-MS/MS. *J. Mass Spectrom.* **45**, 892–899 (08/2010).
38. Krieg, U. C., Walter, P. & Johnson, A. E. Photocrosslinking of the signal sequence of nascent preprolactin to the 54-kilodalton polypeptide of the signal recognition particle. *Proc. Natl. Acad. Sci. U. S. A.* **83**, 8604–8608 (1986).